Limits to global groundwater consumption

Effects on groundwater levels and river low flows

De grenzen van mondiaal grondwaterverbruik

Effecten op grondwaterstanden en lage rivierafvoeren

(met een samenvatting in het Nederlands)

P R O E F S C H R I F T

ter verkrijging van de graad van doctor aan de Universiteit Utrecht
op gezag van de rector magnificus, prof. dr. G. J. van der Zwaan,
ingevolge het besluit van het college voor promoties in het openbaar te verdedigen
op vrijdag 1 april 2016 des middags te 2.30 uur

door

Ingeborg Elisabeth Maria de Graaf

geboren op 5 mei 1987 te Nijmegen

Promotor:
Prof. dr. ir. M. F. P. Bierkens

Copromotor:
Dr. L. P. H. van Beek

This study was funded by the Netherlands Organization for Scientific Research (NWO) in the project Planetary Boundaries Fresh Water Cycle.

Utrecht Studies in Earth Sciences 101

Limits to global groundwater consumption

Effects on groundwater levels and river discharges

Inge de Graaf

Utrecht 2016

Faculty of Geosciences, Utrecht University

Promotor:
Prof. dr. ir. M. F. P. Bierkens

Copromotor:
Dr. L. P. H. van Beek

Examination committee:
Dr. H. Biemans
Wageningen University, Netherlands

Prof. dr. N. van de Giesen
Delft University of Technology, Netherlands

Prof. dr. T. Gleeson
University of Victoria, Canada

Prof. dr. J. Kwadijk
University of Twente, Netherlands

Prof. dr. G. Miguez Macho
University of Santiago de Compostela, Spain

ISBN 978-90-6266-418-4

Published by Faculty of Geosciences, Universiteit Utrecht, The Netherlands, in: Utrecht Studies in Earth Sciences (USES), ISSN 2211-4335

Cover: Center-pivot irrigation systems, Kansas, draw from the High Plains Aquifer. (NASA ASTER image)

Printed by CPI Koninklijke Wöhrmann

Correspondense to: Inge de Graaf, idegraaf@mines.edu, ingedgraaf@gmail.com

Except where otherwise noted, this work is licensed under the Creative Commons Attribution 4.0 International Licence, http://creativecommons.org/licenses/by/4.0/, © 2016 by Inge E.M. de Graaf.
Chapters 2 to 5 and the Appendix are either unpublished submitted articles or last-author versions of previously published articles, © by Inge E.M. de Graaf and co-authors. More information and citation suggestions are provided at the beginning of these chapters.

"I have never tried that before, so I think I should definitely be able to do that"
- Pippi Longstocking

.

Summary

Groundwater is the largest accessible freshwater resource worldwide. Nowadays, many large aquifer systems are depleted and abstraction rates are unsustainable on the long run.

The main objective of this PhD study was to assess the limits of global groundwater consumption. For this assessment past and future trends in groundwater levels and river flows, resulting from changes in climate conditions and water use are estimated and a prediction is made when limits to groundwater consumption are reached. These limits are explored by predicting where and when groundwater levels drop that low groundwater becomes unattainable for abstractions, or groundwater discharge no longer support river low flows.

In this study a coupled version of the global hydrological model PCR-GLOBWB and a global groundwater model based on MODFLOW is developed. The model accounts for lateral groundwater flows and groundwater-surface water interactions and includes water abstractions of the recent past and near future. The model runs at 5 arc-minute spatial resolution (approximately 10 km^2 at the equator) at a daily time-step. Results are evaluated against observed streamflow and groundwater heads. In this study, a water resource model was developed, that dynamically attributes water demands (from industries, households, irrigation, and livestock) to groundwater or surface water resources, based on water availability in the resource. River infiltration and return flows of unconsumed abstracted water are included, and positively affect water availability. The groundwater model, also developed in this study, is parameterized with available global dataset on lithology and permeability and estimates of aquifer thickness and the distribution and thickness of confining layers.

Inclusion of confined aquifer systems (estimated 6% to 20% of the total aquifer area) changes timing and amplitude of groundwater head fluctuations, as well as flow paths and groundwater surface water interactions. Lateral groundwater flows between basins are significant in the model, especially for confined aquifer areas where long paths are simulated crossing catchment boundaries, thereby supporting water budgets of neighbouring catchments or aquifers. This shows that simulating confining layers within global hydrological models is critical for accurately simulating groundwater-surface water interactions, the water table, and groundwater depletion.

Falling groundwater levels, declining groundwater reserves, and decreasing stream flows, due to changes in water abstractions or climate, are evaluated using 1960 as a reference. Falling groundwater levels are assessed relative to two limits; 1) a depth of 100 m below the surface at which groundwater becomes unattainable for local farmers using pumps, as it is the case for irrigated areas in developing countries; 2) a head difference larger than 300 m between phreatic groundwater heads and heads in the well, which is the typical exploitable limit of industrial scale pumps in developed countries. The first depth is interpreted as an economic limit, as investments to exploit deeper cannot be borne by the farmers themselves, the second limit is interpreted as a technical limit.

Global cumulative groundwater depletion is estimated at 10,445 km^3 over 1960-2050. Hotspot areas of groundwater depletion are found for intensively irrigated regions in the dryer climates of the world, like India, Pakistan, North China, Mid and Mid-west of the US. These regions already reached their economic limits (starting from the 1980s). Results show that, next to these regions, new regions experiencing groundwater depletion will develop in the near future in semi-arid climates. In these regions groundwater demand will intensify due to the increase in drought frequency and duration, reflected in the river low flows, combined with population growth, expanding irrigation areas, and rising standards of living. Some of these regions will have groundwater level drops below economic limits (starting from the 2010s). Examples are Spain, Italy, parts of Africa and the Middle East. The increase in global pumping costs to ensure groundwater supply from 1960 to 2050 is estimated at $\sim$4000 Million US$ a year. Regionally, an increase or decline in pumping costs can be an essential factor in economic development, and therefore should be carefully considered in order to warrant a reliable groundwater supply under a changing climate.

Table of Contents

Summary vi

1 Introduction: Limits to global groundwater consumption 1

2 Dynamic attribution of global water demand to surface water and groundwater resources: Effects of abstractions and return flows on river discharges 11

3 A high resolution global scale groundwater model 33

4 A global-scale two-layered transient groundwater model: development and application to groundwater depletion 55

5 Limits to global groundwater consumption 79

6 Synthesis 99

References 109

Appendix: Supplement to Chapter 3 115

Samenvatting (Dutch summary) 119

About the author 123

List of publications 125

Dankwoord (Acknowledgements) 127

.

Chapter 1

Introduction: Limits to global groundwater consumption

1.1 Our thirsty world

Freshwater is essential for human existence. With increasing global population and economic growth, global freshwater demand increased rapidly over the past decades (e.g. Vörösmarty et al., 2010; Shiklomanov & Rodda, 2003). The main water users are industries, households, livestock, and irrigated agriculture. Irrigation is by far the greatest user and is responsible for 70% of the total water demand globally (Döll & Siebert, 2002). Although global water demands can in principle be met by surface water only, from lakes, rivers, and reservoirs, the available surface water stocks are not evenly distributed over the globe and over the year. For example, in monsoon dominated climates a substantial part of the yearly annual runoff occurs during a short period of the year. Also, irrigated regions in arid to semi-arid climates often experience severe water shortage during the crop season, as the available surface water is limited due to low precipitation (e.g. Oki & Kanae, 2006; Vörösmarty et al., 2010).

During dry periods, when available surface water is insufficient to meet human water demands, people often use groundwater as an alternative freshwater resource. Groundwater is the largest accessible source of freshwater globally and provides a substantial reserve of freshwater with constant flow rates and in general good quality. But, often groundwater abstraction rates exceed groundwater recharge for extensive areas and over longer time, leading to persistent groundwater depletion. This means groundwater is permanently lost from its storage (e.g. Rodell et al., 2009; Konikow, 2011; Aeschbach-Hertig & Gleeson, 2012). Regions experiencing serious groundwater depletion are mostly intensively irrigated regions like India, North-China, and the mid-West of the USA (Figure 1.1).

A direct consequence of groundwater depletion is falling groundwater levels. For example, groundwater levels dropped up to 120 m in 100 years over the intensively pumped parts of the Central Valley (Scanlon et al., 2012). With falling groundwater levels pumping costs and maintenance costs of productive wells increases, leading to a rise in crop cost and food prices. The increase in costs impacts all users, but particularly the poorest farmers of the world who cannot afford a deeper well and a stronger pump. Without technical improvements and financial support wells will run dry and agricultural production may decrease, threatining regional food security.

Another consequence of falling groundwater levels is land-subsidence caused by the compaction of the soil when the water is pumped out. Coastal areas become more vulnerable for floods. A well-known example is the Jakarta delta, where river and coastal floods have now become a recurrent phenomenon. Also, groundwater level drops in coastal areas lead to salt water intrusion, contaminating drinking water sources.

Moreover, deeper groundwater levels lead to reduced groundwater discharge needed to sustain river flows, lake levels, and wetlands. Often intensified by over-abstraction of the river water, this will lead to prolonged periods of limited river flows, severely threatening biodiversity in both aquatic and terrestrial ecosystems, as well as deteriorating water quality by concentrating water pollution (Foster & Chilton, 2003; Aeschbach-Hertig & Gleeson, 2012).

Over the past decades global water demands more than doubled (to $\sim$1900 km^3yr^{-1} in 2010 (Wada et al., 2012)). It is expected that these demands increase further in the coming decades driven by population growth, economic development, and expansion of irrigated areas (Döll & Siebert, 2002; Vörösmarty et al., 2010). It is expected that food demands are going to increase most for the less developed countries due to population growth, but also for the upcoming economies where incomes rise and dietary changes towards higher meat intake (UN, 2012). In addition, climate change will have a growing impact on water resources, as it alters rainfall patterns and soil humidity, melts glaciers, and causes water-related disasters such as floods and droughts, which impacts food production (Taylor et al., 2013).

The expected increase in water demands, the decrease in available freshwater, and the mentioned negative effects of groundwater depletion poses the urgent questions how sustainable current water abstractions are worldwide and where and when these abstractions lead to associated problems, such as drying up of wells and falling river flows. Guidance to sustainable groundwater use is needed to overcome potential political water conflicts and reduce potential socio-economic friction, as well as to secure future food productions.

In this PhD research I studied the limits to global groundwater consumption by analysing the effects on surface water and groundwater flows and storages at the global-scale.

1.2 Scientific background

The first study to define limits of global water use within the context of planetary boundaries, is the study of Rockström et al. (2009). They introduced the concept of a safe operating space for humanity, defined as the space for human activity that will not push the planet out of its current equilibrium. Nine earth-system processes were identified and preliminary boundaries were given in the paper. For global freshwater use the boundary was set to safely sustain enough soil water storage for moisture feedbacks, while allowing for terrestrial and aquatic ecosystem functioning. Rockström et al. (2009)

suggests a global threshold for the consumption of freshwater, which is the actual use from lakes, rivers, reservoirs, and groundwater, of 4,000 to 6,000 km^3y^{-1}.

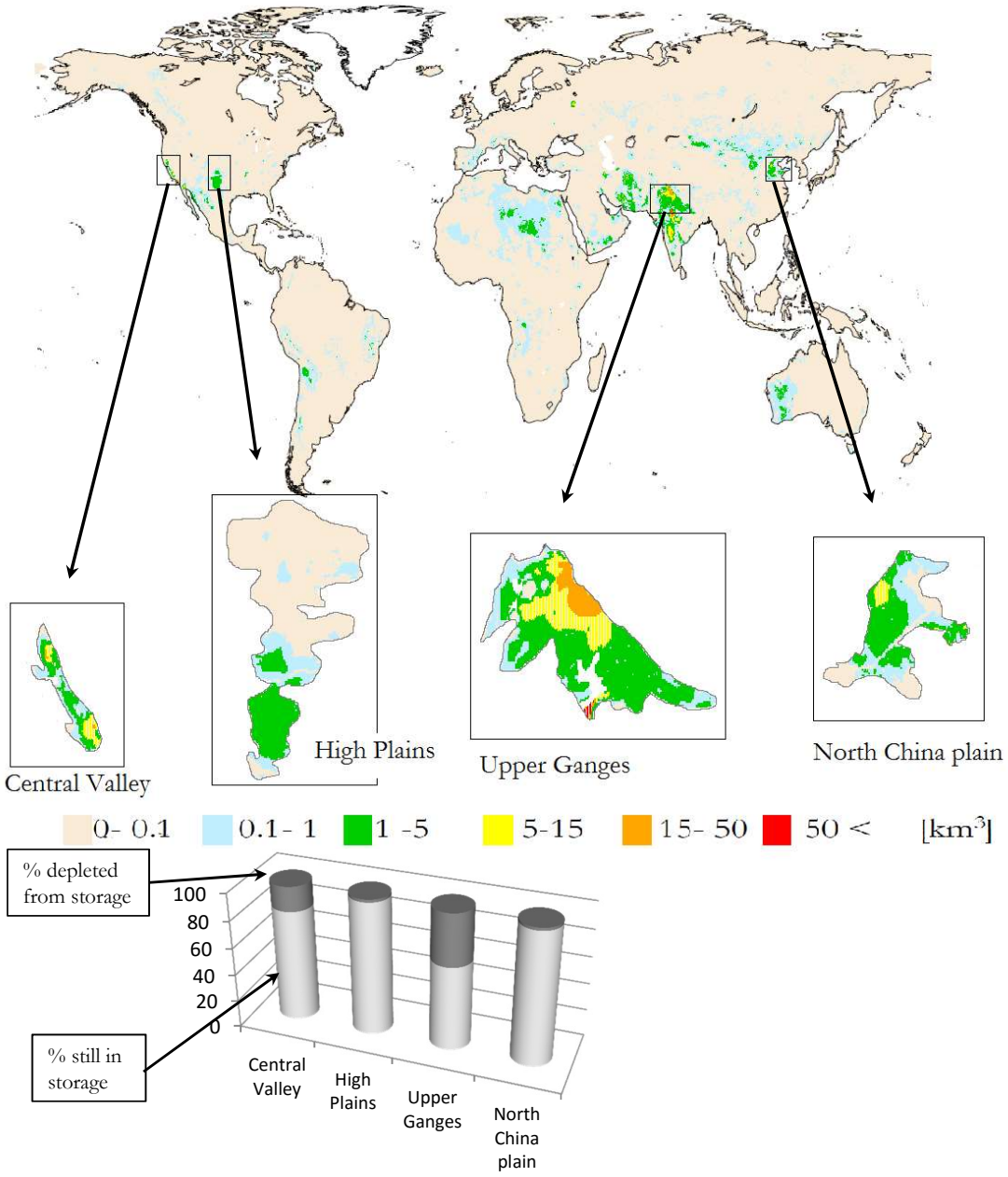

Fig. 1.1: Cumulative groundwater depletion over 1960-2010 in km^3 (this study's result) and zooms for four big aquifer systems of the world. At the bottom of the figure, a diagram of the abstracted volume (in percentage) of the total aquifer storage (calculated with this study's estimates of aquifer thickness and storativities).

However, given the current spatial and temporal variability in freshwater availability, and the rapid increase in water consumption in many parts of the developing world, the global-scale threshold of Rockström et al. (2009) appears not to be particularly useful. Essentially, the concept of a global limit overlooks variabilities at regional and local scales and the role of management in magnifying or ameliorating problems. On the other hand, the suggested thresholds are important because they provide targets for policymakers, giving a clear indication of the magnitude and direction of change. They also provide benchmarks and direction for science.

Rockström's study has been a start for many studies at the global-scale, including this PhD study, focussing on water consumption and its effects on surface water and groundwater flows and storages. General research topics are: How much water is used? How are demands divided over groundwater and surface water resources? How much water can be used in a sustainable way? In the following paragraphs I will discuss the main challenges of current modelling studies and relate these challenges to my own research and I mention this study's specific model aims related to the research questions discussed in the next section of this chapter.

1.2.1 Allocation water demands

Several global-scale hydrological models are developed focussing on consumptive water use and its effects. Examples are: H08 (Hanasaki et al., 2010), WaterGap (Döll et al., 2012), WBMplus (Wisser et al., 2008), PCR-GLOBWB (Wada et al., 2011). All studies had to deal with a data lack on the attribution of water demands to surface water and groundwater resources, and therefore all use their own assumptions. None of these previous studies account for abundance of both surface water and groundwater at the same time. Therefore, the used attribution rules are not robust under changes in water availability, be it from climate change or abstractions.

Moreover, most studies do not include feedback mechanisms connecting surface water and groundwater resources. For example, the increase in river infiltration due to groundwater abstractions is often not included. Nor are the return flows of unconsumed abstracted water -water that can be used again- flowing to the groundwater reservoir or surface water. These return flows support water storage and change residence times of the water when flowing between the resources; from the fast surface water to the slow groundwater, when used for irrigation, or vice versa, when used for industries or domestic uses (de Graaf et al., 2013).

One specific aim of this PhD research was the development of a dynamic scheme that allocates water demands to either surface water or groundwater resources, dependent on the actual water availability in the resource and including feedbacks. Such a scheme is needed to mimic change over time and space in exploitation intensity of surface water or groundwater.

1.2.2 Parameterization of the world's aquifers

Despite the importance of groundwater, most global-scale hydrological models do not include a groundwater flow component. The main reason of this omission is the lack of consistent global-scale hydrogeological information to parameterize the aquifers, such as aquifer thickness, permeability, and specific yields. Such data is needed to obtain a more realistic simulation of groundwater head dynamic and lateral flows (Fan et al., 2007; Schaller & Fan, 2009) and also when effects of groundwater use are to be simulated. The inclusion of a groundwater flow component gets especially important when moving to finer resolutions (e.g. 5 arc-minutes, 10 km^2 at the equator) (Wood et al., 2012, Bierkens et al., 2015), as lateral groundwater flows often cross topographical and administrative boundaries at considerable rates, supporting water budgets of water receiving catchments or aquifers.

Some work has been done toward global-scale groundwater modelling. In the study of Fan et al. (2013) a first global groundwater table depth map is presented (at high-resolution, $\sim$1 km at the equator). Their method however, only returns the steady-state water table, neglecting temporal variations, and does not include the needed hydrogeological information. Also, the hydrological connection between rivers and groundwater, the primary mode of drainage for groundwater in humid regions, is treated only rudimentary. Moreover, their model needs a calibration to head observations, which are not widely available over the globe.

One specific aim of this PhD research was to develop a global-scale groundwater model using hydrogeological information. The main goal was to develop a relative simple method for aquifer parameterization primarily based in available global datasets, such that the method can be expanded to data poor environments. The model is used to simulate groundwater heads and fluctuations, lateral groundwater flows, and aquifer sensitivity for storage changes, be it from climate change or abstractions.

1.2.3 Estimating groundwater depletion

Several previous studies assess the magnitude of groundwater depletion (e.g. Konikow, 2011; Wada et al., 2012; Döll et al., 2012; Döll et al., 2014; Rodell et al., 2009; Aeschbach-Hertig & Gleeson, 2012; Gleeson et al., 2012). Groundwater depletion can be estimated from two different approaches: using a flux-based approach, or volume-based approach. In flux-based methods groundwater depletion derives from the difference between grid-based simulated groundwater recharge and net abstractions (that is groundwater withdrawal minus return flows)(e.g. Döll et al., 2012; Pokhrel et al., 2012; Wada et al., 2012). In volume-based approaches groundwater depletion determines from groundwater head declines (observed or simulated) (Scanlon et al., 2012; Konikow, 2011) multiplied by storage capacities.

The main disadvantage of flux based methods is that increased capture resulting from

decreased groundwater discharge is not included. Therefore, groundwater depletion is generally overestimated by this approach. On the other hand, volume-based depletion estimates, using head declines and storage capacities, are only available for a limited well-monitored aquifers of the world (e.g. High Plains and Central Valley (Scanlon et al., 2012)), such that estimates on the global-scale can only be obtained by extrapolation (Konikow, 2011).

A last approach to obtain groundwater depletion estimates is to use earth's gravity field observations from NASA's Gravity Recovery and Climate Experiment (GRACE) (Rodell et al., 2009; Richey et al., 2015). The satellite mission measures large mass changes of the earth surface. Other sources of mass change, e.g. changes in surface water, ice, snow and global isostatic adjustments have to be corrected for before the storage change from groundwater depletion can be derived. It is only possible to calculate the GRACE signal for large areas (400 km), which is a large disadvantage if the interest lies on spatial variability of depletion, for example within an aquifer.

Available global estimates of groundwater depletion, over the period 1960 to 2010, ranges from 18,000 km^3 (Pokhrel et al., 2012, flux-based approach), to 2,000 km^3 (Konikow 2011, volume-based approach). As said before, the large difference between these estimates is dependent on which approach was used, but also on variability in abstraction rates, differences in climate forcing etc.

In this PhD thesis I present another estimate of global groundwater depletion by using a volume-based method by means of a global groundwater model.

1.2.4 The limits to groundwater use

The limits to groundwater use can be considered from two viewpoints. A first and obvious viewpoint is to consider the total amount of fresh groundwater and see how long it takes before it is exhausted. However, besides that it is not exactly known how much groundwater there is (the most commonly cited estimate 234,106 km^3 of which 105,106 km^3 is fresh (Shiklomanov, 1993)) only a limited part is stored in permeable formations, shallow enough to be exploited. Therefore, it makes more sense to estimate where and when groundwater levels drop that deep that the groundwater has effectively become unavailable for the users, given the level of locally available technology (e.g. stronger pumps) and capital (money to pay for the pump and drill the well) to exploit the groundwater. The economic consequences of increasing cost can be related to this.

Another viewpoint is to consider only renewable groundwater resources, that stores the groundwater that is, at least in the current time frame, is part of the hydrological cycle. This is the groundwater recharged by water infiltration through the soil, and discharges groundwater to rivers, lakes, and wetlands. The limits of groundwater use then include the effects elsewhere, such as reduced stream flows, water level drops of lakes and wetlands, with devastating effects on related ecosystems. The main question here is how much groundwater can be abstracted at maximum to avoid streamflow to

become too low and to avoid groundwater levels to drop below river or lake bottom levels.

Also, with unsustainable groundwater use the question arises how much water can be abstracted before downstream water requirements, from humans or related ecosystems, can no longer be met. It is important here not to study long-year trends only, but also multi-year variability. For example, how much groundwater recharge during multi-year droughts is needed to sustain river low flows. The last part of this thesis deals with the various ways a global groundwater model can be used to determine the limits to groundwater use.

1.3 Research Objectives

In this PhD research I consider the limits to groundwater consumption both from the viewpoint of the limits to locally attainable groundwater (total available groundwater resources) as well as the limits to abstraction in relation to effects on river low flows and groundwater levels critical to lakes, rivers, and wetlands (renewable groundwater resources).

The main objective of this PhD research is **to assess the limits to global groundwater consumption from the perspective of local attainability and regional groundwater-surface water interactions.**

Specifically, the following related research questions (RQ) were asked:

RQ1. What has been the effect of groundwater abstraction on low flows in rivers of the world and which trends in low flow frequency can be attributed to groundwater abstraction?

RQ2. What has been the effect of groundwater abstraction on groundwater levels worldwide and which trends in groundwater level change can be attributed to groundwater abstraction?

RQ3. What are the projected trends in groundwater levels and low flow frequencies as a result of climate change?

RQ4. At what time in the future will limits to groundwater consumption be reached? That is when and where groundwater levels drop that low that groundwater becomes unattainable for abstractions, or that baseflows no longer sustain river discharges.

Basic model approach
As a first step in this PhD research groundwater storages and river discharges were simulated using the global hydrological model PCR-GLOBWB (van Beek et al., 2011).

PCR-GLOBWB is a conceptual, process based hydrological model that simulates daily water balances for every grid-cell (e.g. 5 arc-minute globally, i.e. 10 km^2 at the equator). Water storages are simulated in two vertically stacked soil layers and an underlying groundwater layer (Figure 1.2A). The groundwater is simulated as a linear reservoir and lateral flows are not allowed for.

Therefore, the next step of this PhD research was the development of a global-scale groundwater model. This groundwater model is based on MODFLOW (McDonald & Harbaugh, 2000) and replaces the groundwater store of PCR-GLOBWB (Figure 1.2B). The groundwater model is forced with groundwater recharge and river discharges from the PCR-GLOBWB. Initially the two models ran separately and surface water- groundwater interactions are only one-way. This means that changes in groundwater discharge do not affect river discharges. The last step in this research was to run the two models simultaneously, such that river dynamics are fully coupled to the groundwater.

1.4 Thesis outline

In **Chapter 2** a dynamic attribution scheme for groundwater and surface water abstraction is introduced and used to analyse the impact of abstractions on river discharges focussing on changes in low flow magnitude, frequency, and timing (answering RQ1). Also, past trends of abstractions are given, including an estimate for non-renewable or non-local water abstraction (calculated as groundwater abstraction in excess of groundwater recharge).

In **Chapter 3** the first step towards the global-scale groundwater model is described. Groundwater heads of an upper unconfined aquifer are simulated (steady-state), providing a fist-order estimate of spatial variability of water table heads as a function of topography and climate. The method of aquifer parameterization is described, including an estimation of world's aquifer thicknesses.

In **Chapter 4** the next step towards a global-scale groundwater model is described. The world's aquifers are classified in confined and unconfined systems, holding vital information on the accessibility and quality of groundwater. Groundwater heads and fluctuation as well as fluctuation in groundwater discharges are simulated (answering RQ2). Groundwater depletion is estimated using simulated head declines and globally available data on storage coefficients and specific yields. This is the first estimate of global-scale groundwater depletion that takes account of lateral groundwater flow and river infiltration and drainage.

In **Chapter 5** the limits to global water consumption are investigated by considering economic and physical constraints to groundwater pumping related to groundwater depths. Trends in groundwater levels decline and low flow frequencies are discussed (answering RQ3). Projections of where and when groundwater gets unattainable for users

and where and when river low flows are no longer sustained are given (answering RQ4). Also, the increase in pumping costs due to declining groundwater levels are estimated.

Chapter 6 summarizes and reflects on the main results and findings of the performed research. An outlook to future research is given.

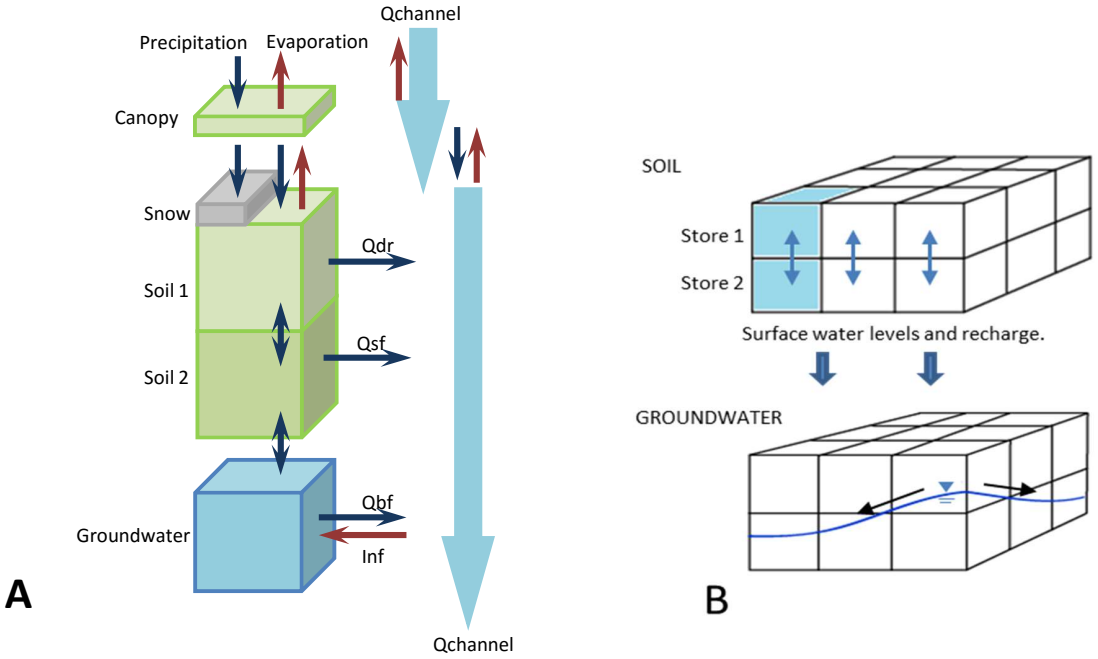

Fig. 1.2: A) Schematic presentation of PCR-GLOBWB; for each grid cell the water balance and fluxes are calculated. Discharge (Qchannel) is the sum of overland flow (Qdr), subsurface flow (Qsf), and groundwater baseflow (Qbf), and is routed along the drainage network. B) The groundwater store (of A) is replaced by the groundwater model, simulating groundwater heads. PCR-GLOBWB is coupled via surface water levels and recharge to the groundwater model.

Chapter 2

Dynamic attribution of global water demand to surface water and groundwater resources: Effects of abstractions and return flows on river discharges

Human water demand is increasing worldwide and the pressure on available water resources grows and sustainable exploitation of the resources is at risk. A dynamic attribution of water demand to surface water and groundwater resources is needed to mimic changes in exploitation intensity and connecting feedbacks between surface water and groundwater systems. However, current global-scale hydrological models lack the ability to do so. This study is the first to develop a dynamic allocation scheme to simulate surface water and groundwater abstractions and corresponding feedbacks, including return flows and a two-way groundwater-surface water interaction. It allows us to analyze the temporal and spatial trends of water availability affected by abstractions and return flows on the global scale. The results show that abstraction and feedbacks strongly affect water allocation over time, particularly for irrigated areas in dry climates. Also, the residence time of the water is affected (from slow groundwater to fast surface water, or vice versa), causing changes in low flow magnitudes, frequencies and timing. The dynamic representation of abstractions and feedbacks makes the model a suitable tool for assessing spatial and temporal impacts of changing global water demand on hydrology and water resources.

Previously published as: de Graaf, I.E.M., van Beek, L.P.H., Wada, Y., Bierkens, M.F.P., 2013: Dynamic attribution of global water demand to surface water and groundwater resources: effects of abstractions and return flows on river discharges, Adv. Water Resour, 64, 21-33, doi:10.1016/j.advwatres. 2013.12.002

2.1 Introduction

Global water demand increased substantially over the past decades due to growing population numbers, expanding irrigation areas and economic development. Water scarcity raises in many parts of the world (Vörösmarty et al., 2000), and an increasing number of rivers runs dry for substantial periods of the year before reaching the sea (Postel, 2000).

In regions with frequent surface water stress and large aquifer systems groundwater is often used as an additional source of freshwater to meet human water demands. In many of these regions groundwater is abstracted at rates that exceed groundwater recharge and the existing groundwater stores are depleted. The resulting drop in groundwater levels leads to a decline in groundwater base flows, what negatively affects stream flow of groundwater fed rivers, groundwater fed wetlands and ecosystems (Gleeson et al., 2010).

Previous model studies, focusing on global-scale water consumption and related effects, had to deal with the lack of information on the attribution of water demand to surface water and groundwater resources. Consequently, these studies all use different assumptions for the attribution of water demands over the available resources. Limiting ourselves to models that explicitly account for human water abstractions, examples of attribution rules are: H08 (Hanasaki et al., 2010), where surface water is preferentially abstracted, WBMplus (Wisser et al., 2008), where water from reservoirs and groundwater is preferentially abstracted, LPJmL (Rost et al., 2008), where irrigation demand is attributed to surface water and groundwater resources using temporal invariant fractions, WaterGap (Döll et al., 2012) where sector specific abstractions are calculated with temporally invariant but country-specific fractions of total water demand, and PCR-GLOBWB (Wada et al., 2011) where also sector specific gross and net abstractions are calculated, and where groundwater abstractions are constrained to reported values (from IGRAC www.un-igrac.org).

None of these attribution rules accounts for the abundance of both surface water and groundwater resources at the same time. This makes the distribution rules of these models not very robust under changes in water availability, caused by changes in climate or human water consumption. A first attempt to include such changes is done by Wada et al. (2014), and improved the previous scheme to account for feedbacks between supply and demand. In their study water demand is allocated to surface water or groundwater resources using the fraction between groundwater base flow and the long-term average river discharge. But, the used fraction does not reflect the actual change in surface water availability. Besides that, return flows are static and therefore do not affect actual water availability in surface water or groundwater resources. So further improvements of the suggested method of Wada et al. (2014) are needed.

The goal of this study was to explore a dynamic attribution scheme that is able to mimic changes in exploitation intensity of surface and groundwater. This scheme explicitly considers feedbacks that connect surface water and groundwater systems and their exploitation. More specifically, compared to previous work, the following features are added in this study: 1) the dynamic attribution of water demand to surface water and groundwater resources. based on the actual availability in the water resources; 2) changes in groundwater and surface water storages caused by abstractions and corresponding return flows are simulated at run time (full integration of the hydrological cycle); 3) a two-way interactions between surface water and groundwater by allowing drainage of groundwater to surface water bodies and infiltration of surface water to the

groundwater through riverbed infiltration. With these additions we are able to simulate adjustments of preferred water use based on changes in surface water and groundwater availability due to changes in climate or increased water consumption. Apart from the validation of the abstraction rates produced by this scheme we specifically focus on the effects of return flows on river discharge.

We used the global hydrological model PCR-GLOBWB (van Beek et al., 2011) to simulate water storages and river discharges over the period 1960-2010 (daily time step, 0.5° resolution, which is about 50 km at the equator). In this study, total water demand stems from irrigation, industry, and domestic use and defines the total abstraction if sufficient water is available. Abstractions are variably taken from surface water and groundwater resources driven by simulated water availability and are sector independent. Return flows of unconsumed abstracted water are simulated at the same time as the abstractions. Return flows are sector specific and return to a single source; those of irrigation to the groundwater, those of industry and domestic use to the surface water. In other words, return flows cause a redistribution of abstracted water over the water resources. Three model runs are used to test for the effects of abstractions and return flows on water allocation and river discharges: 1) no abstractions (NA), 2) abstractions only (AB), 3) abstractions and return flows (ABRE).

We validated the suggested dynamic allocation scheme by comparing simulated groundwater abstraction magnitudes and fractions (for the year 2000) to reported values at the global and continental scales. The impacts of abstractions on river discharges are analyzed, focusing on changes in low flow magnitudes, frequencies and timing. We focus the analysis specifically on low flows, as the contribution of groundwater base flows in biggest then and help to sustain river discharges during times of droughts. We provide past trends of groundwater and surface water abstraction (over the period 1960-2010). These trends show temporal changes in abstraction intensity under the influence of feedback mechanisms.

2.2 Methods

2.2.1 Hydrological model

We use the global hydrological model PCR-GLOBWB (van Beek et al., 2011) to simulate water storages and fluxes of the terrestrial part (excluding Greenland and Antarctica) of the hydrological cycle for the period 1960-2010. A schematic representation of the model is given in Figure 2.1. A summarized description of the model is given here, for a more detailed description we refer to (van Beek et al., 2011).

PCR-GLOBWB is a grid-based hydrological model (here 0.5° grid resolution globally) that operates at a daily time step. Each grid cell contains surface water elements and a vertically structured representation of the canopy, two soil layers, and an underlying

groundwater reservoir. For each time step and each grid cell the water balance of the soil columns and groundwater layer is calculated.

Sub-grid variability is used to represent fractions of different vegetation (i.e. short and tall), saturated soil (to quantify surface runoff and lateral outflow from the unsaturated zone), and surface water (i.e. lakes, reservoirs, wetlands, floodplains). Precipitation can be stored as canopy interception or as snow when temperatures are below 0°C. Through-fall and meltwater are passed to the upper soil layer. Actual evapotranspiration is calculated from potential evaporation and soil moisture conditions. Vertical exchange between the soil and groundwater layers occurs by percolation and capillary rise. Drainage from the soil column to the river network takes place as overland flow, subsurface flow from the two soil layers, and base flow from the groundwater reservoir. This last reservoir is parameterized based on lithology (Dürr et al., 2005) and topography, and is represented as a linear reservoir model (Kraaijenhof van der Leur, 1958).

The combined runoff is accumulated and routed as river discharge along the drainage network based on DDM30 (Döll & Lehner, 2002) using a kinematic wave approximation on a sub-daily time scale. Open water evaporation, water storage in lakes, and attenuation by floodplains and wetlands are taken into account within the routing scheme. Reservoirs are located on the river network based on GLWD1 (Lehner & Döll, 2004). Reservoir storage and release are dynamically calculated by evaluation of the downstream water demand. This encompasses all blue water demand within an area 600 km downstream of the reservoir outlet (approximately a week with an average discharge velocity of 1 ms^{-1}). When more than one reservoir is present directly upstream, demand is partitioned proportionally to reservoir capacity.

PCR-GLOBWB was forced with daily fields of precipitation, temperature, and reference potential evapotranspiration over the period 1960-2010. For the period 1960-2000 precipitation and air temperature were prescribed by the CRU TS 2.1 monthly dataset (Mitchell & Jones, 2005; **?**), which was downscaled to daily fields by using the ERA-40 reanalysis (**?**). For the period 2000-2010 climate data were retrieved for the ERA-Interim (Dee et al., 2011) reanalysis. Reference potential evapotranspiration was calculated using the Penman-Monteith equation according to FAO guidelines (Allen et al., 1998). For the period 1960-2000 radiation and wind speed were prescribed by CRU CLIM 1.0 climatology data (New et al., 2002). For compatibility, data from ERA-Interim (precipitation, temperature, potential evaporation) was bias-corrected by scaling the long-term monthly means of these fields to the CRU TS 2.1 dataset over the overlapping period (1979-2001).

2.2.2 Water Demand

Throughout the paper total water demand is used to denote the water requirements for three sectors: 1) irrigation, 2) industry, and 3) households. It denotes potential water

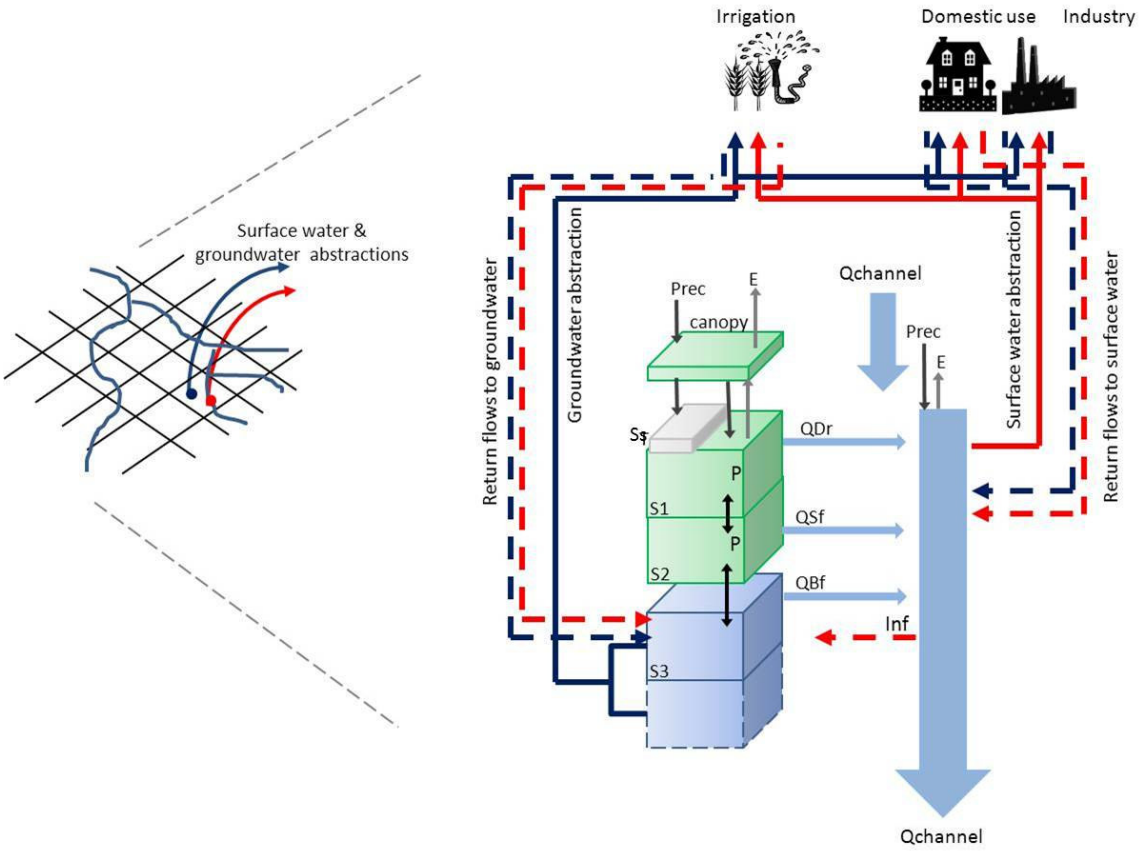

Fig. 2.1: The model concept of PCR-GLOBWB and used allocation scheme. Middle part: the soil compartment, divided into two soil layers (S1 and S2) and one linear groundwater reservoir (S3). Precipitation (Prec) falls as rain or snow (temperature dependent) and can be stored in canopy or as snow accumulation (Ss). Vertical transport within the soil column appears from percolation or capillarity rise (P). The total local gains from all cells, i.e. drainage (QDr), subsurface flow (QSf), and baseflow (Qbf), are routed along the drainage direction to yield the channel discharge (Qchannel). In every grid cell water can be abstracted from surface water or groundwater. Return flows go to surface water or groundwater, dependent on the water use.

withdrawal, i.e. the water that would be abstracted if sufficient water were available (gross water demand).

Sectoral water demand data for the model period were adopted from the previous study of Wada et al. (2011). To overcome the lack of available spatially explicit data, sectoral water demands were estimated using country statistics on the extent of irrigated areas and population numbers downscaled to 0.5° resolution. To approximate economic development over the period 1960-2010 data of Gross Domestic Product (GDP), electricity produced, and household consumption were used.

Industrial demand is kept constant over the year. Domestic demand reflects seasonal variability according to air temperature fluctuations. Water recycling ratios for industry

and domestic use are adopted from (Wada et al., 2011) and were calculated per country, on the basis of GDP and the level of economic development, i.e. high income (80%), middle income (65%), and low income (40%) economies.

Irrigation water demand is calculated assuming optimal crop growth (i.e. maximum crop transpiration), and taking into account bare soil evaporation and soil water availability. The bare soil evaporation is simulated in PCR-GLOBWB as actual transpiration from the unsaturated zone (S1 and S2 in Figure 2.1). Losses during abstraction and transport are calculated by multiplying the required irrigation water demand with a country specific efficiency factor taken from Rohwer et al. (2007). Irrigation water demand is increased with 10-40% upon implementing this efficiency factor. Evaporation losses during application are not accounted for in the estimation of irrigation water demand. Domestic irrigation (e.g., gardens) is not considered, as it is small compared to crop irrigation water demand.

2.2.3 Water abstractions and feedbacks

Total water demand can be met from three resources: 1) surface water, 2) groundwater, and 3) desalinated water. Although global desalinated water use is very small (0.2% of global water abstractions (FAO, 2010)) it can be an important resource of water locally (e.g. Middle East). Country scale data of desalinated water use are taken from FAO AQUASTAT (FAO, 2010), and downscaled onto a coastal ribbon (around 40 km) based on gridded population intensities (Wada et al., 2011). Desalinated water use is assumed to be constant over the year and subtracted from the total water demand, as it is assumed to be consumed entirely.

The remaining water demand is dynamically attributed to surface water and groundwater resources, depending on simulated water availability in the resources. Return flows (i.e. unconsumed abstracted water) and riverbed infiltration affect water availability and are simulated at the same time as the abstractions and are included at runtime in the hydrological model. The developed allocation scheme is illustrated by the outer arrows of Figure 2.1. In every grid cell, total water abstractions are variably, and sector-independent taken from surface water and groundwater resources. Sector-independent abstractions means that irrigation, industrial, and domestic demands can be satisfied both from surface water or groundwater resources. Local preferences are not accounted for. Return flows contribute to a single source (surface water or groundwater) and are sector dependent, thereby redistributing abstracted water over groundwater and surface water resources. The redistribution of water causes a shift from the fast surface water to the slower groundwater, or vice versa, and affects (long-term) local and downstream water availability and residence times.

A first estimate of surface water and groundwater abstractions is obtained by allocating total water demand to groundwater and surface water resources using the ratio two-year running-averages of local baseflow (Q_{Bf}) over upstream accumulated discharge (Q

$_{channel}$). This ratio is variable over time reflecting the dynamics of water availability in the surface water and groundwater resources. A main advantage of this allocation is that these abstraction estimates are not dependent on data. It is estimated that close to the main river branches the ratio of Q_{Bf} over $Q_{channel}$ is small and potentially more surface water is abstracted than groundwater. Further from the main river branches, the ratio is larger and potentially more groundwater is abstracted than surface water. The two-year running-average is used to smoothen out one-year fluctuations, e.g. a dry year between two wet years, and to highlights longer-term trends. It is used based on the assumption that more structural water management actions (e.g. infrastructure) are taken when water shortage last at least two years. Total water demand is divided over the grid-cell, WD_{tot} [L], and potential surface water and groundwater abstractions (GWA_{pot} and SWA_{pot} [L]) are calculated as:

$$GWA_{pot} = (\overline{Q_{Bf}}/\overline{Q_{channel}}) \times WD_{tot} \tag{2.1}$$

$$SWA_{pot} = (1 - \overline{Q_{Bf}}/\overline{Q_{channel}}) \times WD_{tot} \tag{2.2}$$

Additionally, SWA is limited by an environmental flow condition, in this study defined as the 90th percentile of the 7-day running averaged low flow of the no-abstraction scenario (Q90NA) over the period 1960-2010. Surface water abstraction (SWA) is simulated by evaluating potential surface water abstraction against simulated daily surface water availability (routed along drainage network). When river discharge gets below the Q90NA, surface water abstractions dwindles.

Simulated surface water availability is negatively affected by abstractions and losses through riverbed infiltration (Inf), but equally positively affected by groundwater discharge and return flows from surface water and groundwater abstractions for industry and domestic use (SW_{retID} and GW_{retID} respectively). Groundwater abstraction possibly results in riverbed infiltration. To avoid simulating extremely large riverbed infiltration over hydrologically inactive groundwater reservoirs, we limit riverbed infiltration to areas where under the no abstractions scenario base flow is present. For these areas riverbed infiltration occurs whenever groundwater abstractions exceed base flows. Riverbed infiltration is parameterized with saturated conductivity of the underlying sediments or bedrock (based on Dürr et al., 2005). Most likely this leads to an overestimation because the resistance of bottom sediments is not accounted for; however infiltration is small compared to aquifer size.

The actual change in surface water storage (Q_{loc}) for the present step in the sub-loop due to local fluxes is calculated as:

$$Q_{loc} = Q_{in} - SWA - Inf + SW_{retID} + GW_{retID} \tag{2.3}$$

Where Q_{in} is inflow from baseflow and specific runoff (all in L^3T^{-1}). River discharge

($Q_{channel}$ L^3T^{-1}) is calculated from Q_{loc} using the kinematic wave approximation.

If the available surface water is insufficient to satisfy the potential surface water abstraction, the deficit is abstracted from the groundwater. In this study groundwater can be abstracted from two types of resources: 1) renewable groundwater and 2) non-renewable or non-local water. Renewable groundwater is water stored in the groundwater reservoir (S3 in Figure 2.1) and is naturally or artificially recharged. In this study non- renewable groundwater or non-local water is assumed to be an additional unlimited source of water, abstracted when insufficient renewable groundwater is available.

Renewable groundwater abstraction (GWA_{renw}) is simulated by evaluating total GWA_{pot} (sum of GWA_{pot} and surface water deficit) against available groundwater (stored in S3) and recharge (both natural (R) and artificial recharge, the latter stemming from irrigation return flow in case of the ABRE scenario). Irrigation return flows from surface water or groundwater abstractions (SW_{retIRR} and GW_{retIRR} respectively) are simplified for the modeling purpose, and directly recharge to the groundwater. Evaporation losses during application are therefore not accounted for in the simulation of irrigation return flows. This results in an overestimation of irrigation return flow, however it is expected to be small compared to the abstracted irrigation water. Groundwater storage [L] is calculated as:

$$S3_t = S3_{t-\Delta t} + (R3 - GWA_{tot} + Inf + GW_{retIRR} + SW_{retIRR})\Delta t \tag{2.4}$$

When $S3_t$ is positive, all groundwater abstractions are renewable. When S3 becomes negative, part of the groundwater demand is abstracted from non-renewable or non-local water resources. As little to no data is available on the actual availability of non-renewable or non-local water, this resource is assumed to be a virtual unlimited groundwater source, calculated as negative groundwater storage in the model. When non-renewable groundwater or non-local water is abstracted, natural and artificial recharge is still available for GWA_{renw}. After a period of non-renewable groundwater or non-local water abstractions, negative groundwater storage recovers when total recharge becomes larger than GWA_{tot}. Renewable groundwater abstractions [L] are then calculated as:

$$If\ S3_t > 0 : GWA_{renw} = min(GWA_{tot}, S3_t/\Delta t) \tag{2.5}$$

$$If\ S3_t \leq 0 : GWA_{renw} = min(GWA_{tot}, R3 + GW_{retIRR} + SW_{retIRR}) \tag{2.6}$$

Non-renewable groundwater or non-local water (NRGNLW) abstraction is then calculated as [L]:

$$NRGNLW = GWA_{tot} - GWA_{renw} \tag{2.7}$$

2.2.4 Runs and analysis

Three model runs were formulated: no abstractions (NA), abstractions (AB), and abstractions and return flows (ABRE). In the AB and ABRE runs, total water demand did not change. Contrary to AB, in the ABRE case additional water becomes available for reuse by return flows, where in the AB case return flows are treated as losses to the system. However, for industrial and domestic water net surface water abstraction rates are applied for both cases, as surface water to surface water return flows are implicitly included. Net irrigation water abstractions are for ABRE smaller than for AB.

To gain confidence in the proposed water allocation scheme, first simulated groundwater abstraction magnitudes and groundwater fractions of the total abstracted water are validated against reported data per country from the FAO AQUASTAT database (FAO, 2010). The FAO AQUASTAT database reports water statistics at country level with emphasis on irrigation and agricultural water use. Not for all countries the data are coherent and reliable, due to the fact that national statistics are not available and water demands had to be estimated (FAO, 2010). Simulated groundwater abstraction magnitudes are also validated for the USA against reported data from the USGS database (www.usgs.gov). Results are compared in the same way to the previous study of Wada et al. (2012) where reported groundwater abstraction data from IGRAC (www.un-igrac.org) were used to condition groundwater abstractions.

Second, similar to van Beek et al. (2011), minimal monthly river discharges over the model period reported for 2219 stations from the GRDC long-term dataset were compared to simulated minimal monthly discharges for the three model runs. This discharge comparison shows how accurate minimal monthly flows are simulated under the condition of abstractions and return flows. The effects of abstractions and return flows on water availability are analyzed by looking at river discharges globally. We focus especially on the effects on low flows, as the contribution of baseflow is largest then. In addition, we studied in more detail four selected major rivers, that differ in term of climatic region, dominant type of abstraction (groundwater vs surface water), and dominant water use sector; 1) the Rhine and 2) Danube, where industrial and domestic water use are dominant, 3) the Mississippi, with irrigation, industrial and domestic water use, and 4) the Indus, with predominantly irrigation. For these rivers flow duration curves (FDCs) of 7-day averaged discharges and hydrographs over the period 1994-2001 are compared for the three model runs. For an extensive validation of PCR-GLOBWB for these and many other major rivers we refer to van Beek et al. (2011).

2.3 Results

2.3.1 Model validation

Reported FAO AQUATAT data is compared against simulated groundwater abstractions magnitudes and fractions for the AB and ABRE runs per country for the year 2000 (upper two scatter Figure 2.2). Simulated abstractions on 0.5° resolution were

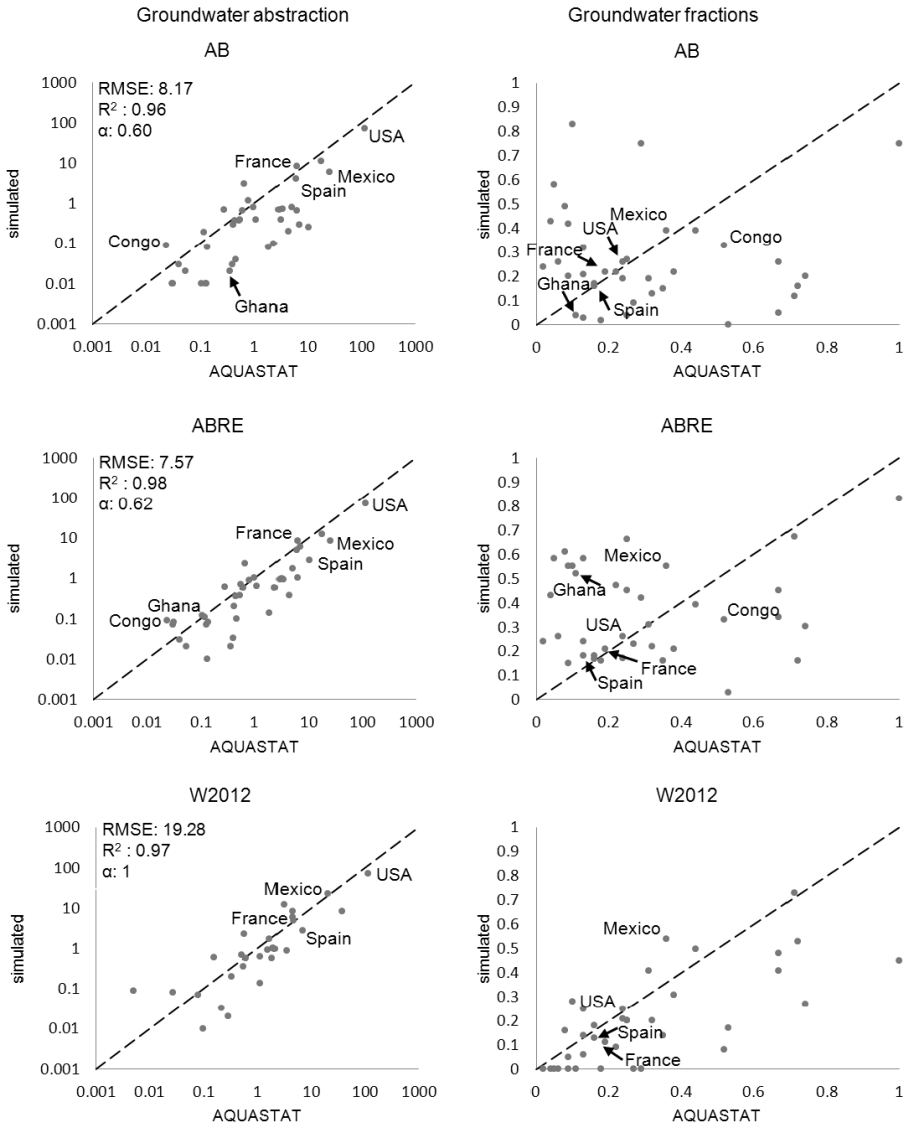

Fig. 2.2: Continental scale validation of simulated (gross) groundwater abstraction rates, of AB, ABRE, and W2012, to reported AQUASTAT data ($10^6 m^3 y^{-1}$) and groundwater fractions (-). Root Mean Square Error, coefficient of determination (R^2) and regression coefficient (α) are given.

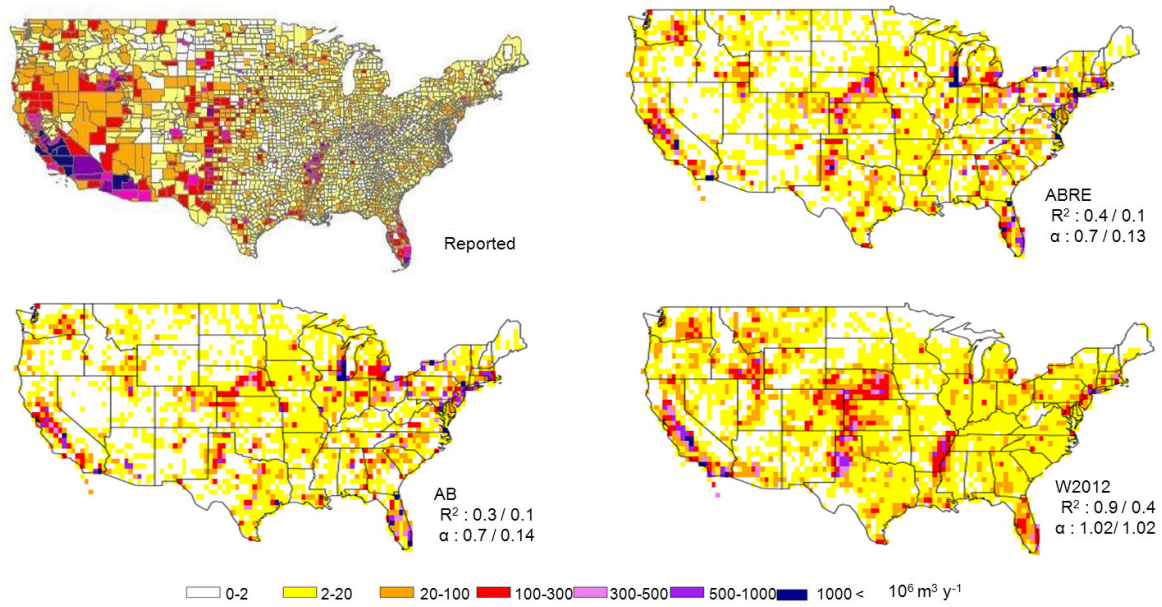

Fig. 2.3: Groundwater abstractions rates in the conterminous USA (10^6 m^3y^{-1}) for the year 2000. Reported data by U.S. Geological Survey (www.usgs.gov) per county, compared with simulated abstractions, without return flows (AB), simulated abstractions, including return flows (ABRE), and simulated abstractions of the previous study of W2012. Statistics of the validation are given: coefficient of determination (R^2), and regression (α) (state / county scale).

aggregated to country scale. In the lower scatters simulated results are compared with the previous study of Wada et al. (2012) (from now on called W2012) also per country for the year 2000.

Results show larger abstractions are better estimated than smaller abstractions (e.g. USA, Mexico, Spain, France), as seen from the smaller scatter for larger abstractions (closer to the 1:1 line). Estimates of ABRE are slightly, but not significantly, better than for AB. The coefficient-of-determination (R^2) for AB and ABRE is respectively 0.96 and 0.98, however regression coefficient (α) is 0.6 and 0.62. The simulated values of W2012 are similar to the FAO AQUASTAT data (close to 1:1 line), R^2 is 0.97 and α is 1.

The difference in model accuracy between this study and W2012 is explained by difference in model approach. In this study additional model uncertainties arise from the fact that demand is allocated purely based simulated base flow and channel flow. In W2012 groundwater abstractions are constrained to reported data from IGRAC, which are comparable to the FAO AQUASTAT data.

The Root Mean Square Errors calculated for AB, ABRE, and W2012 are respectively 8.12, 7.57, and 19.28 (all x $10^6 m^3y^{-1}$). This shows estimates of ABRE are better than AB and both are better than W2012. Better estimates are mainly caused by countries

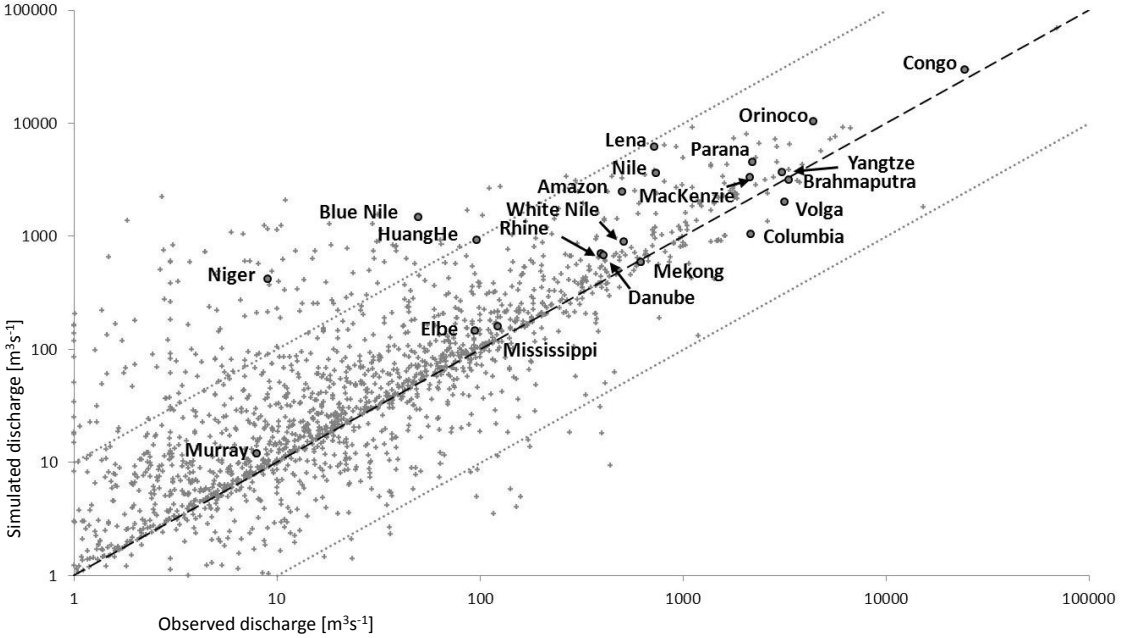

Fig. 2.4: Observed versus simulated minimal river discharges of ABRE run, for 2219 stations of the long-term GRDC dataset and 21 selected large river basins. The solid line represents 1:1 line, the dashed lines indicate bound values differing by less than order of magnitude.

with low abstraction rates that are simulated in this study but not included in the IGRAC database (Figure 2.2). Most of these low abstraction magnitudes are found for in countries with low economic development (e.g. Ghana, Congo). For these countries R^2's of AB, ABRE, and W2012, are 0.8, 0.9, and 0.5 respectively with α being 0.6, 0.8, and 0.3. Here, model uncertainties of W2012 are large due to differences in reported data between the two datasets, while AB and ABRE results are not dependent on reported abstraction data. Still groundwater abstractions are underestimated with AB and ABRE, possibly from lack of including user or sector specific preferences, e.g. the use of clean groundwater above polluted surface water.

The plots of simulated and observed groundwater abstraction fractions show a large scatter, partly explained by the scatter in groundwater abstractions magnitudes. Due to the nature of ratio calculations a limited mismatch in magnitude results automatically in larger scatter for the groundwater fraction. Again the scatter is smaller for ABRE than for AB and best for W2012. For countries with relative large groundwater abstractions ($\pm \geq 100$ km^{3}y^{-1}), and dominantly industrial and domestic use, simulated fractions correspond well with reported fractions (e.g. USA, France). For some irrigation dominant countries, groundwater fractions are highly overestimated (e.g. Spain). This may be explained by the overestimation of irrigation return flow magnitudes that directly recharge the groundwater without accounting for distribution and application. This also explains the fact that this is largest for ABRE.

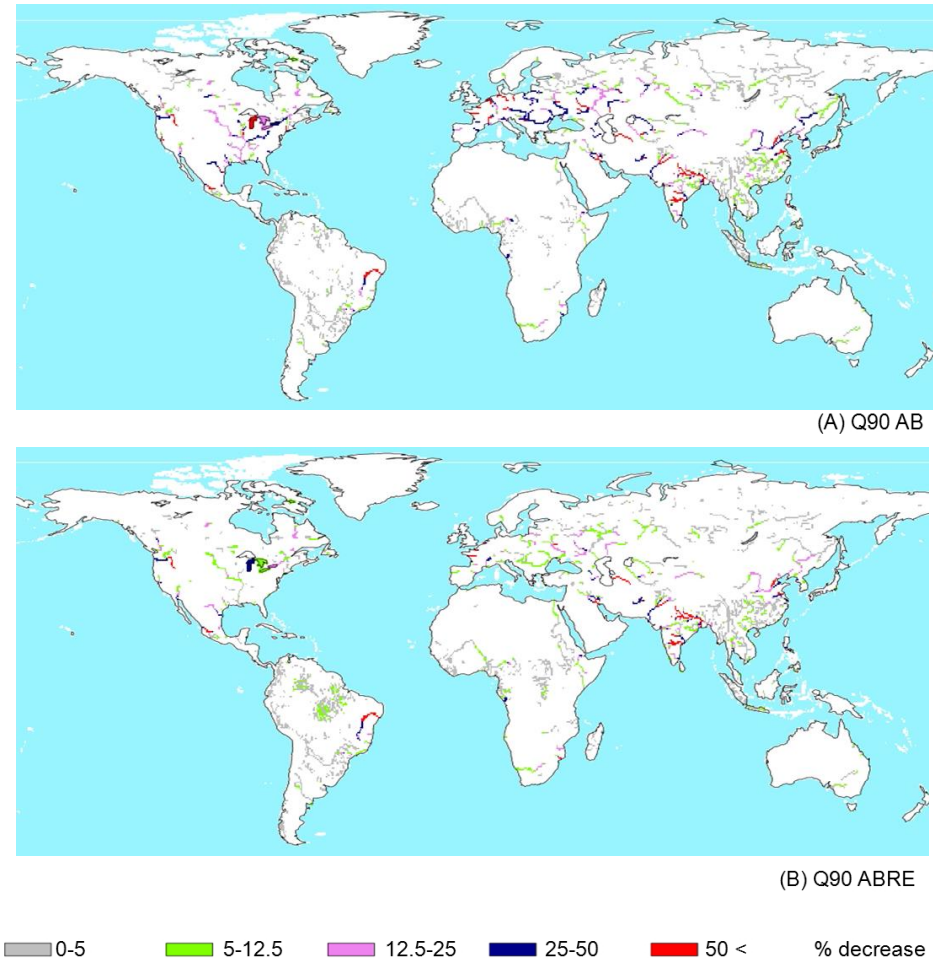

Fig. 2.5: Relative change in magnitude of low flow (7-day-Q90) compared to the no-abstraction (NA) situation caused by (A) abstractions (AB) and (B) abstractions and returnflows (ABRE)

For the USA groundwater abstraction magnitudes were validated at two spatial scales; at state level and at county level (Figure 2.3). The simulated spatial pattern of estimated groundwater abstraction correspond well with the reported map. Large groundwater abstraction rates are e.g. simulated for the Ogallala Aquifer, Central valley aquifer, Florida, and the Columbia Plateau basaltic rock aquifer. However, R^2 for both scales is low (≤ 0.5) and decreases with higher resolution. For W2012 at state level R^2 is 0.9, however at county scale R^2 is ≤ 0.5. At state level, α for this study equals 0.7 and decreases with smaller scale, for W2012 α is 1.02 and does not change. At the finer resolution model uncertainties increase for both model approaches. First, because a significant part of the counties is smaller than the used 0.5° grid cells. For counties larger or equal to the grid cell resolution all three model approaches showed better estimates compared with the reported data. For ABRE and AB R^2 is still low, 0.2 and 0.1 respectively, however α increased to 0.6 and 0.62 respectively, meaning that the underestimation of groundwater abstraction is smaller for larger counties. For W2012 for the

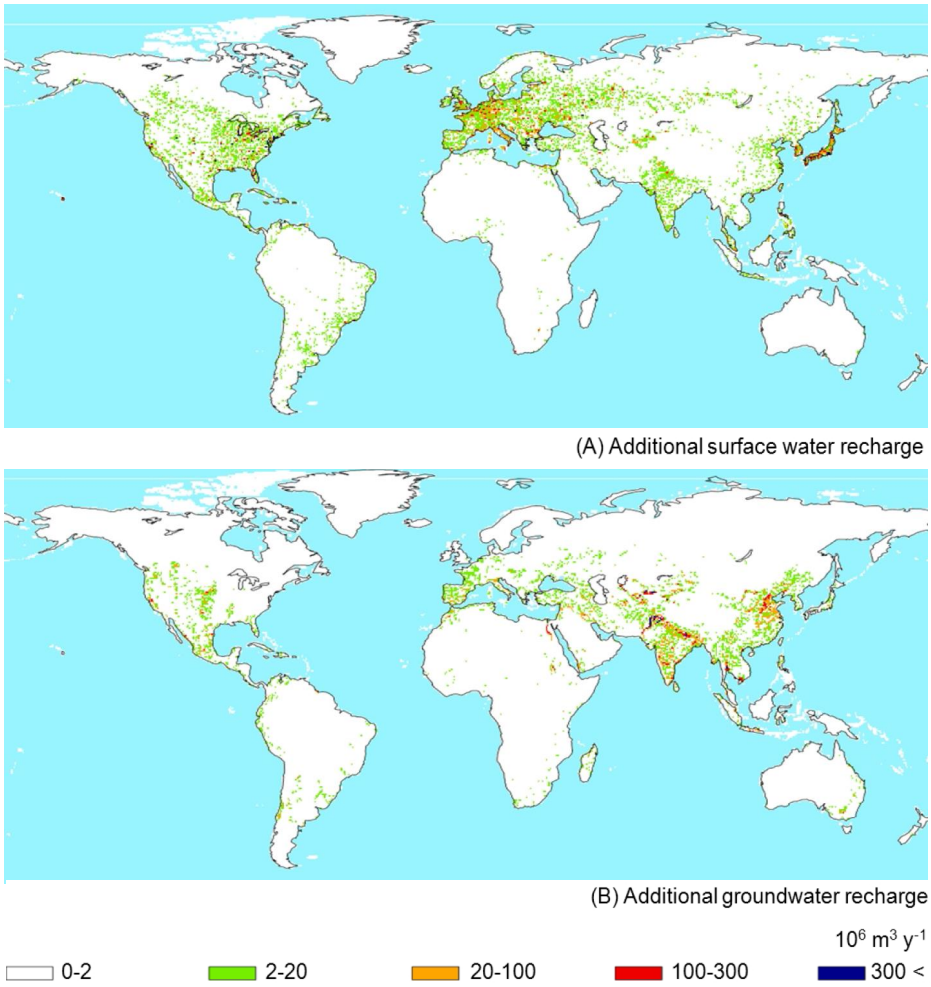

Fig. 2.6: Simulated additional return flows ($10^6 m^3 y^{-1}$), for the year 2000: (A) surface water return flows from industrial and domestic groundwater abstractions and (B) groundwater return flows from surface water irrigation.

larger counties R^2 remains 0.4 and α is 0.94. Second, for this study, specific local preferences for surface water or groundwater abstractions are not averaged out at smaller scales and deviations from global-scale datasets of water demand are likely to be larger. From Figure 2.3 it follows that in general groundwater abstractions for large irrigation areas in the USA (e.g. High Plains, Mississippi embayment) are underestimated by our method. This is explained by the fact that, due to the low model resolution (0.5°), simulated river discharges will be higher than simulated river discharges on higher resolution (Haddeland et al., 2002). Consequently, surface water is ubiquitously available for irrigation in most of the cells, and is abstracted instead of groundwater. Groundwater abstractions are overestimated for the Great Lake regions (Wisconsin, Illinois, Michigan), where industries rely on surface water rather than on groundwater. However, this is not captured by the model due to the inability of the model scheme to abstract standing water from lakes. Again these estimates would be better when sector-specific

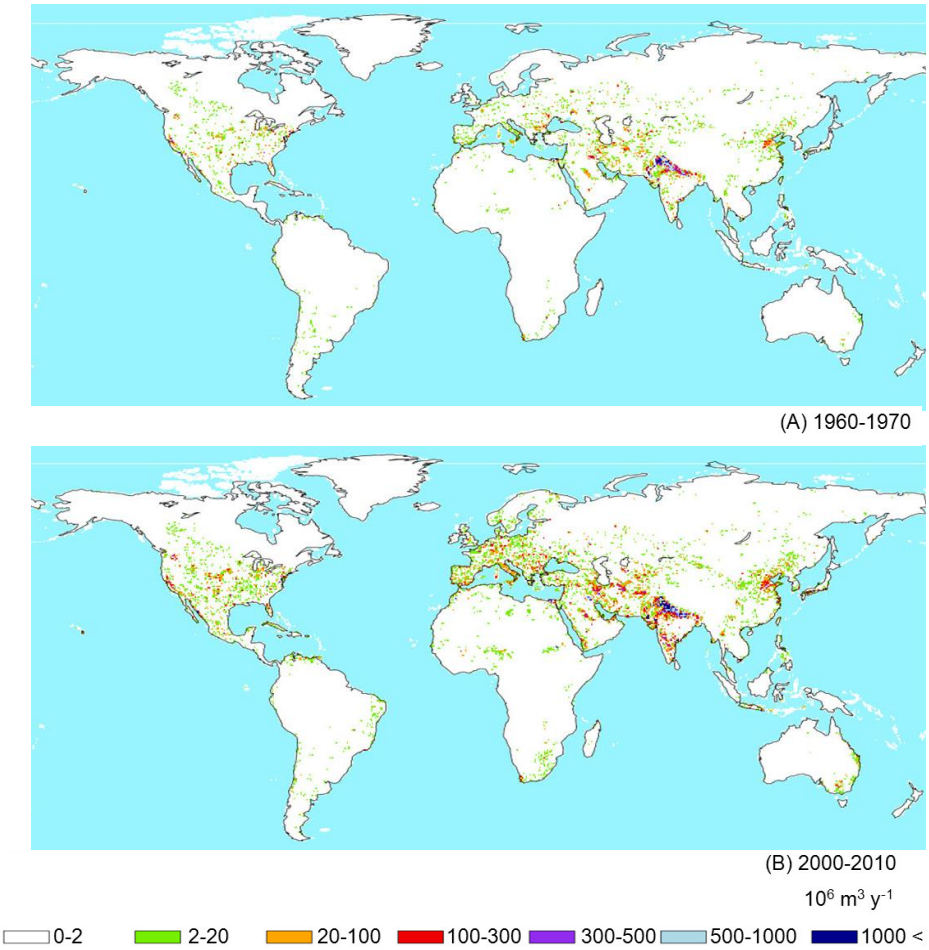

Fig. 2.7: Simulated average yearly non-renewable, or non-local water abstractions ($10^6 m^3 y^{-1}$), accounting for return flows, over the periods (A) 1960-1970 and (B) 2000-2010.

preferences were accounted for.

Observed and simulated (ABRE run) minimum monthly discharge are compared over the model period for 2219 GRDC stations (Figure 2.4). Differences between the three runs are small, all coefficients-of-determination (R^2) were high (for AB and ABRE 0.9, for NA 0.8), although the scatter is large. It is already known from van van Beek et al. (2011) that the model has the tendency to overestimate extreme discharges, especially minimum flows. Regression coefficients (α) are 1.07, 1.03, and 0.8 for AB, ABRE, and NA respectively. Also the abstraction scheme used in this study does not regard reducing abstraction rates when approaching environmental flow conditions, or poor infrastructure when river discharges decrease. From the figure it can also be concluded that the spread around the 1:1 line decreases when the basin area increases and more runoff is accumulated. The 21 indicated stations still show this overestimation (alpha for ABRE 1.25), but the data points center more around the 1:1 line, especially for the larger basins. The R^2 for these 21 stations is 0.91 for ABRE (0.88 and 0.86 for AB and NA

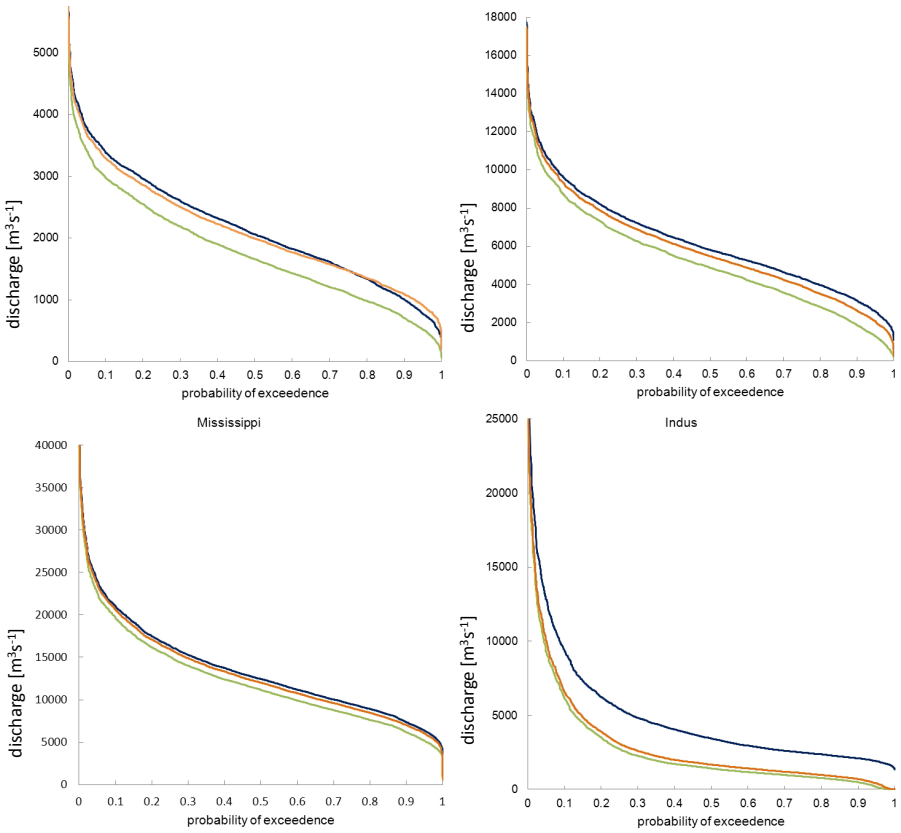

Fig. 2.8: Seven day averaged flow duration curves of the four selected rivers for the different model runs, no abstractions (NA in blue), abstractions (AB in green), and abstractions and return flows (ABRE in oragne). (River name, and GRDC station number): Rhine 6335020, Mississippi 4127800, Danube 6742900, Indus 2335950

respectively with α's 1.26 and 1.23). For rivers in intensively irrigated basins (e.g. Nile, Huang He) minimum river discharges were significantly better estimated compared with the NA run. The better estimated minimum river discharges are the result of surface, directly affecting river discharge, and groundwater abstractions, resulting in lower base flows to the river channel. The difference for basins in dominated industrial rivers are also significant, e.g for the Rhine and Danube, where large magnitudes of surface water and groundwater are abstracted.

2.3.2 Effect of water abstractions on river discharges

Figure 2.5 shows the relative decrease in magnitude of averaged 7-day low flows after abstractions and after including return flows compared to the scenario without water use. Water use upstream affects water availability locally and downstream, as local runoff is routed along the drainage network. Surface water abstractions and return flows to the surface water affect river discharges directly. Groundwater abstractions

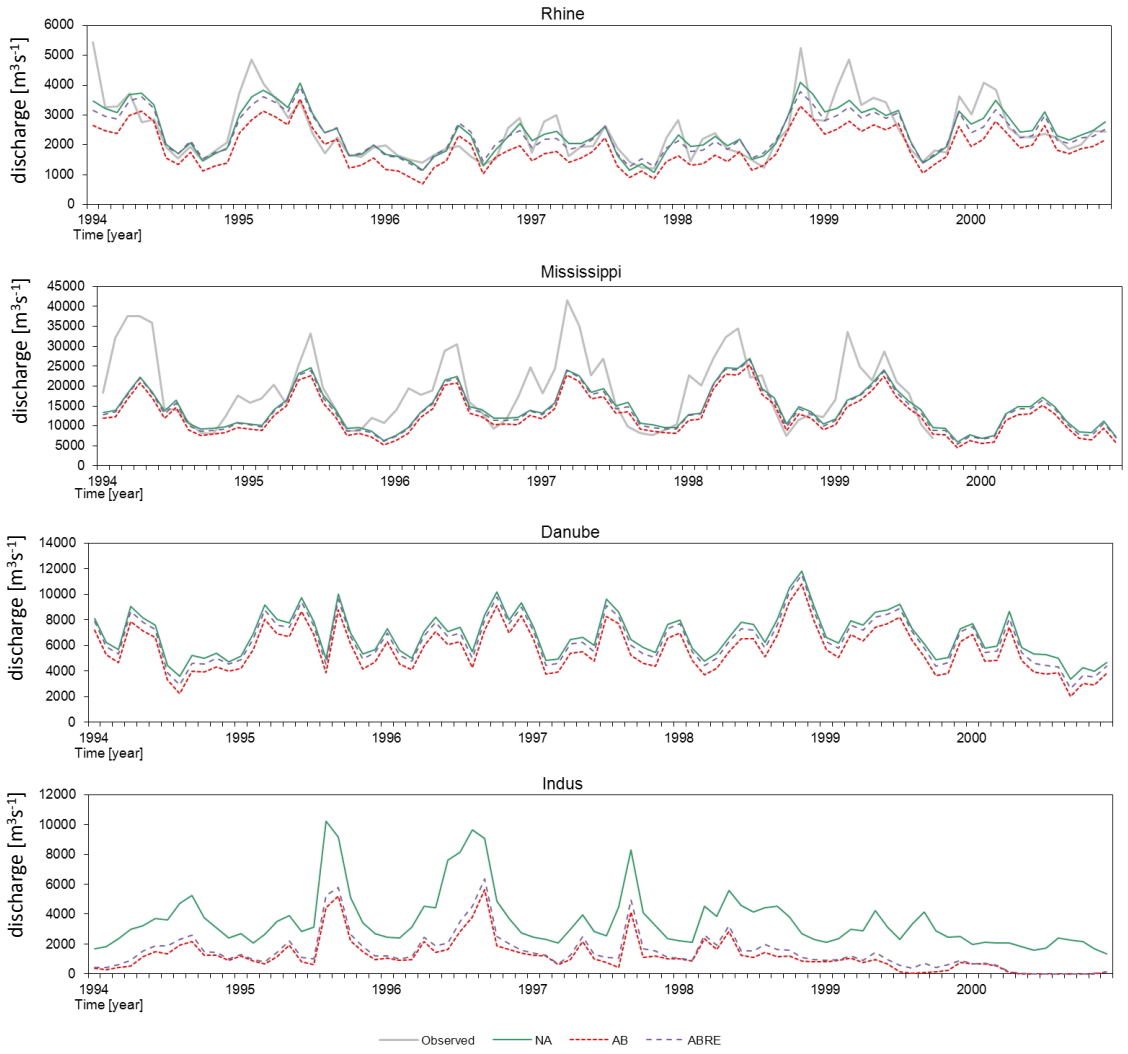

Fig. 2.9: Hydrographs of monthly discharge over the period 1994-2000 for the four selected rivers. For the Danube and Indus no GRDC observations over the given period were available. (River name, GRDC station number).: Rhine 6335020, Mississippi 4127800, Danube 6742900, Indus 2335950

and return flows to the groundwater influence groundwater storage and river discharges through changes in baseflows. The impact is largest during low flows when the baseflow contribution is dominant.

Many rivers across the world show a decrease in low flow magnitude due to abstractions (Figure 2.5A), while the effect of return flows differs, depending on the dominant sector (Figure 2.5B). For areas where industrial use is dominant (e.g.USA, Europe) the impact of return flows is largest, as the largest part of the abstracted water flows back to surface waters raising low flows. This results in higher low flows and thus higher surface

water availability. For example, the decrease of low flow after abstractions is between 25-50% for the Danube, upstream Mississippi, and downstream Rhine (Figure 2.5A). Including return flows largely minimizes the effects of abstractions, e.g. for the Danube the decrease is 5-12.5%, downstream Mississippi 0-5% (Figure 2.5 B). For e.g. the Rhine and Elbe low flows even increase (Figure 2.5B) as a result of additional return flows from groundwater abstractions by industry (Figure 2.6A). The effect is that groundwater discharge, that would otherwise occur later, is bypassed by abstraction and return flow to the surface water. As such, it increases low flows at the expense of discharge later on in time.

For irrigated basins, e.g. the Indus, Ganges, Yellow River, the effects of abstractions are large. Low flows for the downstream Indus decrease with 25-50%, for the Ganges more than 50%, and for the Yellow River between 12.5-25% and 25-50% (Figure 2.5A). The effect of return flows is not significant. For the Indus and Ganges the effect is minimal, while for the Yellow River low flow decreases 12.5-25%, both up- and downstream (Figure 2.5B). However, for these intensively irrigated basins, additional irrigation return flow to the groundwater is large, as can be seen from Figure 2.6B. For these basins, the additional groundwater recharge from surface water abstractions does not lead to an increase of base flow, but the availability of renewable groundwater is increased and the allocation of water demand changes. As a result, less non-renewable groundwater or non-local water will be abstracted for ABRE, compared to AB. Figure 2.7 shows the spatial and temporal development of nonrenewable groundwater or nonlocal water for ABRE. Hotspots are present over well-known intensively irrigated areas (see e.g. Wada et al. (2010)); India, Pakistan, China, Saudi-Arabia, USA, Mexico.

For the four selected rivers Flow Duration Curves (FDCs) and hydrographs are plotted for GRDC-stations closest to the river outlet (Figure 2.8 and Figure 2.9). All FDCs of the AB-run show a decrease in low flows. However, the effects of including return flows are different between rivers. For the Rhine and the Mississippi, additional return flows from surface water irrigation (Figure 2.7B) increase the contribution of base flow during low flows (flatter FDC for ABRE than for AB). For the Danube the negative effects of abstractions are clearly reduced by return flows, although base flow contribution during low flows slightly decreases (steeper FDC). Also for the Indus, return flows have a positive effect, although small.

The hydrographs indicate a similar response and additionally show changes in timing and regime. Under ABRE the Rhine shows a decrease in peak flows due to surface water abstractions and the relative small contribution of base flow to these events. For periods directly following low flows (e.g. 1996, 1997), river discharge of ABRE is higher than NA. Here, the direct recharge of abstracted groundwater for industry or domestic to the river leads to a direct increase of low flows. The same holds for the Mississippi. For the Indus, the effects of irrigation return flows are clear. Before a low flow (e.g., 1996, 1997, 1998), the base flow component is clearly higher for ABRE than for AB. Surface water used for irrigation additionally recharges the groundwater after which it contributes via baseflow to the river discharge. As a result, the timing of peak flows

and low flows changes, both for AB and ABRE (e.g. 1995, 1996 and 1996, 1997). To a smaller extent this is also found for the Danube (e.g. 1994, 1999).

2.3.3 Global trends in abstraction rates

Figure 2.10 presents global-scale trend of demand, surface water, and groundwater abstractions over the period 1960-2010 for the AB and ABRE runs (numbers are given in Table 2.1).

For both runs, the ratio of surface water abstraction to total groundwater abstractions is close to 50%. However, for ABRE more surface water is abstracted, and the relative increase in surface water abstraction in slightly larger compared to AB, 48% and 42% respectively. The figure shows that around 40% of the total abstracted water can be reused via surface water return flows.

A clear difference between the two model scenarios is found for the water allocation to renewable groundwater and non-renewable or non-local water resources. For ABRE roughly 50% of the total abstracted groundwater comes from renewable groundwater resources, for AB this is 40%. As already shown in Figure 2.6, hotspots of NRGNLW are intensively irrigated areas. Especially in these regions, return flows limit the expansion of NRGNLW areas and less groundwater depletion takes place. Our numbers on abstractions correspond well with the previous study of W2012 (Table 2.1). For the year 2000 we estimate for ABRE a total groundwater abstraction of 910 km^3y^{-1}, of which 456 km^3y^{-1} is NRGNLW. Previous studies found for example 1070 km^3y^{-1} total groundwater abstractions of which 494 km^3y^{-1} is NRGNLW (Wada et al., 2012), and 400-800 km^3y^{-1} (Vörösmarty et al., 2000) and 450 km^3y^{-1} (Pokhrel et al., 2012) for NRGNLW.

The basic assumption made in this study is that the NRGNLW reservoir is unlimited, and all water demand is satisfied. As a first attempt to limit this resource, an maximum exploitation depth of 100 m was set based on the assumption that below 100 m groundwater becomes unattainable. For the year 2000, 141 km^3y^{-1} becomes unattainable, and has to be satisfied by non-local resources or deeper aquifers. The regions where this occurs are the intensively irrigated areas. In order to simulate deep groundwater abstractions and groundwater dynamics properly, the existing model should be extended with a groundwater flow model.

2.4 Conclusion and discussion

As human water demand is increasing worldwide, it is important to simulate how water demand is potentially allocated to surface water and groundwater resources and to account for the dynamic effects of abstractions and return flows on water availability. This study is the first to develop a dynamic allocation scheme to simulate surface water

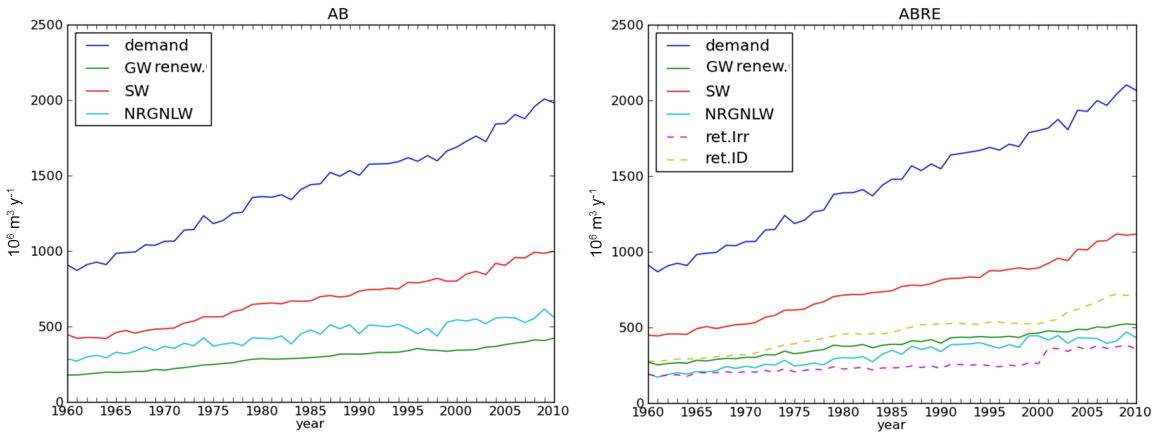

Fig. 2.10: Global trends, over the period 1960-2010 of simulated demand, abstractions, and return flows, for (a) abstractions, excluding return flows (AB) and (b) abstractions, including return flows (ABRE).

Table 2.1: Simulated global abstractions (km^3y^{-1}) of nonrenewable groundwater or nonlocal water (NRGNLW), renewable groundwater (renew.GW), and surface water (SW) for two model runs (AB and ABRE) compared with results of Wada et al. 2012.

	AB			ABRE			W2012	
	1960	2000	2010	1960	2000	2010	1960	2000
NRGNLW	285	546	561	193	446	432	171	494
renw.GW	178	344	422	271	463	517	271	582
SW	446	803	1000	450	896	1116	456	843

and groundwater abstractions and corresponding feedbacks, including return flows and a two-way groundwater- surface water interaction. It allows us to analyze the temporal and spatial trends of water availability affected by abstractions and return flows on the global scale.

In the dynamic scheme local water availability is affected by local and upstream surface water and groundwater abstractions and return flows. Return flows cause a redistribution of unconsumed water over the water resources and change residence times of the water (channel discharge, base flow). The advantage, compared to existing schemes, is that this scheme does not rely on preconceived assumptions about the preferences of surface water over groundwater abstractions or vice versa, or on fixed ratios between the two. As a result, the distribution rules of our scheme are more robust under changes in water availability caused by water consumption or climate. However, the spread in simulated water abstractions increases compared to previous schemes because of the dynamic attribution instead of the use of data or fixed fraction for surface water or groundwater abstractions. Especially for intensively irrigated regions groundwater abstractions are overestimated, caused by e.g. the overestimation of groundwater availability due to

return flows that directly recharge to the groundwater; i.e. irrigation return flows may also end up in surface water or evaporate.

Changes in river discharges and river regimes show the effects of abstractions and return flows. Largest impacts are found during low flows, when the contribution of groundwater through base flow is largest. For industrial regions, the negative effects of abstractions in terms of magnitude largely diminish when return flows are included. Up to 80% of the abstracted water flows directly back to the channel as return flow.

For irrigated regions, return flows are smaller (up to 60%) and the impact of abstractions on river discharges is larger. However, return flows do change timing and duration of low flows for these regions. By the redistribution of water, base flow is maintained longer and the timing and duration of low flows changes. Also, for these regions, due to the increase in local attainable groundwater by return flows, less non-renewable groundwater, or non-local water is abstracted. The largest impact of return flows on the temporal and spatial expansion of non- renewable groundwater or non-local water abstraction are therefore found in irrigation hotspots like India, Pakistan, and China.

Obviously large model uncertainties remain. Not only in the proposed abstraction and return flow scheme, but also the forcing as well as abstraction data. In previous studies, using the same hydrological model, uncertainties in recharge and abstractions are analyzed (Wada et al., 2010), as well as uncertainties in meteorological forcing (Wada et al., 2013). And indeed the uncertainties are considerable, although not so large that trends and variability are obscured. Uncertainties arising from the abstraction scheme can only be reduced by testing and improving the underlying assumptions with empirical evidence from local case studies.

Improvements can be expected from making the ratio of groundwater to surface water abstractions not only dependent on the availability of these resources, but also sector specific and dependent on local preferences. Likewise, increasing model resolution would lead the better estimates of abstracted water by removing scale effects such that more local preferences of groundwater to surface water abstraction and availability can be taken into account. However, this requires information about accessibility of water, e.g. available and required infrastructure, which is not an issue on 0.5° resolution. Also distance to surface water and reservoirs, between-basin water transfer as well as specific yield and groundwater depth are factors to consider.

Acknowledgements
We thank three reviewers, Huan Wu Ph.D. of the University of Maryland and two and two anonymous reviewers, for their constructive and thoughtful suggestions, which substantially helped to improve the quality of the manuscript. This study was funded by the Netherlands Organization for Scientific Research (NWO) in the project Planetary Boundaries Fresh Water Cycle .

.

Chapter 3

A high resolution global scale groundwater model

Groundwater is the world's largest accessible source of fresh water. It plays a vital role in satisfying basic needs for drinking water, agriculture and industrial activities. During times of drought groundwater sustains baseflow to rivers and wetlands, thereby supporting ecosystems. Most global scale hydrological models (GHMs) do not include a groundwater flow component, mainly due to lack of geohydrological data at the global scale. For the simulation of lateral flow and groundwater head dynamics, a realistic physical representation of the groundwater system is needed, especially for GHMs that run at finer resolutions. In this study we present a global scale groundwater model (run at 6′ resolution) using MODFLOW to construct an equilibrium water table at its natural state as the result of long-term climatic forcing. The used aquifer schematization and properties are based on available global datasets of lithology and transmissivities combined with the estimated thickness of an upper, unconfined aquifer. This model is forced with outputs from the land-surface model PCR-GLOBWB, specifically net recharge and surface water levels. A sensitivity analysis, in which the model was run with various parameter settings, showed that variation in saturated conductivity has the largest impact on the groundwater levels simulated. Validation with observed groundwater heads showed that groundwater heads are reasonably well simulated for many regions of the world, especially for sediment basins ($R^2 = 0.95$). The simulated regional scale groundwater patterns and flowpaths demonstrate the relevance of lateral groundwater flow in GHMs. Inter- basin groundwater flows can be a significant part of a basin's water budget and help to sustain river baseflows, especially during droughts. Also, water availability of larger aquifer systems can be positively affected by additional recharge from inter-basin groundwater flows.

Previously published as: de Graaf, I.E.M., E.H. Sutanudjaja, van Beek, L.P.H., Bierkens, M.F.P., 2015: A high resolution global scale groundwater model. Hydrol. Earth Syst. Sci., 19, 823-837, doi:10.5194/hess-19-823-2015

3.1 Introduction

Groundwater is a crucial part of the global water cycle. It is the world's largest accessible source of fresh water and plays a vital role in satisfying basic needs of human society. It is a primary source for drinking water and supplies water for agriculture and industrial activities (Wada et al., 2014). During times of drought stored groundwater provides a buffer against water shortage and sustains baseflow to rivers and wetlands, thereby supporting ecosystems and biodiversity. However, in many parts of the world groundwater is abstracted at rates that exceed groundwater recharge, causing groundwater levels to drop while baseflow to rivers is no longer sustained (Konikow, 2011; Gleeson et al., 2012).

In order to understand variations in recharge and human water use affect groundwater head dynamics, lateral groundwater flow and groundwater surface water interactions should be included in global scale hydrological models (GHMs), especially as these GHMs progressively move towards finer resolutions (Wood et al., 2012; Krakauer et al., 2014). Several studies (e.g. Bierkens & van den Hurk, 2007; Fan et al., 2007) have suggested that lateral groundwater flows can be important for regional climate conditions as they influence soil moisture and thus the water cycle and energy exchange between land and the lower atmosphere. Moreover, lateral groundwater flowing over catchment boundaries, i.e. inter-basin flows, can be a significant part of the water budget of a catchment, dependent on certain climate and geological conditions (Schaller & Fan, 2009). By supplementing the water budget, incomming inter-basin groundwater helps to sustain baseflows during droughts thereby increasing surface water availability for human water needs (de Graaf et al., 2013).Up to now, the current generation of GHMs typically does not include a lateral groundwater flow component mainly due to the lack of worldwide hydrogeological information (Gleeson et al., 2014). These data are available for parts of the developed world, but even there it is difficult to obtain data in a consistent manner. To cope with the unavailability of hydrogeological data Sutanudjaja et al. (2011) proposed the use of global datasets of surface lithology and elevation for aquifer parameterization. This method was tested by building a groundwater flow model for the Rhine–Meuse basin ($30''$ resolution) with promising results. Similarly, Vergnes et al. (2012) used global and European datasets to delimit the main aquifer basins for France (at 0.5 resolution) and parameterized these based on lithological information.

Recently, a pioneering study by Fan et al. (2013) presented a first ever high-resolution global groundwater table depth map. Their method however, does not include hydrogeological information such as aquifer depths and transmissivities, but uses estimates from soil data. Also, the hydraulic connection between rivers and groundwater, which is the primary mode of drainage for groundwater in humid regions, is ignored. Moreover, their model requires calibration to head observations.

In this paper we present a global-scale groundwater model of an upper aquifer which is assumed to be unconfined. For the parameterization of the aquifer properties we relied entirely on available global lithological maps (Hartmann & Moosdorf, 2012) and

databases on permeability (Gleeson et al., 2011). To overcome the lack of information about aquifer thickness worldwide, this is estimated based on extrapolation of available data from the USA. This can equally be extended to data-poor environments.

We forced the groundwater model with output from the global hydrological model PCR-GLOBWB (van Beek et al., 2011), specifically the net groundwater recharge and average surface water levels derived from routed channel discharge. This approach builds on earlier work by Sutanudjaja et al. (2011) and Sutanudjaja et al. (2014).

With this approach we were able to simulate groundwater heads of a upper unconfined aquifer, providing a first-order estimate of the spatial variability of water table heads as a function of climate and geology. In this paper we limit ourselves to a steady-state simulation as a prelude to transient simulations in forthcoming work. Also we did not yet perform a formal calibration of the model. We performed a sensitivity analysis using a Monte Carlo framework in which we ran the model with various hydrogeological parameter settings. Simulated groundwater heads from all realizations were evaluated against reported piezometer data and the parameter set with the highest coefficient of determination was used for further analysis. This resulted in a global map of average groundwater table depth in its natural state, i.e. in equilibrium with climate and without groundwater pumping. We simulated flowpaths from the location of infiltration towards the location of drainage. Flowpaths show areas where lateral groundwater flows are important and inter-basin groundwater flows are significant and contribute to water availability in neighbouring watersheds. They also provide an indication of groundwater travel times.

Hereafter follows a description of the methods, in particular the parameterization of the upper aquifer, after which results of the sensitivity analysis and validation are presented. Next, the groundwater table depth map and flowpath maps for Europe and Africa are presented. We end with conclusions and discussion.

3.2 Methods

3.2.1 General

The hydrological model of the terrestrial part of the world (excluding Greenland and Antarctica) developed in this study consists of two parts; (1) the dynamic land surface model (PCR-GLOBWB) and (2) the steady state groundwater model (MODFLOW). Both the land-surface model and groundwater model are run at $6'$ resolution (approximately 11 km at the equator). PCR-GLOBWB and MODFLOW are coupled offline where both models are run consecutively (Sutanudjaja et al., 2011).

Hydrological model

The model PCR-GLOBWB is a global hydrological model that simulates hydrological processes in and between two soil stores and one underlying linear groundwater store. For a detailed description of the model PCR-GLOBWB we refer to van Beek et al. (2011), and a summarized model description is given here. PCR-GLOBWB was run at 6′ resolution using a daily time step. Monthly climate data were taken from the CRU TS2.1 (Mitchell & Jones, 2005) with a spatial resolution of 0.5° and downscaled using the ERA-40 (Uppala et al.,2005)and ERA-Interim reanalysis (Dee et al., 2011) to obtain a daily climatic forcing (see de Graaf et al. (2013) for a more detailed description of this forcing dataset). Each grid-cell contains a land surface that is represented by a vertical structured soil column comprising two soil layers (maximum depth 0.3 m and 1.2 m respectively), an underlying groundwater reservoir, and the overlying canopy. Sub-grid variability is included with regards to land cover (in this case using fractions of short and tall vegetation), soil conditions, and topography. The model employs the improved Arno Scheme (Todini, 1996; Hagemann et al., 1999) to simulate variations in the fraction of saturated soil in order to quantify direct surface runoff. For each time step and for every grid cell the water balance of the soil column is calculated on the basis of the climatic forcing that imposes precipitation, reference-crop potential evapotranspiration, and temperature. Actual evapotranspiration is calculated from reference-crop potential evaporation, time-varying crop- factors, and soil moisture conditions. Vertical exchange between the soil and groundwater occurs through percolation and capillary rise. Specific runoff from the soil column, comprising direct surface runoff, interflow, and baseflow, is accumulated along the drainage network that consists of laterally connected surface

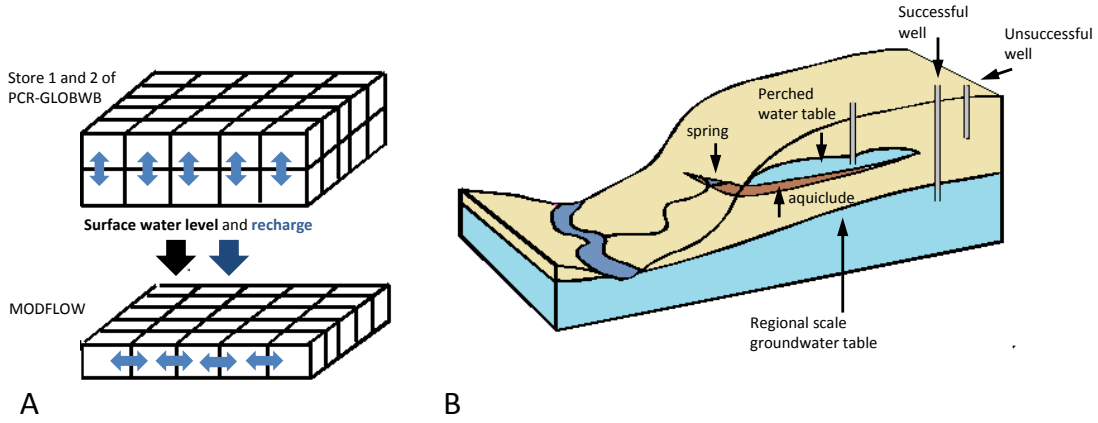

Fig. 3.1: A) Model structure used to couple the land-surface model PCR-GLOBWB with the groundwater model MODFLOW: first average annual net recharge and average annual channel discharge is calculated with PCR-GLOBWB. The latter is translated into surface water levels. Both recharge and surface water levels are used to force MODFLOW (after Sutanudjaja et al., 2011). B) Cross-section illustrating the difference between the simulated regional scale groundwater level and the perched groundwater levels that are often sampled.

water elements representing river channels, lakes or reservoirs. The accumulated runoff is routed to obtain discharge using the kinematic wave approximation of the Saint-Venant equations at a sub-daily time step. In the original version of PCR-GLOBWB no lateral groundwater flow is simulated. Groundwater flow within a cell is described as a linear store and recharge is simulated as percolation to the groundwater store, minus capillary rise from the groundwater store to the soil. However, in the current set-up, the capillary rise is disabled to force a one-way coupling from PCR- GLOBWB to MODFLOW.

Groundwater model

In this study the linear groundwater store of PCR-GLOBWB is replaced by a MODFLOW layer (McDonald & Harbaugh, 2000; Schmitz et al., 2009) simulating lateral groundwater flows and groundwater heads in a single-layer unconfined aquifer. Aquifer properties are prescribed and the MODFLOW layer is forced by outputs from PCR-GLOBWB, i.e. long-term averages of surface water levels and groundwater recharge (running period 1960-2010). Figure 3.1A illustrates the modelling strategy.

3.2.2 Estimating aquifer properties

Aquifer properties were initially based on two datasets; (1) the high resolution global lithological map (GLiM) of Hartmann & Moosdorf (2012), and (2) the global permeability estimates of Gleeson et al. (2011).

The GLiM describes 15 lithology classes (see Tabel 3.1) (similar and expanding on Dürr et al., 2005). It is assumed that the lithological map represents the geology of the shallow subsurface accurately (Hartmann & Moosdorf, 2012). For the global permeability map the lithology classes of Dürr et al. (2005) were combined to 5 hydrolithologies, representing broad lithologic categories with similar hydrogeological characteristics (Gleeson et al., 2011). In the GLiM, these hydrolithological units were subdivided further on the basis of texture in the case of unconsolidated and sedimentary rocks (Tabel 3.1). (Gleeson et al., 2011) found that for all hydrolithologies permeability is representative for larger scales and that there is no discernible additional dependence of permeability on scale, with the exception of carbonates, most likely due to karst. The resulting map shows regional scale permeability over the globe with the geometric mean permeability attributed to each hydrolithological unit. The geometric mean was obtained from calibrated permeabilities from groundwater models for units larger than 5 km in extent within 100 m depth. The polygons in the GLiM, delineating a hydrological unit, were subsequently gridded to $30''$ ($\sim$ 1 km) and aggregated as the geometric mean at $6'$ resolution.

To estimate aquifer transmissivities (kD in m^2d^{-1}), aquifer thicknesses are required. Since no globally consistent dataset on aquifer thickness is available, this was estimated

Table 3.1: Lithologic and hydrolihologic categories.

Lithologic categories[a]	Hydrolithologic categories[b]	$\log k\ \mu_{\text{geo}}\ [m^2]$[b]	$\sigma\ [m^2]$[b]	$S_y\ [m/m]$[c]
Unconsolidated sediments	unconsolidated	−13.0	2.0	0.235
	c.g. unconsolidated	−10.9	1.2	0.360
	f.g. unconsolidated	−14.0	1.8	0.110
Siliciclastic sediments	siliciclastic sedimentary	−15.2	2.5	0.055
	c.g. siliciclastic sedimentary	−12.5	0.9	0.100
	f.g. siliciclastic sedimentary	−16.5	1.7	0.010
Mixed sedimentary rocks Carbonate sedimentary rocks Evaporites	Carbonate	−11.8	1.5	0.140
Acid volcanic rocks Intermediate volcanic rocks Basic volcanic rocks	Crystalline	−14.1	1.5	0.010
Acid plutonic rocks Intermediate plutonic rocks Basic plutonc rocks pyroclastics metamorphic	Volcanic	−12.5	1.8	0.050
water bodies Ice and Glaciers	not assigned	–	–	–

[a] Hartmann & Moosdorf (2012).

[b] Based on Gleeson et al. (2011), $\log k\ \mu_{\text{geo}}$ is the geometric mean logarithmic permeability; σ is the standard deviation; f.g. and c.g. are fine-grained and coarse-grained, respectivaly.

[c] S_y is the storage coefficient, average per category.

using predominantly terrain attributes. Based on the assumption that unconfined productive aquifers coincide with sediment basins below river valleys the distinction was made between (1) mountain ranges with negligible sediment thickness, consisting mainly of hard rock with secondary permeability and (2) sediment basins with thick sediment layers, presenting aquifers.

Aquifer thicknesses were then estimated as follows:

1. Mountain ranges and sediment basins were distinguished based on the difference between surface elevation and floodplain elevation within a cell. We used elevation data at $30''$ from the HydroSHEDS dataset to determine the floodplain elevation at $6'$. First, for each $6'$ cell we identified the lowest elevation at $30''$ (maximum 144 values for a cell comprising only land area) and assigned this as the floodplain elevation for the entire cell (see Figure 3.2, top panel). Next, the difference between surface elevation, also taken from the HydroSHEDS database, and floodplain elevation at $6'$ was calculated. All cells with a floodplain elevation within $50m$ below the surface level were assumed to form a sediment basin that constitutes an unconfined and relatively permeable aquifer (Figure 3.2, top panel). These defined sediment basins included 70 % of the unconsolidated sediments mapped in the GLiM. The sediment basins consist of 56 % unconsolidated sediments, 25%

consolidated sediments and 19 % metamorphic or plutonic rocks. The latter are mainly found over the old cratons of Africa and the flat, recently glaciated areas of Laurasia.

2. By definition basins are linked to sedimentary environments in fluvial systems and deltas. Sediments are deposited perpendicular to the main gradient (constituting the transversal axis of the basin), with grain size and volumes decreasing at greater distance away from the transversal axis. Grain size also decreases along the transversal axis, distinguishing proximal (near the source of sediment) and distal parts. We assumed that gradation in grain size is captured in the GLiM but differentiation in depth is not. Instead, we used relative elevation as a measure of proximity to the river measured along the transversal axis and as an indicator of the associated depth. We standardized the relative elevation and used this to define the distribution of aquifer thickness using a log-normal distribution, assuming thickness is non-negative and positively skewed. In more detail, we used the following procedure:

   First, for each cell-location x belonging to the sediment basins a measure expressing the relative difference between land surface elevation and floodplain elevation was calculated:

$$F'(x) = 1 - \frac{F(x) - F_{\min}}{F_{\max} - F_{\min}} \tag{3.1}$$

   where $F(x)$ is the difference of surface and floodplain elevation at location x. $F_{\min}$ and $F_{\max}$ are the minimal and maximal value, corresponding to a difference between land surface and floodplain elevation of 0 and $50m$ respectively (following from the method to distinguish sediment basins from mountain ranges). This measure leads to a thinning layer further from the river towards the edge of the sediment basin (Figure 3.2 bottom panel). $F'(x)$ can be seen as the likelihood of finding a thick sedimentary aquifer at a particular location. A map of the spatial distribution of $F'(x)$ is given in the Supplementary material (Figure 6.1).

   Second, the associated z-score is then calculated as:

$$Z(x) = G^{-1}(F'(x)) \tag{3.2}$$

   where $G^{-1}()$ is the inverse of the standard normal distribution.

3. Next, statistics on the thickness of unconsolidated sediments were obtained from available regional scale groundwater studies in the USA (e.g. Central Valley California, (Faunt, 2009); Mississippi basin, (Clark & Hart, 2009).As a measure of difference between aquifer systems, for each study the average thickness was determined resulting in a range of average thickness between 50 and 500 m. We assume that the thicknesses of the delineated sediments basins correspond with the total thickness of the upper aquifer and that this thickness is log-normally

distributed. Therefore, this distribution is described using the average thickness of the ln-transformed thickness $\overline{\ln D}$. This $\overline{\ln D}$ is chosen uniform over the globe and sampled from the range of thicknesses:

$$\overline{\ln D} = U(50; 500). \tag{3.3}$$

Moreover, as a measure of variation in thickness within aquifers systems, an average coefficient of variation was determined from the same USA regional groundwater studies. The coefficient of variation of the ln-transformed thickness $Cv_{\overline{lnD}}$ was fixed when calculating the global distribution of aquifer thickness.

4. For each realization a spatial distribution of aquifer thickness is generated,assuming a log-normal distribution with random average $\overline{\ln D}$, sampled from $U(50; 500)$ with a fixed coefficient of variation $Cv_{\overline{\ln D}}$, and using the standard normal ordinate $Z(x)$ that is based on the topographical controls within each delineated basin:

$$Y(x) = \overline{\ln D}(1 + Cv_{\overline{\ln D}}Z(x))D(x) = e^{Y(x)}. \tag{3.4}$$

So in this representation $Y(x)$ and $D(x)$ are random because $\overline{\ln D}$ is random, while spatial variation is determined in $Z(x)$ reflecting the likelihood of a thick aquifer. Average aquifer thicknesses was simulated randomly from $U(50, 500)$ resulting in 100 equally likely maps of aquifer thickness. The result of the best performing run (selected after evaluation to groundwater head data) is presented in Figure 3.3.

Transmissivities were calculated using the estimated aquifer thickness. To estimate permeability at greater depth we combined the concept of exponentially decreasing permeability of the continental crust with depth (Ingebritsen & Manning, 1999) with data on near surface permeability from Gleeson et al. (2011). The permeability decline with depth is prescribed by the sediment-bedrock profile at a location, which depends strongly on terrain slope; the steeper the land, the thinner the weathered layer and the sharper the decrease in permeability with depth. This is expressed through the e-folding depth f (range and global spatial distribution of e-folding depth is given in the supplementary material, Figure 6.2 and Figure 6.4 and taken from Miguez-Macho et al. (2008)). With near surface permeability k_0 md^{-1}, from Tabel3.1 the transmissivity $T(x)$ $\mathrm{m}^2\mathrm{d}^{-1}$) over the aquifer depth $D(x)$ m) can then be calculated as:

$$T(x) = \int_0^{D(x)} k_0 e^{\frac{-z}{f}} \mathrm{d}z \tag{3.5}$$

As Eq 6. is an exponential function, permeabilities will approximate zero at greater depth.

It is assumed that conductivities are horizontally homogeneous within a hydrolithological class. The globally calculated transmissivities are presented in Figure 3.3B. Note

that for mountain ranges low permeabilities are calculated that represent the permeabilities of the bedrock, thereby neglecting weathered regolith soils with high permeabilities that develop on the more gentle slopes. As a result perched water tables that develop in these soils are not included in the simulated lateral groundwater flow (illustrated in Figure 3.1B). Instead, runoff associated with these perched water tables is taken care of in the land-surface model (PCR-GLOBWB) as stormflow or interflow from the second soil reservoir. It should be recognized that our MODFLOW model is built at $6'$ and cells thus have different lengths units. To account for this a spatially variable anisotropy factor can be introduced. We have not yet implemented this option, but will do so in future work.

3.2.3 Boundary conditions, recharge, and drainage levels

For large lakes and the ocean a Dirichlet boundary condition was used. For the ocean the groundwater head was set at $0m$, water levels of the lakes were set at elevation levels provided by the HydroSHEDS digital elevation map.

The steady-state groundwater recharge, shown in Figure 3.4 and obtained from PCR-

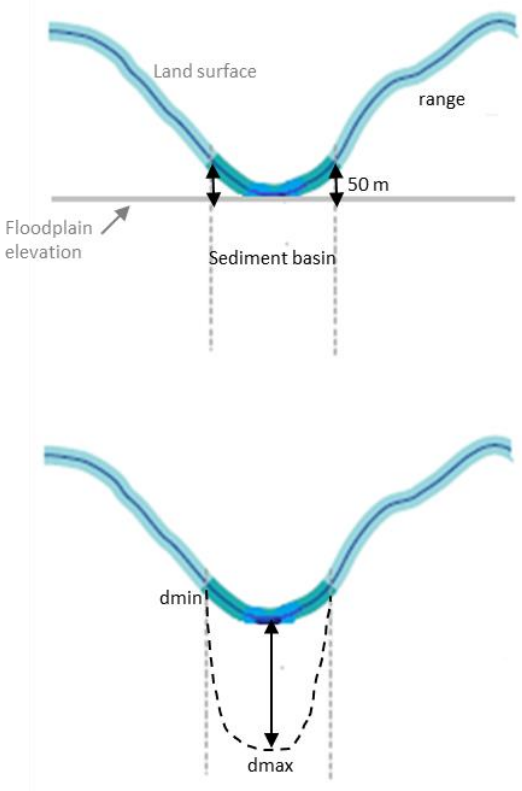

Fig. 3.2: (top) definition of sediment basins and mountain ranges, based on terrain attributes (land surface elevation and floodplain elevation). (bottom) estimation of aquifer thickness.

GLOBWB as the long-term average (for 1960-2000), was used as input for the recharge package of MODFLOW. In the MODFLOW calculation, the input value of recharge is multiplied by the MODFLOW cell dimension to get a volume per unit time, L^3T^{-1}. However, the input coming from our hydrological model is calculated for a geographic projected cell, thus varying surface areas. For this reason we modified our recharge input as follow:

$$\mathrm{RCH_{inp}} = \mathrm{RCH_{act}} \times \frac{A_{\mathrm{cell}}}{A_{\mathrm{MF}}} \tag{3.6}$$

where A_{cell} is the cell area of the projected cell, A_{MF} is the cell area of the MODFLOW cell, $\mathrm{RCH_{act}}$ is the groundwater recharge coming from PCR-GLOBWB (Figure 4), and $\mathrm{RCH_{inp}}$ is the modified input for the MODFLOW calculation.

We used the MODFLOW river (RIV) and drain (DRN) packages to incorporate in-

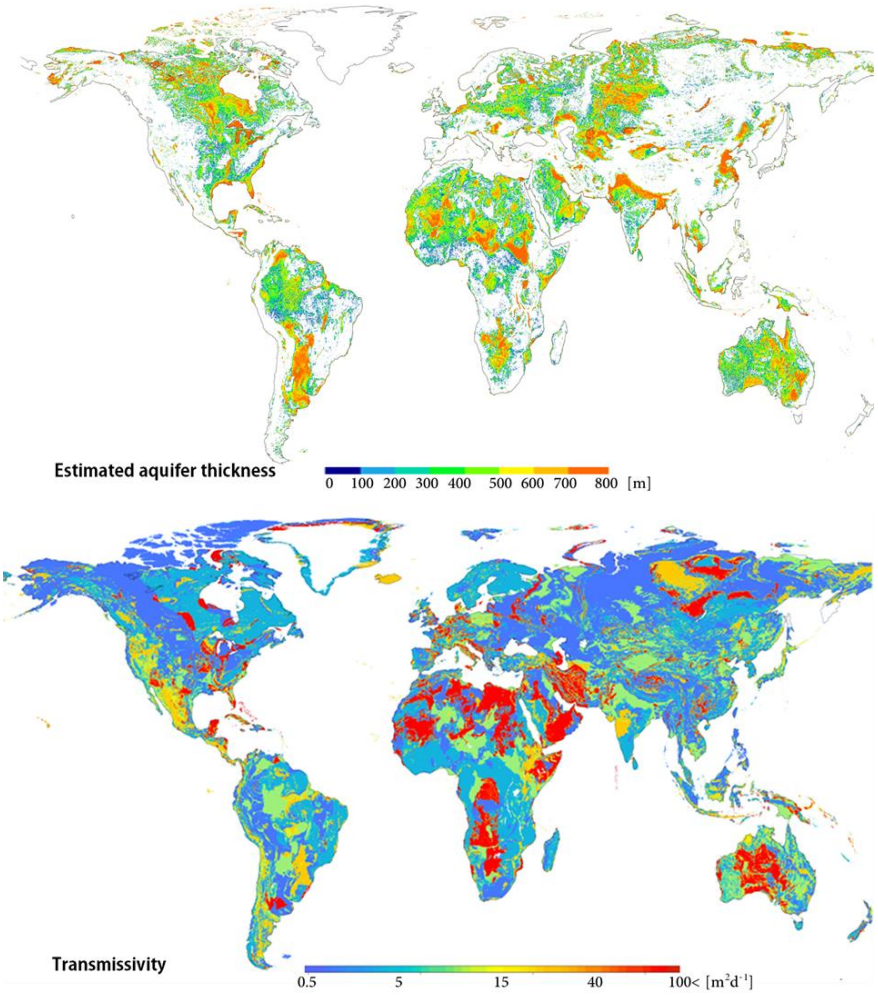

Fig. 3.3: Calculated aquifer thickness and tranmissivities.

teractions between groundwater bodies and the surface water. We distinguished three levels of groundwater-surface water interactions: (1) large river with a width >10 m, (2) smaller rivers, with a width <10 m, and (3) springs and streams higher up in river valleys.

1. For the larger rivers the interactions are governed by actual groundwater heads and surface water levels. The latter can be obtained from the long-term average naturalized river discharge, $\overline{Q_{\text{chn}}}$ (calculated by PCR-GLOBWB), by using assumed channel properties. These are: channel width, W_{chn} (L), channel depth, D_{chn} (L), Manning roughness coefficient, n ($L^{-1/3}T^{-1}$), and channel longitudinal slope, Sl (–).

   The channel width was calculated using Lacey's formula (Lacey, 1930):

$$W_{\text{chn}} \approx P_{\text{bkfl}} = 4.8 \times Q_{\text{bkfl}}^{0.5} \tag{3.7}$$

   where P_{bkfl} (m) is the wetted perimeter, Q_{bkfl} is the long-term averaged natural bankfull discharge (m^3d^{-1}) and 4.8 ($s^{0.5}m^{-0.5}$) is an emperical factor derived from the relationship between discharge and channel geometry (Savenije, 2003). In large natural braided rivers P_{bkfl} is slightly larger than W_{chn}. The bankfull discharge was calculated from the simulated river discharges and occurs, as a role of thumb, every 1.5 year. Combining Lacey's formula with Manning's formula (Manning, 1891) assuming a rectangular channel gives for channel depth:

$$D_{\text{chn}} = \left(\frac{n \times Q_{\text{bkfl}}^{0.5}}{4.8 \times \text{Sl}^{0.5}} \right)^{\frac{3}{5}} \tag{3.8}$$

   By subtracting D_{chn} from surface elevation we estimated the bottom elevation of the river bed RBOT (m). The average river head HRIV (m) was subsequently calculated from the long- term average naturalized river discharge $\overline{Q_{\text{chn}}}$ using the Manning formula:

$$\text{HRIV} = \text{RBOT} + \left(\frac{n \times \overline{Q_{\text{chn}}^{0.5}}}{W_{\text{chn}} \times \text{Sl}^{0.5}} \right)^{\frac{3}{5}} \tag{3.9}$$

   The RBOT and the HRIV were used as input for the RIV package in MODFLOW to calculate the flow between the river and aquifer: Q_{riv} (m^3d^{-1}). If the head in the cell connected to the river drops below the bottom of the river bed, water enters the groundwater system from the river at a constant rate. If the head is above the bottom of the river bed, water will either enter or leave the aquifer system depending on whether the head is above or below the river head. Q_{riv} is positive when water from the river enters the aquifer and is calculated as follows:

$$Q_{\text{riv}} = \begin{cases} c \times (\text{HRIV} - h) & \text{if } h > \text{ RBOT} \\ c \times (\text{HRIV} - RBOT) & \text{if } h \leq \text{RBOT} \end{cases} \tag{3.10}$$

where h is groundwater head (m), and c is a conductance ($\text{m}^2\ \text{d}^{-1}$) calculated as:

$$c = \frac{1}{\text{BRES}} \times P_{\text{chn}} \times L_{\text{chn}} \tag{3.11}$$

where BRES is bed resistance (d, taken 1 day here), L_{chn} (m) is the channel length (approximated the diagonal cell length), and P_{chn} is the wetted perimeter (approximated by W_{chn}. The river package was used only for cells with large rivers, i.e. $W_{\text{chn}} \geq 10\,\text{m}$.

2. To simulate smaller rivers, $W_{\text{chn}} < 10\,\text{m}$, the DRN package was used. Water can only leave the groundwater system through the drain when head rises above the drainage level which was taken equal to the surface elevation, DEM. The drainage Q_{drn} ($\text{m}^3\ \text{d}^{-1}$) is then calculated as follows:

$$Q_{\text{drn}} = \begin{cases} c \times (\text{DEM} - h) & \text{if } h > \text{DEM} \\ c \times 0 & \text{if } h \leq \text{DEM} \end{cases}. \tag{3.12}$$

Figure 4 shows larger rivers and active smaller rivers for Europe and Africa.

3. Q_{riv} and Q_{drn} quantify flow between streams and aquifer and are the main components of the baseflow Q_{bf} which is negative when water flows into the river. However, at $6'$ resolution the main stream is insufficient to represent truthfully all locations within a cell where groundwater levels intersect the terrain and additional drainage is needed to represent local sags, springs, and streams higher up in valleys in mountainous areas. To resolve this issue, we assumed that groundwater above the floodplain level can be tapped by local springs (illustrated in Figure 3.1B) which were presented by means of a linear storage-outflow relationship. To be consistent with the RIV and DRN packages, this term is also negative when water is drained. Thus, total groundwater drainage was simulated as:

$$Q_{\text{bf}} = (Q_{\text{riv}} + Q_{\text{drn}}) - (JS_{3,\text{flp}}) \tag{3.13}$$

where $S_{3,\text{flp}}$ (m) is the groundwater storage above the floodplain as obtained from PCR-GLOBWB and J (d^{-1}) is a recession coefficient parameterized based on Kraaijenhof van der Leur (1958):

$$J = \frac{\pi T}{4 S_y L^2} \tag{3.14}$$

where T (m^2d^{-1}) is the transmissivity as used in the groundwater model, S_y is the storage coefficient assumed for each hydrolithological category (see 3.1), and L is the average distance between streams and rivers as obtained from the stream density (see van Beek et al. (2011)).

3.2.4 Sensitivity analysis of aquifer properties and recharge

In groundwater modelling the transmissivity and groundwater recharge are important parameters and subject to large uncertainty. In this study we investigated the sensitivity of the model outcome to changes in the aquifer parameters (conductivity, thickness) and recharge.

For each parameter a Monte Carlo simulation of 100 samples was performed. This simulation followed a log-normal distribution for layer thickness and saturated conductivity. For groundwater recharge a normal distribution was used. For layer thickness, mean and standard deviation were obtained by combining several case studies of the USA and

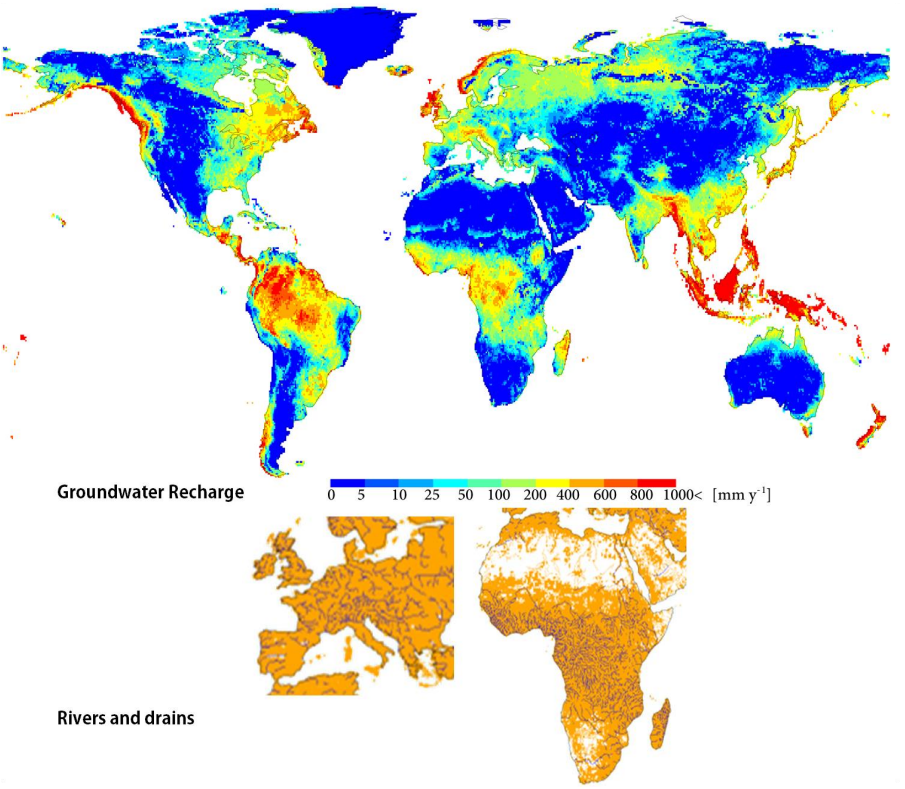

Fig. 3.4: (top) Steady-state recharge input as obtained from averaging PCR-GLOBWB recharge output over the period 1957-2002. (bottom) The hydrography of the imposed stream-network is superimposed: large rivers, with widths >10 m (blue) and smaller rivers, with widths 10 m (orange).

extrapolating this globally (see section 3.2.2, eq. 3.1-3.5). Means and standard deviations of saturated conductivities per hydrolithological class were taken from Gleeson et al. (2011) (see Tabel 3.1). Mean and standard deviations for groundwater recharge were taken for the PCR-GLOBWB sensitivity study of Wada et al. (2014).

The variation in groundwater depth caused by changing one parameter was evaluated by calculating maps coefficients of variation (presented in Figure 3.5). To obtain the uncertainty from the combination of these parameters, for each parameter 10 evenly distributed quantiles were determined and combined into 1000 parameter sets to run the model with. Again variation in groundwater depth was evaluated by calculating maps of coefficients of variation.

3.2.5 Validation of groundwater heads

Simulated groundwater depths were validated against a compilation of reported piezometer data (Fan et al., 2013). The average of the reported data was used if more than one observation was available within a $6'$ cell, giving a total of 65 303 cells with observations worldwide (of the total 6 480 000 cells). The water table head, instead of depth, was evaluated as it measures the potential energy that drives flow and is therefore physically more meaningful. The coefficient of determination (R^2) and regression coefficient (α) were calculated for every run (results presented in Figure 3.6). Residuals (res) were calculated as simulated heads minus observed heads and maps are presented Figure 3.7).

3.2.6 Simulating flowpaths

Particle tracking, using MODPATH (Pollock, 1994), was included to track flowpaths and estimate travel times of groundwater flows. For this simulation cell-to-cell flux densities, defined as the specific discharge per unit of cross-sectional area, were used. A flowpath is computed by tracking the particle from one cell to the next until it reaches a boundary or sink. It shows the path through the subsoil that the groundwater follows from the location of infiltration towards the location of drainage. In our case the particle was stopped when it reached the ocean, a lake, or the local drainage (rivers or drains). It provides insights in regional scale groundwater movements and groundwater age, indicating areas where lateral groundwater flows are significant and inter-basin groundwater flows are important. The latter positively affects water budgets of neigboring catchments or recharges the larger aquifer systems, thereby increasing water availability of these neigboring catchments. Results are presented for Europe and Africa, showing paths and travel times (Figure 3.9).

3.3 Results and discussion

3.3.1 Sensitivity analysis

Figure 5 shows the coefficient of variation (CV) of calculated groundwater depths with changing parameter settings for saturated conductivity, aquifer thickness, and recharge. Overall CVs are small; less than 1. Higher CVs are found for the Sahara and Australian desert, where recharge is low, transmissivities are high, and groundwater levels become disconnected from the surface. This emphasizes the influence of regional scale lateral flow in these areas. Higher variations are also found for areas with shallow groundwater tables and higher transmissivities and recharge, like the Amazon and Indus basin.

Figures of CVs of simulated groundwater depths resulting from changing a single parameter only are presented in the supplementary material of this paper (Figure 6.3). The CVs from changing saturated conductivity are almost simular to the total CV, illustrating that saturated conductivity is the predominant control of groundwater depth. This is expected as the standard deviation of saturated conductivity is large for several hydrolitological classes (Tabel 3.1), changing saturated conductivity by orders of magnitude. In general a higher saturated conductivity leads to lower water tables and more significant regional groundwater flow, and vice versa.

The other two parameters, aquifer thickness and groundwater recharge, are of lower importance. Although different thicknesses do change transmissivities, impact on calculated groundwater depths is small. Also, the effect of changing groundwater recharge is small. This is the direct result of the small relative uncertainty compared to hydraulic conductivity. Beside this, drainage is self-limiting; as recharge increases, the water table rises and the hydraulic gradient is steepened, accelerating drainage and lowering the water table. This dampens the water table sensitivity to recharge uncertainties.

3.3.2 Validation of groundwater simulated heads

Simulated groundwater heads were compared to piezometer observations. A scatter plot of the best performing run (after changing three parameters) is presented in Figure 3.6 and spatial patterns are presented in Figure 3.7. It should be mentioned here that for most regions of the world no observation data are available (see supplementary material Figure 6.5) or are incomplete (i.e. no elevation measurement). While interpreting the results it should be noted that observation locations are biased towards river valleys, coastal ribbons, and the areas where productive aquifers occur. Also, observations are taken at a certain moment in time, and thus are liable to seasonal effects and drawdown as a result of abstractions, while simulated groundwater heads represent the steady state average. Beside this, for the mountain ranges it is likely that observations are located in small mountain valleys with shallow local water tables, partly from infiltrating streams. Our grid resolution is too coarse to capture these small-scale features. Also,

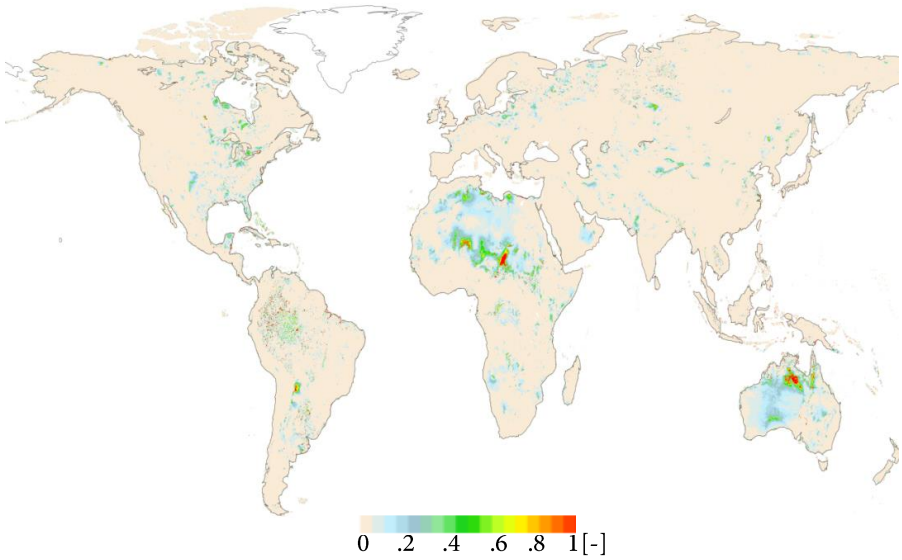

Fig. 3.5: Coefficient of variation of groundwater depth of 1000 runs with different parameter settings for aquifer thickness, saturated conductivity, and groundwater recharge

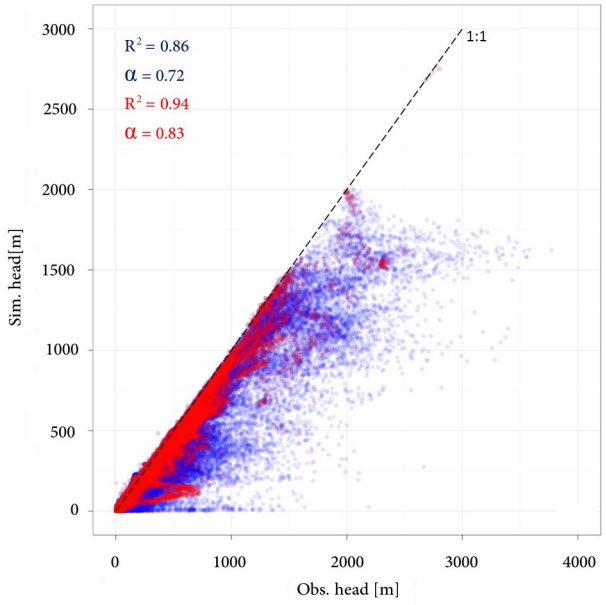

Fig. 3.6: Scatter plot of observed heads against simulated heads for sediment basins (red) and mountain ranges (blue).

occasionally observations of perched water tables in hill slopes are included. These perched groundwater tables are not described by our large-scale groundwater model (simulating the regional scale groundwater, see Figure 3.1B), but captured in the land surface model as interflow.

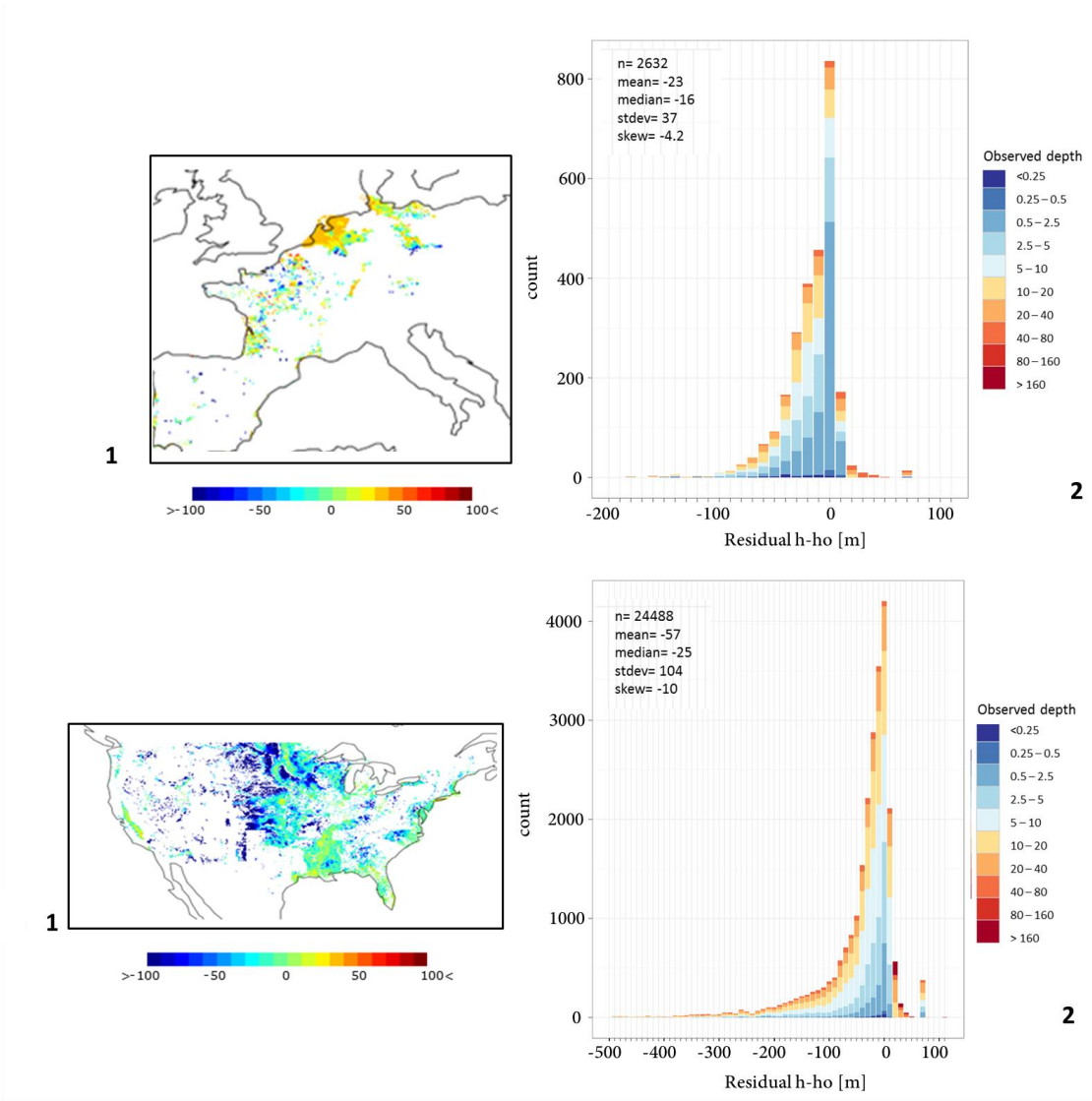

Fig. 3.7: Maps of residuals for NW-Europe and USA. (1) residuals and (2) histograms of residuals. Each bar in the histogram is clustered based on observed on classified groundwater depths.

For all runs the computed coefficient-of-determination (R^2) was calculated and found to fall between 0.75 and 0.87. For the 10 best performing runs it ranges between 0.85 and 0.87. The scatter of the best performing run is given in Figure 3.6. The presented scatter and statistics of R^2 and regression coefficient α in Figure 3.6 show that the model performance is good. However, the scatter shows a strong underestimation of groundwater heads, meaning that simulated groundwater tables are too deep compared with the observations. This appears especially for higher elevated areas (also shown in Figure 3.7). This underestimation is expected as most likely for higher elevated areas shallow local water tables are sampled which are not captured by our model as a result

of the limited grid resolution. Therefore we evaluated R^2 and α for mountain ranges and sediment basins separately shown in Figure 6 in blue and red respectively. The R^2 for the sediment basins is slightly better than for mountain ranges, but in general water table elevations here are still underestimated. The R^2 for sediment basins ranges between 0.90 and 0.95, and for the 10 best performing runs between 0.945 and 0.946. For the lower elevations (approx. 0- 500 m) a small overestimations of heads can be seen as well.

In Figure 3.7 the spatial distribution of the residuals of groundwater heads and corresponding histograms are shown for Europe and the USA. The figures confirm the above stated conclusion that heads are generally underestimated compared to the observations. The largest underestimations area found for higher elevated areas, such as the Rocky Mountains. Groundwater heads are best estimated for lower flatter areas, like the Mississippi embayment and the Netherlands. The histograms show that larger residuals are found for areas where groundwater levels are deeper, and smaller residuals are found for more shallow groundwater levels. This shows that, although absolute values of groundwater heads are underestimated, the general pattern of deep and shallow groundwater is well captured by the model.

3.3.3 Global groundwater depth map

Figure 3.8 shows for the best performing run the simulated steady-state groundwater table depths at its natural state (without pumping), in meter below the land surface (result of the best performing run).

General patterns in water table depths can be identified. At the global scale, sea level is the main control of groundwater depth. Throughout the entire coastal ribbon shallow groundwater tables occur. These areas expand where flat coastal plains meet the sea, including major river basins like Mississippi, Indus, and large wetlands. At the regional scale, recharge is the main control in combination with scale topography. For regions with high groundwater recharge rates shallow groundwater tables are simulated, for example the tropical swamps of the Amazon. The influence of the regional topography is also evident in the central Amazon and for the flat lowlands of South America as these regions receive water from elevated areas.

Regions with low recharge rates correspond with deep groundwater where groundwater head gets disconnected from the local topography. The great deserts stand out (hyper-arid regions dotted in Figure 3.8). Also for the mountain ranges of the world deep groundwater tables are simulated. As stated before, small local valleys with higher local groundwater tables are not captured by the model due to the used grid resolution. The mountainous regions where local and perched water tables are likely to occur are masked in the figure with a semi-transparent layer.

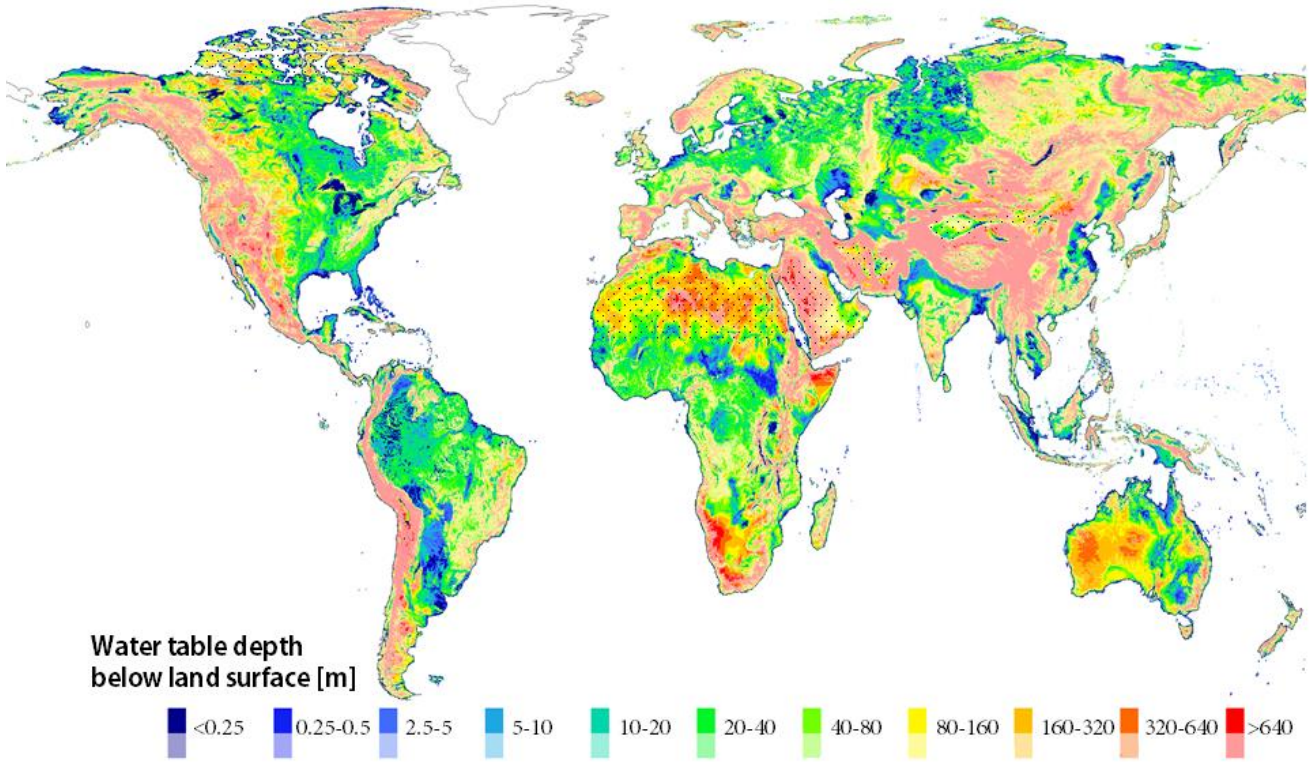

Fig. 3.8: Simulated water table depth in meters below the land surface. The result of a steady-state natural run, using the best estimated parameter set. Semi-transparant colours indicate deep groundwater regions where most likely more shallow perched and local water tables not captured by the model. Dotted areas indicate hyper- arid zones, distinguished at the grid resolution. White areas indicate no-data values.

3.3.4 Groundwater flowpaths and travel time

Figure 3.9 shows the simulated large-scale flowpaths for Europe and Africa where different colors indicate the simulated travel times. These figures show both short and long inter-basin flowpaths, that are stopped when they reach the local drainage, such as a lake or the ocean. Long flowpaths are for example found in Eastern-Europe, where flowpaths cross several catchment boundaries and end as submarine groundwater discharge. Also, inter-basin flowpaths recharge larger aquifer systems, such as is the case for the upper-Danube aquifer system. For Africa long inter-basin flow paths are evident for the desert area as well. The flowpath simulations show that especially for sediment areas, inter-basin groundwater flow is important and significant at least at longer time scales. It should be noted that these larger-scale flowpaths are associated with the scale of the model. Obviously, superimposed on these areas subregional to local-scale flowpaths of shallow groundwater systems exist that are not captured by our model (Toth, 1963).

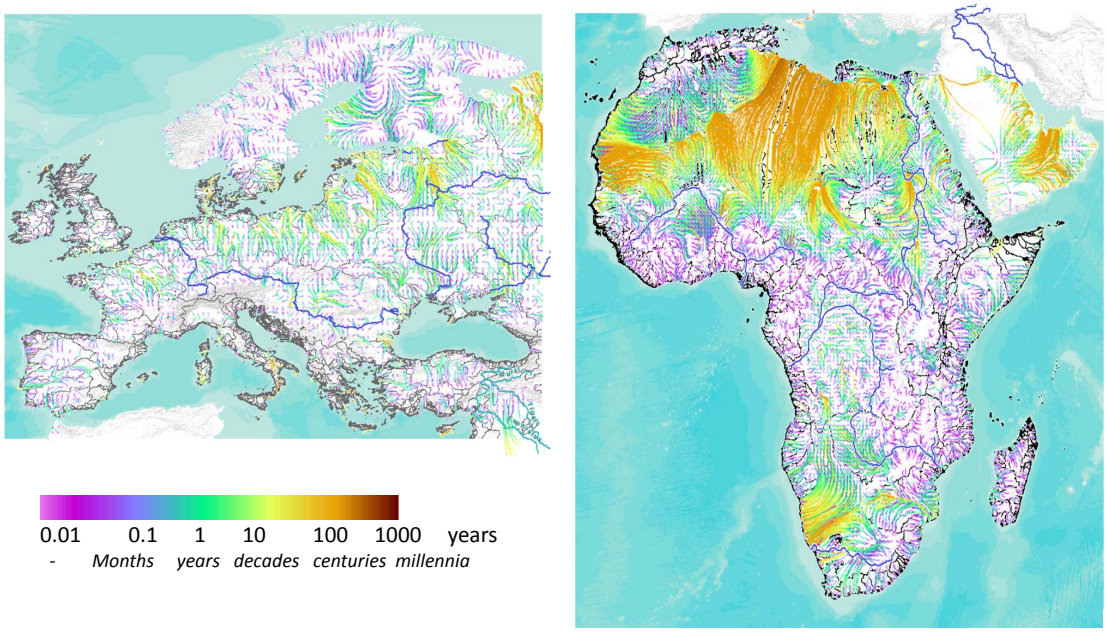

Fig. 3.9: Flow paths simulated for NW-Europe and Africa, underlain by river basin boundaries, overlain with major rivers.

3.4 Conclusions

In this paper a global scale groundwater model of an upper unconfined aquifer layer is presented. A feasible and relatively simple method is introduced to overcome the

limited information available for aquifer parameterization; available global datasets for lithology and saturated conductivity were used such that the parameterization method can be expanded to data poor environments.

By applying this method we are able to produce a global picture of water table depths at fine resolution ($6'$) within good accuracy in many part of the world, especially for sediment basins ($R^2 = 0.95$ and $\alpha = 0.84$). The sediment basins are specific areas of interest, as these include the major aquifer systems of the world (e.g. Indus, Ganges, High Plains). For the higher and steeper terrain groundwater depths are in general overestimated compared to observations (simulated depths deeper than observed), likely because perched water tables on hillsides, are not included in the groundwater model but are present in the observations. Additionally, the model resolution and the aquifer property estimation are still too coarse to capture shallow water tables in small sediment pockets in small mountain valleys.

The results presented in this study confirm the relevance of taking lateral groundwater flow into account in global scale hydrological models. Short and long flowpaths, also over catchment boundaries as inter-basin flowpaths, are simulated. The latter can be of major importance as it provides additional recharge to a catchment and thereby helps to sustain river baseflow in times of droughts, supporting ecosystems and wetlands and increasing surface water availability for human water use. Also, inter-basin groundwater flows can act as additional recharge to large aquifer systems, thereby increasing water availability in these aquifers.

Obviously the model presented here must be considered as a first-order attempt towards global groundwater modelling and consequently has a number of limitations that prevent it from simulating groundwater dynamics completely truthfully.

Firstly, the model simulates a natural dynamic steady-state; it does not provide any information about groundwater fluctuations caused by climate (seasonal and inter-annual) or human water use. Obviously, as we have estimated specific yield as well, extension to transient simulations is straightforward and will be attempted in a next study.

Secondly, only one unconfined layer is modelled here, while in reality, multi-layered aquifers including unconsolidated and consolidated layers can be present. Before we can include human groundwater use globally, these multi-layered aquifers should be included in the model as this holds vital information on the accessibility and quality of global groundwater resources. However, the information on these aspects is sparse and incomplete.

Thirdly, capillary rise of the water table into the soil has not yet been implemented, although several studies have pointed out that it can affect soil moisture, evaporation, or even precipitation (e.g. Bierkens & van den Hurk, 2007; Fan et al., 2013; Lam et al., 2011). Further, there is no dynamic interaction between groundwater and surface water, as the drainage level of rivers does not change over time.

That being said, our model has the ability to capture the large scale distribution of

groundwater levels and as such can serve as a starting point leading to a tool to assess groundwater level fluctuations and their sensitivity to human water intervention and climate.

The next step of this work will be to expand the current aquifer schematization with multi-layered and confined aquifer systems. The model will become transient and fully coupled to the land-surface model in order to incorporate capillary rise to the soil moisture and link river dynamics with groundwater. Human water use will be included as well. The goal will be to represent the impact of human water use on groundwater dynamics and river discharges. It will show where and when limits of groundwater abstractions will be reached. This is vital information needed to ensure sustainable and efficient groundwater use, particularly for semi-arid regions where groundwater demand will intensify due to the increase of drought frequency and duration, combined with population growth, expansion of irrigation areas, and rising standard of living.

Acknowledgements
The autors thank Peter Vermeulen (Deltares) for his assistance with iMOD used for the particle tracking. The autors also would like to thank the three reviewers, Nir Krakauer (The City College of New York), Mary Hill (USGS), and one anonymous reviewer for their constructive and thoughful suggestions on an earlier version of this paper. This study was funded by the Netherlands Organization for Scientific Research (NWO) in the project Planetary Boundaries Fresh Water Cycle.

Chapter 4

A global-scale two-layered transient groundwater model: development and application to groundwater depletion

Groundwater is the worldâs largest accessible source of freshwater to satisfy human water needs. Moreover, groundwater buffers variable precipitation rates over time; thereby effectively sustaining river flows in times of droughts as well as evaporation for areas with shallow water tables. Lateral flows between basins can be a significant part of the basins water budget, but most global-scale hydrological models do not consider surface water-groundwater interactions and do not include a lateral groundwater flow component. In this study we simulate groundwater head fluctuation and groundwater storage changes in both confined and unconfined aquifer systems using a global-scale high-resolution (5 arc-minutes) groundwater model by deriving new estimates of the distribution and thickness of confining layers. Inclusion of confined aquifer systems (estimated 6% to 20% of the total aquifer area) changes timing and amplitude of head fluctuations, as well as flow paths and groundwater-surface water interactions rates. Also, timing and magnitude of groundwater head fluctuations are better estimated when confining layers are included. Groundwater flow paths within confining layers are shorter compared to paths in the underlying aquifer, while flows within the confined aquifer can get disconnected from the local drainage system due to the low conductivity of the confining layer. Lateral groundwater flows between basins are significant in the model, especially for confined aquifer areas were long, slow paths are simulated crossing catchment boundaries, thereby supporting water budgets of neighboring catchments or aquifer systems. This study reveals hotspots of groundwater depletion in confined aquifers for the first time, and estimates global depletion over 1960-2010 is estimated at 6700 km^3, which is consistent with previous estimates. Simulating confining layers with global hydrologic models is critical for accurately simulating groundwater surface water interactions, the water table, and groundwater depletion.

Under review in Hydrology and Earth System Sciences as: de Graaf, I.E.M., L.P.H. van Beek , T. Gleeson, N. Moosdorf, O. Schmitz, E.H. Sutanudjaja, M.F.P. Bierkens, A global-scale two-layered transient groundwater model: development and application to groundwater depletion

4.1 Introduction

As the world' s largest accessible source of freshwater, groundwater plays a vital role in satisfying the basic needs of human society. It serves as a primary source of drinking water and supplies water for agricultural and industrial activities. During periods of low or no rainfall, groundwater storage provides a large natural buffer against water shortage, preserves evaporation in areas with shallow water tables, and sustains baseflows to rivers and wetlands, thereby supporting ecosystem habitats and biodiversity (e.g. Bierkens & van den Hurk, 2007; de Graaf et al., 2013; Wada et al., 2014). Moreover, groundwater often flows across topographical and administrative boundaries at considerable rates, supporting water budgets of water receiving catchments or aquifers. However, groundwater resources are increasingly threatened by excessive abstractions, particularly in irrigated areas where abstraction rates are high and groundwater is only slowly renewed (Gleeson et al., 2011). The most direct effects of groundwater depletion are falling water tables and the irreversible loss of storage. As a consequence, pumping costs increase, and baseflows to rivers and wetlands are reduced, negatively affecting ecosystems, and causing land subsidence.

Despite the importance of groundwater, most global-scale hydrological models do not include a groundwater flow component. The main reason of this omission is the lack of consistent global-scale hydrogeological information. Such data is needed to obtain a realistic physical representation of the groundwater system, allowing for a more realistic simulation of groundwater head dynamics and lateral flows (e.g. Fan et al., 2007; Schaller & Fan, 2009) and especially needed when these models move to finer resolutions (e.g. 5 arc-minutes) (Wood et al., 2012, Bierkens et al., 2015).

Previous work on global-scale groundwater models has been done by e.g. Fan et al. (2013); de Graaf et al. (2015). The study of Fan et al. (2013) produced a first high-resolution global groundwater table map. However, their method has its limitations as it method does not include hydrogeological information on aquifers (e.g. depths and transmissivities). In addition the hydrological connection between groundwater and rivers, which is the primary drainage of groundwater in humid regions, is ignored. Moreover, their model requires calibration to head observations and only returns the steady state head distribution.

The recent study of de Graaf et al. (2015) presents the first high-resolution global-scale groundwater model including hydrogeological information and accounting for groundwater-surface water interactions. Lateral groundwater flows for an upper, unconfined aquifer at the steady-state are simulated. A relative simple method for aquifer parameterization is used based on available global datasets of lithology (Hartmann & Moosdorf, 2012) and permeability (Gleeson et al., 2011) such that the method provides results for data-poor environments. Also, aquifer thickness is derived globally using terrain attributes. The results are promising, shown by the high correlation between observed and simulated averaged groundwater heads. However, the studyâs greatest limitation is that only the steady-state head distribution is reported and temporal changes in groundwater head

patterns due to climate or human impacts are not considered. Also, only a single unconfined aquifer is described and vital information on the accessibility and quality of the groundwater water resource is missing. This information is needed to simulate the aquifer sensitivity to storage changes due to climate fluctuations or abstractions. Also, abstractions are preferentially positioned in confined aquifer systems, as these systems are less sensitive for climate fluctuations and groundwater quality is often better than from unconfined systems (Foster & Chilton, 2003).

The first objective of this study is to represent the groundwater system more realistically, including for confined aquifers, and simulate groundwater head dynamics affected by changes in climate and human water use. The groundwater system is more realistically described by including information on the presence of confining layers, leading to the categorization of worldâs aquifers in confined and unconfined systems. The improved physical groundwater presentation leads to a more realistic estimate of aquifer sensitivity to changes in storage by climate or human impacts.

The second objective of this study is to provide estimates of groundwater depletion and head declines worldwide. Previous estimates of groundwater depletion (e.g. Döll et al., 2012; Wada et al., 2010; Konikow, 2011; Pokhrel et al., 2012) vary by an order of magnitude. For example the flux-based approaches of Wada et al. (2010) estimate groundwater depletion (283 ± 40 km^{3}yr^{-1} for 2010) as the residual of grid-based groundwater recharge and withdrawal. Their approach overestimates depletion as it does not account for increased capture due to decreased groundwater discharge, nor for long-distance surface water transports. The volume-based approach of Konikow (2011) estimates groundwater depletion (145 ± 39 km^{3}yr^{-1} between 2001 and 2008) based on data for the US and other big aquifer systems by extrapolation of groundwater depletion globally using the average ratio of depletion to abstractions observed in the US. Our study will be, to our knowledge, the first including lateral groundwater flow and groundwater-surface water interaction to simulate changes in global groundwater storage. We expect our depletion estimate to be lower than earlier flux-based estimates and more similar to volume-based estimates.

4.2 Methods

4.2.1 General

In this study a two-layered groundwater model for the terrestrial part of the world is developed (excluding Greenland and Antartica). The model consist of two parts: (1) the hydrological model PCR-GLOBWB (van Beek et al., 2011) and (2) the groundwater model using MODFLOW (McDonald & Harbaugh, 2000). Both models were run at 5 arc-minute resolution (approx. 10 km at the equator) over the period 1960-2010. The groundwater model was forced with outputs from PCR-GLOBWB, specifically via

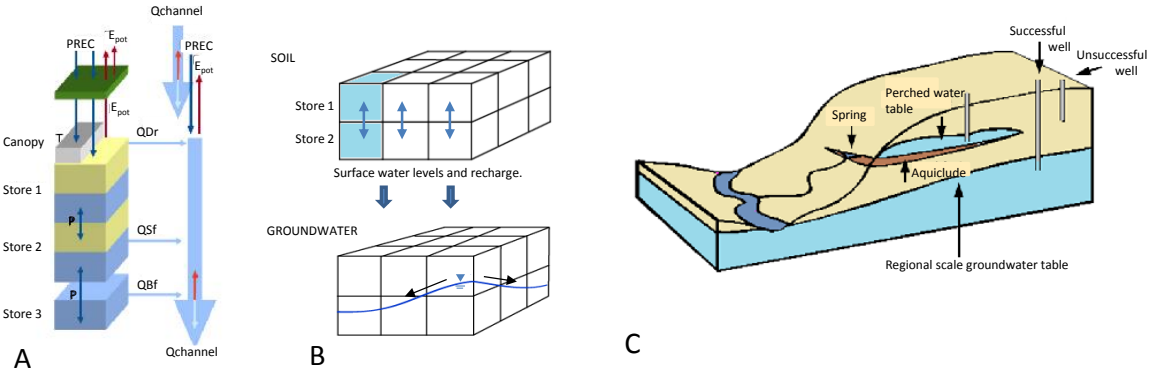

Fig. 4.1: A) Original model structure of the hydrological model PCR-GLOBWB. B) Coupling to the groundwater model, the PCR-GLOBWB cell of A is coloured blue. The groundwater model is forced with recharge and surface water levels, and groundwater heads and lateral flows are calculated. C) A cross-section illustrating the differnce between the simulated regional-scale groundwater levels and perched water levels. The latter are often sampled.

groundwater recharge and river discharges (Figure 4.1). A brief description of the models and coupling is given here, a more detailed description is given in de Graaf et al. (2015).

Global hydrological model

The model PCR-GLOBWB simulates hydrological processes in and between two vertically stacked soil stores (maximum thickness 0.3 and 1.2 m respectively) and one underlying groundwater store. The model was run at 5 arc-minutes resolution at a daily time step. For the climate forcing, monthly data from CRU TS 2.1 (Mitchell & Jones, 2005) was downscaled using ERA-40 (Uppala et al, 2005) and ERA-interim (Dee et al., 2011) reanalysis to obtain a daily climate forcing (see de Graaf et al., 2013) for a more detailed description of this forcing dataset). For each time step and every grid cell the water balance of the soil column is calculated based on the climatic forcing that imposes precipitation (rain or snow depending on temperature), reference potential evapotranspiration, and temperature. Vertical exchange between the soil and groundwater occurs through percolation and capillary rise. Specific surface runoff snowmelt, interflow, and baseflow are accumulated along the drainage network that consists of laterally connected surface water elements representing river channels, lakes, or reservoirs. A kinematic wave approximation at a sub-daily time step is used to route surface water to the basin outlet.

In the original version of the PCR-GLOBWB model no lateral groundwater flow is simulated. Groundwater flow is described by means of a linear store fed by groundwater recharge simulated as percolation minus capillary rise from the soil layers to the groundwater reservoir.

Global groundwater model

A 2-layered MODFLOW model (McDonald & Harbaugh, 2000; Schmitz et al., 2009) replaces the linear groundwater store of PCR-GLOBWB. Aquifer properties are prescribed and include confined and unconfined aquifer systems (discussed in the next paragraph). The MODFLOW model is forced with outputs from PCR-GLOBWB, specifically groundwater recharge and river discharge. The recharge is the input for the MODFLOWâs recharge (RCH) package, while the MODFLOWâs river (RIV) and drain (DRN) packages are used to incorporate interactions between the groundwater and surface water. Three levels of groundwater-surface water interactions are distinguished: (1) large rivers, with a width larger than 25 m, (2) smaller rivers with a width smaller than 25 m, and (3) springs and streams higher up in the valley.

1. For large rivers, interactions are governed by actual groundwater heads and river levels ($HRIV$ [m]). The latter was calculated from river discharges (Q_{chn} [m^3s^{-1}]) simulated by PCR-GLOBWB and using channel properties based on geomorphological relations to bankful discharge (Q_{bkfl} [m^3s^{-1}]) (Lacey, 1930; Savenije, 2003; Manning, 1891). The RIV-package calculates the water flux between the river and groundwater Q_{riv} [m^3d^{-1}]. Water infiltrates the aquifer if the groundwater head lies below the river head: Q_{riv} is then positive. Water is drained from the aquifer when groundwater head lies above the river head: Q_{riv} is then negative. Q_{riv} for the larger rivers ($Q_{riv.Big}$ [m^3d^{-1}]) was calculated as:

$$Q_{\text{riv.Big}} = \begin{cases} c \times (\text{HRIV} - h) & \text{if } h > \text{ RBOT} \\ c \times (\text{HRIV} - RBOT) & \text{if } h \leq \text{RBOT} \end{cases} \tag{4.1}$$

   where c [d] is the river bed resistance (assumed 1 day), h [m] is groundwater head, and $RBOT$ [m] is the river bottom calculated for bankful conditions (taken as a rule of thumb happening every 1.5 year). Surface elevation (DEM [m]) is taken as the reference level here.

2. Smaller rivers were defined as drains; water can only leave the groundwater system through the drain when heads get above the drainage level. In this case, the drainage levels were taken equal to the DEM. The drainage was then calculated as $Q_{riv.Small}$ [m^3d^{-1}]:

$$Q_{\text{riv.Small}} = \begin{cases} c \times (\text{DEM} - h) & \text{if } h > \text{DEM} \\ 0 & \text{if } h \leq \text{DEM} \end{cases} \tag{4.2}$$

3. $Q_{riv.Big}$ and $Q_{riv.Small}$ quantify flow between streams and aquifers and are the main components of the baseflow, Q_{bf}, which is negative when water is drained from the aquifer. At the 5 arc-minute resolution however, the mean stream is insufficient to represent local sags, springs, and streams higher up in the mountainous area.

We assume that groundwater above the floodplain level can be tapped by local springs that are represented by means of a linear storage-outflow relationship. To be consistent with the RIV and DRN packages, this linear storage term is also negative when water is drained. Total drainage Q_{bf} [$m^3 d^{-1}$] was thus calculated as:

$$Q_{bf} = (Q_{riv.Big} + Q_{riv.Small}) - (JS_{3,flp}) \tag{4.3}$$

where $S_{3,flp}$ [m^3] is the groundwater storage above the floodplain (obtained from PCR-GLOBWB) and J [d^{-1}] is the recession coefficient parameterized based on Kraaijenhof van de Leur (1958):

$$J = \frac{\pi T}{4 S_y L^2} \tag{4.4}$$

where T [m^2 d^{-1}] is transmissivity, S_y [-] is the specific yield (for each hydrolithological unit; Tabel 4.1) and L [m] is the average distance between streams and rivers as obtained from the drainage density (van Beek et al., 2011).

4.2.2 Aquifer parameterization

The aquifer parameterization is based on available global datasets on lithology (Global Lithology Map (GLiM) Hartmann & Moosdorf (2012)) and permeability (Gleeson et al., 2011, 2014), combined with an estimate of aquifer thicknesses (de Graaf et al., 2015). A detailed description of the aquifer parameterization is given in de de Graaf et al. (2015), a summary is given below since the focus of this study is to extend the aquifer parameterization by categorizing world's aquifers in confined and unconfined systems.

General: Aquifer permeability and transmissivity

Aquifer permeabilities were defined by lumping the lithology classes defined by Hartmann & Moosdorf (2012) to 7 combined hydrolithologies (adopted from Gleeson et al. (2011)), representing broad lithological categories with similar hydrogeological characteristics. These units were subdivided further on the basis of texture for unconsolidated and sedimentary rocks (Table 4.1), resulting in a global map representing regional scale permeability. The polygons of the lithological map, delineating a hydrogeological unit, were subsequently gridded to 30 arc-seconds (approx. 1 km^2 at the equator) and aggregated as the geometric mean at 5 arc-minutes resolution (approx. 10 km^2 at the equator).

To calculate transmissivities (T [m^2 d^{-1}]) aquifer thicknesses are needed. These were estimated since no global dataset of observed aquifer thickness is available. Using the assumption that productive aquifers coincide with sediment basins below river valleys

Table 4.1: Lithologic and hydrolihologic categories.

Lithologic categories[a]	Hydrolithologic categories[b]	$\log k\ \mu_{\text{geo}}$ [m^2][b]	σ [m^2][b]	S_y [m/m][c]
Unconsolidated sediments	unconsolidated	−13.0	2.0	0.235
	c.g. unconsolidated	−10.9	1.2	0.360
	f.g. unconsolidated	−14.0	1.8	0.110
Siliciclastic sediments	siliciclastic sedimentary	−15.2	2.5	0.055
	c.g. siliciclastic sedimentary	−12.5	0.9	0.100
	f.g. siliciclastic sedimentary	−16.5	1.7	0.010
Mixed sedimentary rocks Carbonate sedimentary rocks Evaporites	Carbonate	−11.8	1.5	0.140
Acid volcanic rocks Intermediate volcanic rocks Basic volcanic rocks	Crystalline	−14.1	1.5	0.010
Acid plutonic rocks Intermediate plutonic rocks Basic plutonc rocks pyroclastics metamorphic	Volcanic	−12.5	1.8	0.050
water bodies Ice and Glaciers	not assigned	–	–	–

[a] Hartmann & Moosdorf (2012).

[b] Based on Gleeson et al. (2011), $\log k\ \mu_{\text{geo}}$ is the geometric mean logarithmic permeability; σ is the standard deviation; f.g. and c.g. are fine-grained and coarse-grained, respectivaly.

[c] S_y is the storage coefficient, average per category.

the distinction was made between (1) mountain ranges, and (2) sediment basins representing the aquifers. Subsequently, aquifer thicknesses were estimated by relating these to terrain attributes (e.g. curvature) after calibration of these relations with reported aquifer thicknesses from U.S. groundwater modeling studies (see de Graaf et al. (2015) for an extensive description of this procedure to delineate aquifer systems and estimate thicknesses).

Delineation of confining layers

In this study we delineated confining layers and categorized the aquifers of the world in confined and unconfined systems. The categorization was done using information on grain sizes of unconsolidated sediments in the lithological map (GLiM) and additional information in the sediment property description of GLiM. Figure 4.2 the resulting map of confining layers. Some clear spatial inconsistencies can be seen, e.g. for the US over the High Plain aquifer, or the German-Polish border (inconsistencies are discussed in Hartmann & Moosdorf (2012)). We interpreted the GLiM lithologies of 'fine-grained unconsolidated sediments' and 'mixed-grained unconsolidated sediments' as potential near-surface confining units. About 30% of the mixed grained unconsolidated sediments have layers of clay, silt or till in the sediments description. We assume, based

on the uncertainty in the sediment descriptions, that this 30% represents the minimum percentage of unconsolidated mixed grained sediments with a confining unit. The maximal percentage is if all mixed grained unconsolidated sediments would have a confining unit. These two percentages are used to test the sensitivity of groundwater patterns and fluctuations to absence or presence of confining layers.

Additionally, we classified regions of the world where we know confining layers are present but are not fully represented in GLiM: the coastal zones. We reconstructed the inland extent of Holocene fine-grained coastal plains that overlay older, coarser sediments from the Pleistocene. A reconstruction of sea-level rise (e.g Toscano & Macintyre, 2003)) and coastal sedimentation (e.g Syvitski et al., 2005)) implies that 6000 years ago along many Holocene coastal plains the coastline was more inland compared to the modern situation. Coastlines have receded tens of kilometers since in many deltas (e.g Stanley & Warne, 1994)). With sea-level rise during the Holocene, the downstream gradient along the river flattened, and in the downstream part sediments accumulated. The apex of the delta and deposition areas indicate the point where accumulation originated. This accumulation point is reconstructed using the profile curvature along the river, with its occurrence where the curvature changes from convex to concave starting from the coast.

The accumulation point was identified globally for larger rivers ($>$ 25 m wide) with their outlet on, or near the coast (i.e. within 50 km). Points at high elevations, clearly not related to sedimentation in the coastal zone, were excluded.

Figure 4.3 (top) shows a schematic cross-section of a coastal aquifer with a confining layer on top. Thickness of the confining layer at the coast is estimated using ocean bathymetry (elevation taken one 5 arc-minute grid-cell out of the coast). The thickness at the coastline is interpolated along the river using the river gradient until the apex, where thickness is minimal. The interpolation is done for all identified large rivers and thickness of the coastal plains is derived by interpolation between the rivers, bounded by the elevation contours on which the apex are situated (Figure 4.3 bottom). Following this approach approximately 11% of the global coastline is classified as confined after interpolation.

Confined systems: Aquifer transmissivity and storativity

Confined systems are described as an aquifer overlain by a fine grained confining layers. Parameter settings used for confined systems are shown in Figure 4.4. All other rocks and sediments the values from Table 4.1 where used. In absence of any other information vertical conductivity was assumed to be the same as the horizontal conductivity. Storage capacities were parameterized using specific yields for unconfined aquifers (Table 4.1) and for confined aquifers a storage coefficient of 0.001 (Heath, 1983) was assumed. Thickness of coastal confining layers is estimated using ocean bathymetry and interpolation (as described). For 80% of the coastal confined grid- cells the estimated confining layer thickness is approximately 10% of the total estimated aquifer thickness. Based on

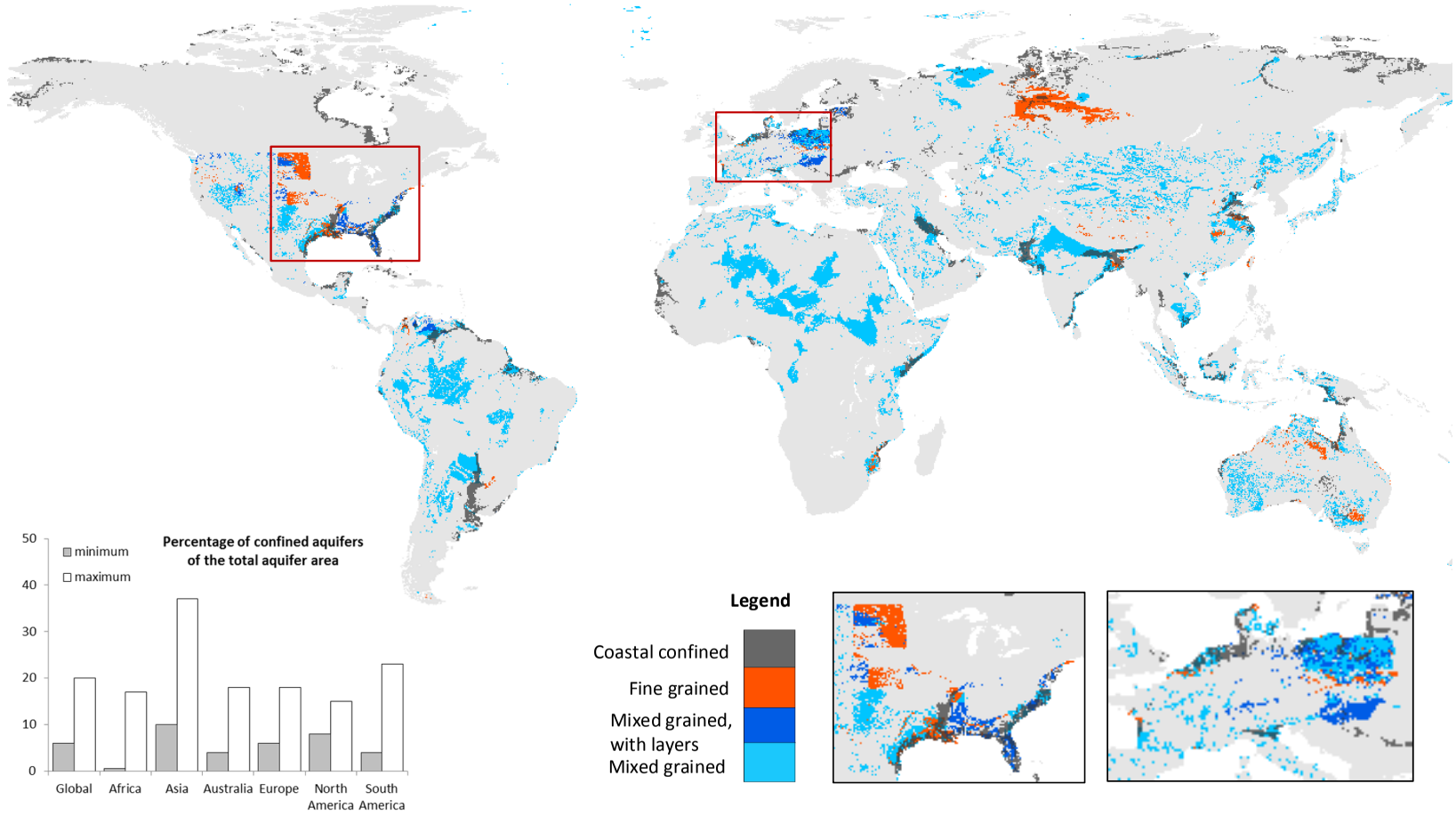

Fig. 4.2: Map of defined confining layers for unconsolidated sediments. The zooms illustrate the difference in quality of the input data used for the lithological map. The histogram shows the global percentage of confining layers assumed for the minimum and maximum scenario, and per continent.

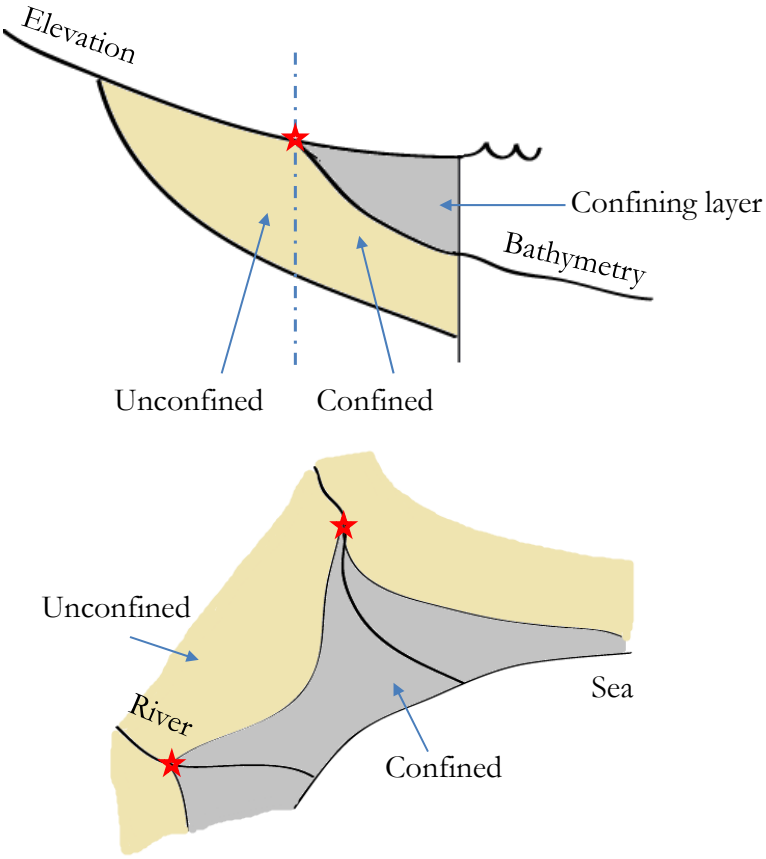

Fig. 4.3: Top) 2-dimensional schematization of coastal confined aquifer classification. The star indicates the apix. Bottom) spatial expansion coastal confined aquifer.

this finding and by lack of any other information, we decided to apply a thickness of 10% of the total estimated thickness to all confining layers not located near the coast.

4.2.3 Sensitivity analysis

The focus of the sensitivity analysis lies on the effect of confined aquifer systems on groundwater head fluctuations, groundwater flow patterns, groundwater-surface water interactions and storage changes. Three scenarios are formulated describing different spatial distributions of confined and unconfined aquifer systems: (1) unconfined systems only ((following de Graaf et al., 2015), (2) confined systems for fine grained unconsolidated sediments and mixed grained unconsolidated sediments with fine grained layers (30%) (in GLiM) and coastal confined regions (minimum confining scenario), and (3) confined systems for fine grained and all mixed grained unconsolidated sediments and coastal confined regions (maximum confining scenario). The parameter settings of confined and unconfined systems are used as described above (Figure 4.4 and Table 4.1)

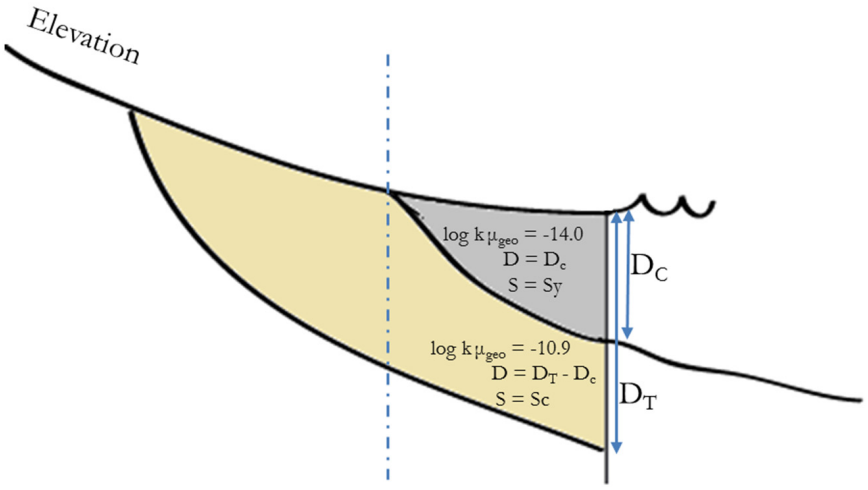

Fig. 4.4: Used aquifer parameter settings for unconsolidated sediments for confined aquifer systems. D is thickness [m], D_T is the total estimated aquifer thickness, D_c is estimated thickness of the confining layer. For conductivity the geometric mean logarithmic permeability, $logk\mu_{geo}$ [m^2], for fine grained (confining layers) and coarse grained sediments (confined aquifers) is used. S is the storage coefficient, defined as specific yield (confining layer, values Table 4.1) or storage coefficient (confined aquifer).

4.2.4 Human water use

Data on human water use were incorporated in the PCR-GLOBWB run and adopted from Wada et al. (2014) and de Graaf et al. (2013). To overcome the lack of available spatially explicit data, sectorial water demands were estimated using country statistics and population numbers downscaled to 30 arc-minutes resolution. To approximate economic development over the model period, data of Gross Domestic Product, electricity, and household consumption were used. Industrial water demands were kept constant over the year, while domestic demand reflects seasonality in air temperature. Irrigation demand is calculated assuming optimal crop growth, accounting for bare soil evaporation and soil water availability (see Wada et al. (2014) for more details on the calculation of irrigation water demand). Total water demands were dynamically attributed to surface water and groundwater resources, based on the simulated availability of the water resource (see de de Graaf et al. (2013)) for more details on the dynamic attribution).

The groundwater abstractions following this attribution in PCR-GLOBWB were subsequently used as input for the MODFLOW model through the WELL-package. For confined systems all abstractions were located in the confined aquifer, for unconfined systems abstractions were located in the bottom layer, however this bottom layers has the same conductivities and storativities as the top layer. The MODFLOW model was additionally forced with PCR-GLOBWB river discharge and recharge outputs that

include abstractions and corresponding return flows over the model period 1960-2010.

Over the past decades, total water demand increased globally from approximately 900 km^3y^{-1} for 1960 to 2000 km^3y^{-1} for 2010 (Wada et al., 2010). Total groundwater abstractions increased globally from approximately 460 km^3y^{-1} for 1960 to 980 km^3y^{-1} for 2000 (de Graaf et al., 2013). These values are in the same range as reported rates, 321 km^3y^{-1} for 1960 to 734 km^3y^{-1} for 2000 (www.un-igrac.org).

4.2.5 Summary of the model coupling

PCR-GLOBWB and MODFLOW are only coupled one-way. PCR-GLOBWB is first run over the period 1960-2010 with daily time steps. Next, the following outputs are passed to MODFLOW as monthly averages: surface water levels are passed to the RIV-package, net recharge (seepage from the second soil reservoir plus groundwater return flows minus capillary rise) is passed to the RCH-package and groundwater abstractions are passed to the WELL-package. Finally, MODFLOW is run over the period 1960-2010 at monthly time steps with these fluxes and boundary conditions imposed.

This type of coupling ensures that the same amount of water passes through the groundwater model as through the groundwater zone (third reservoir) of PCR-GLOBWB and also yields the same global average flux between surface and groundwater. Thus the coupling ensures full terrestrial balance closure. Also, it implicitly includes capillary rise which is calculated in PCR-GLOBWB (see van Beek et al. 2011) and is included in the net recharge. However, it does not include feedback effects of groundwater levels on the partioning of surface fluxes as a full coupling would do. In a next paper we will present a setup that includes a full coupling between PCR-GLOBWB and the global groundwater model.

4.2.6 Groundwater flow patterns

The effect of confined systems on groundwater flow patterns is analyzed by simulating groundwater flow paths and groundwater-surface water interactions. Groundwater flow paths and travel times were simulated for heads averaged over the simulation period, comparing two model setups: unconfined and confined aquifer systems (the unconfined and maximum confining scenarios from the sensitivity analysis). Flow paths were calculated with particle tracking in MODPATH (Pollock, 1994), using cell- to-cell flux densities [volume/time/area] as input. In MODPATH a flow path is computed by tracking the particle through the subsoil from one cell to the next, from the location of infiltration toward the point of drainage.

Following Schaller & Fan (2009) the spatial redistribution of local recharge can be evaluated using the ratio between groundwater drainage and recharge: Qgw / Rgw. The ratio is estimated for sub-basins that we defined using stream-orders, starting from

the second stream-order at 5 arc-minutes. The local drainage network was defined at the 5 arc-minute grid-cell, and for every cell a stream is present. It follows that, for a ratio of 1, all water recharged in the basin is also drained in the basin, or cross basin- boundary groundwater inflows and outflows are approximately equal. If part of the water recharged in the catchment flows to a neighboring catchment and it is not compensated by cross-boundary inflow, the catchment‘ s groundwater drainage is less than groundwater recharge, thus Qgw / Rgw < 1. The catchment is then classified as a net ‘groundwater exporter‘İf more water is drained than recharged in the catchment the catchment, the catchment is classified as a net ‘groundwater importer‘ and Qgw / Rgw > 1. Deviations from 1 are primarily a function of geology, while climate and basin size influence the magnitude of these deviations (Schaller & Fan, 2009). The spatial pattern of net importers and exporters is expected to change by including confined aquifer systems.

4.2.7 Evaluation of simulated groundwater heads

The model performance was validated by evaluating simulated- to observed water table head time-series. Heads (with reference to ocean level) instead of depths were used as heads measure potential energy and are therefore more meaningful than depths.

Time-series were selected for the US (available from the USGS: www.usgs.gov/water) and Europe (Rhine-Meuse delta Sutanudjaja et al., 2011). The used time-series have a record covering at least five years and include seasonal variation; for the US ∼28000 stations, for Europe ∼6000 stations were available. In case multiple stations were positioned in one grid cell, we elected not to average these but use them as they are, because the different stations generally have observations over different time periods. Also, stations have different surface elevations or are placed in different aquifers (i.e. deep or shallow).

The evaluation focused on mean monthly values, timing of fluctuations (given by the cross-correlation coefficient R), and amplitudes. The latter is compared by the (relative) inter-quantile range error, Q_{RE}, calculated as:

$$Q_{RE} = \frac{IQ^m_{7525} - IQ^o_{7525}}{IQ^o_{7525}} \tag{4.5}$$

where, IQ^m_{7525} and IQ^o_{7525} are the inter-quantile ranges of the modeled and observed data time series.

The sample correlation is calculated as:

$$R = \frac{s_{xy}}{s_x s_y} \tag{4.6}$$

where s_x and s_y are the sample standard deviations, and s_{xy} is the sample covariance.

Maps of the different performance indicators are given at the grid-cell scale. In these maps the results of the best performing stations are given.

4.3 Results and Discussion

4.3.1 Delineation of confining layers

Figure 4.2 shows the spatial distribution of the confining layers. For the minimum confining scenario about 6% of the total aquifer area is classified as confined that belongs to either coastal confined, or fine grained and layered mixed grained unconsolidated sediments (in GLiM). This 6% is assumed to be the minimum extent of confined aquifer systems worldwide. For the maximum confining scenario about 20% of the total aquifer area is classified as confined, belonging to either coastal confined or fine grained and mixed grained unconsolidated sediments. This scenario is assumed to represent the maximum extent of confined systems. The distribution per continent does not differ much between the two scenarios (bar plots Figure 4.2). Combining the two scenarios 5.39 x 10^6 km^2 17.34 x 10^6 km^2 of the world's aquifers are expected to be confined.

4.3.2 Global pattern of groundwater depths

Figure 4.5 (top) shows the long-term average groundwater depth simulated for the maximum confining scenario. General patterns in groundwater depths can be identified, and are more or less similar for the three scenarios and comparable to previous results from de Graaf et al. (2015). At the global-scale, sea level is the main control of groundwater depth and throughout the entire coastal ribbon shallow groundwater tables are found. These areas expand inland where the flat coastal ribbon meets the major river deltas, like the Mississippi, Indus, and large wetland areas of e.g. South America. At the regional scale, recharge is the main control together with topography. Topography influences for example the heads in the flat areas of central Amazon and the lowlands of South America which receive groundwater from the higher elevated areas. High, flat recharge regions show shallow groundwater tables, e.g. the tropical swamps of the Amazon. Regions with low recharge rates show deep groundwater tables; the deserts stand out where groundwater gets disconnected from the local topography. Also, for mountain regions deep groundwater tables are simulated. In these areas local sediment aquifers smaller than the grid resolution (<10 km) are not captured, and groundwater heads are therefore underestimated (de Graaf et al., 2015).

The differences in groundwater depth between the two model layers (top: confining layer, bottom: confined aquifer) are small. Zooms of parts of the US and Europe illustrate this (Figure 4.5 bottom). For unconfined systems, where top and bottom layers have equal conductivities, any groundwater depth differences are expected to be small.

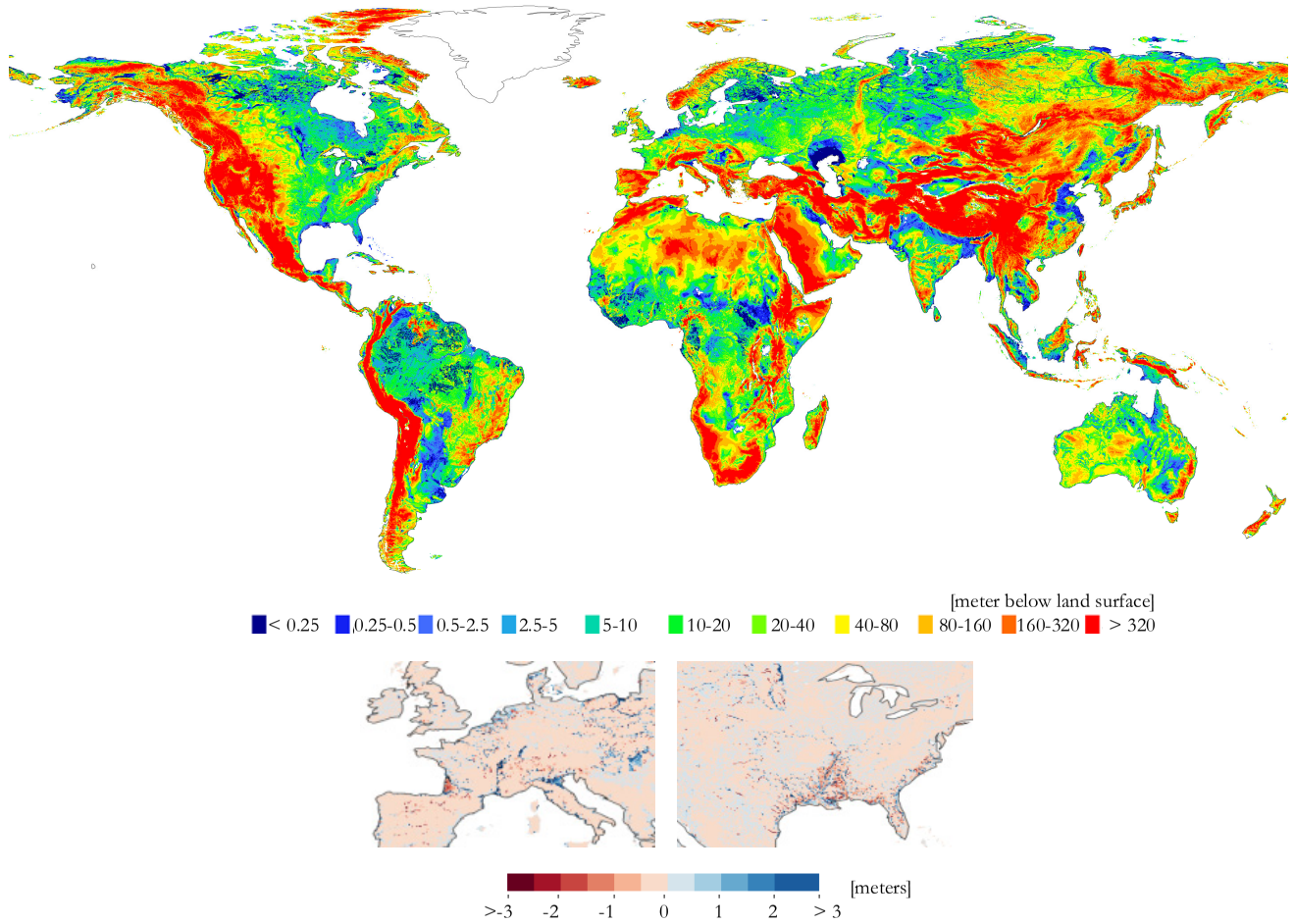

Fig. 4.5: Top) Simulated water table depths in meters below the land surface in the upper aquifer under natural conditions for the maximum confining scenario (averaged for the period 1960-2010). Bottom) head differences; bottom minus top layer. For water under pressure in the confined aquifer (bottom layer) a positive value is shown. When head in the confining layer are higher, a negative values is shown.

For confined systems, where conductivities are different for the top confining layer and bottom confined aquifer, the groundwater in confined aquifers often exhibits higher hydraulic heads than those with overlying layers. This is for example seen along the Dutch coast, Po river, Rhone, and along the Gulf of Mexico, including the Mississippi. However, when groundwater recharge does not seep through the confining layer groundwater tables can exceed the hydraulic heads of the confined aquifer. This is seen for example for in the Mississippi embayment and the Garonne region (France).

4.3.3 Evaluation of simulated groundwater head fluctuation

Model performance was evaluated for the three scenarios (unconfined, minimal, or maximal confining) focusing on mean monthly values, timing of fluctuations and amplitudes of groundwater heads. Simulated head fluctuations were compared to reported heads (for Europe and US). Note that observations (in this case long time-series covering all seasons) are often biased towards river valleys, coastal ribbons, and productive aquifers. Examples of time-series of the observed and simulated heads for the three scenarios are shown in Figure 4.6. Instead of plotting actual head values, we plotted the anomalies related to their mean values. We can conclude that the model is able to capture both timing (good timing when $R > 0.5$) and amplitude (small error when $\mid \mathrm{Qre} \mid < 50\%$) of the observed heads quite well. Also, fluctuation timing and amplitude error are better

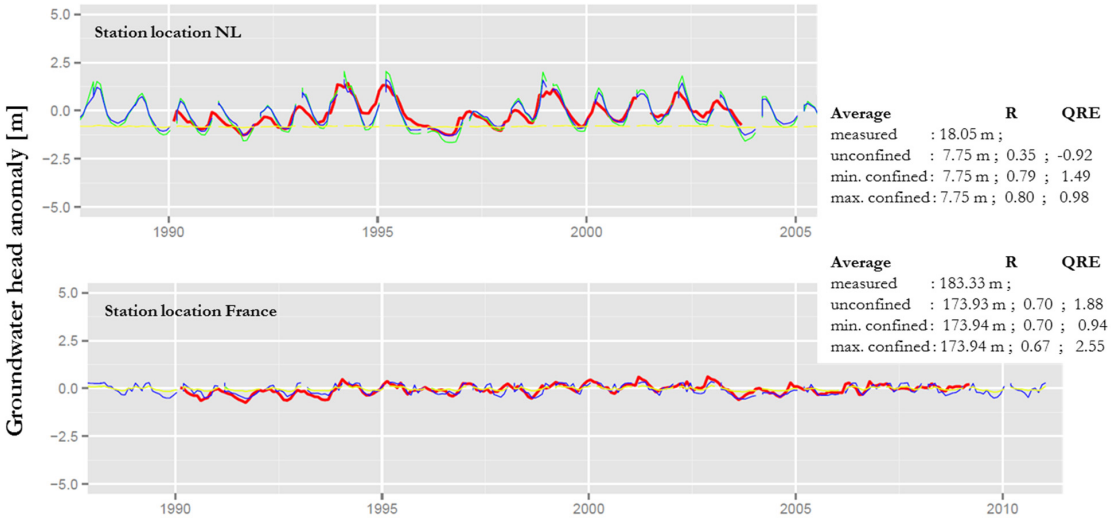

Fig. 4.6: Groundwater head anomaly comparison between measured data (red) and simulated data from the different scenarios; unconfined (yellow), minimal confined (green), maximal confined (blue).

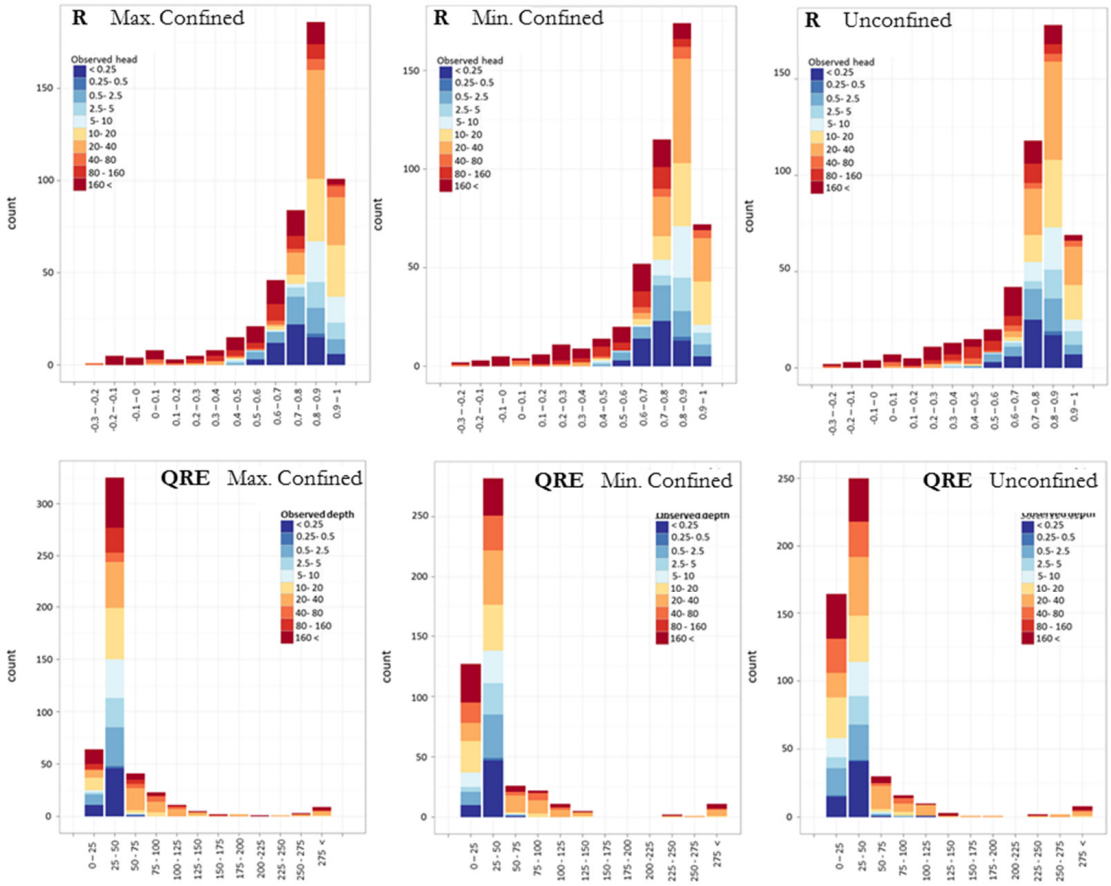

Fig. 4.7: Histograms of correlation (R) and amplitude error ($|QRE|$) for the different scenarios. Each bar in the histogram shows clustered observed groundwater depth values, averaged over the model period (1960-2010). When more than one observed head time-series was available in a grid-cell, the result shows the highest model performance value.

captured when a confined aquifer system is included (Figure 4.6).

The histograms of grid-cell maximum R, and minimum | Qre | for the three scenarios show overall good agreement in timing ($R > 0.5$), which slightly improves when confined aquifer systems are included, showing larger frequencies in classes 0.8-0.9 and 0.9-1 (Figure 4.7). Also amplitude errors are small (| Qre | $< 50\%$), and cover not only shallow groundwater depths but deeper groundwater depths as well (Figure 4.7). When including confining layers amplitude errors increase slightly shifting from 0-25% to 25-50% and from 25-50% to 50-75%. The better timing, but slightly bigger amplitude errors, are the result of the changed flow paths and residence time when confined systems are included. It also indicates that the storage coefficient of the confined aquifer is underestimated for some systems, as more storage will lead to a damped effect. However, model results are promising and show that we are able to mimic groundwater head

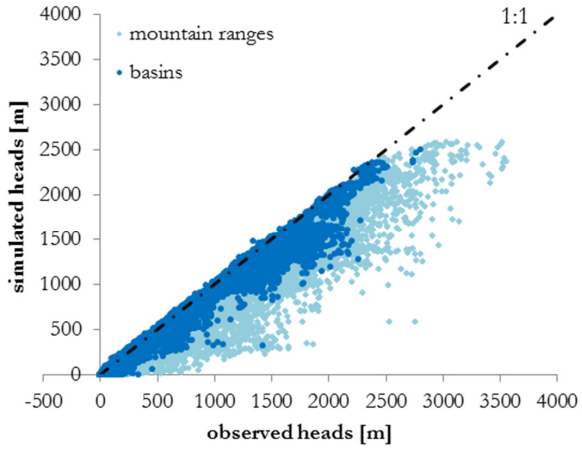

Fig. 4.8: Comparing averaged observed heads against simulated heads for the maximum confining scenario, for mountain ranges (in general deep groundwater levels) and basins (in general shallow groundwater tables).

Table 4.2: Coefficients of determination (R^2) and regression coefficient (α) corresponding to the scatter of Figure 4.8.

	All	Basins
R^2	0.95	0.99
α	0.75	0.85

fluctuations well if confined layers are considered.

The scatter and statistics (Figure 4.8, Tabel 4.2) of temporal mean simulated values against mean observed values for the maximum confining scenario show that averaged values are reproduced well (very high R^2 and α), and slightly better when only sediment basins were considered in the comparison. Model performance of the other scenarios is comparable.

4.3.4 Groundwater patterns

Flow paths simulations were done using averaged groundwater heads (1960-2010) for the unconfined and maximum confining scenarios. We focus the discussion on part of the US (Figure 4.9) as this region contains shallow and deep groundwater tables and confined and unconfined aquifer systems, and has been the focus of related previous studies (Schaller & Fan, 2009; Gleeson et al., 2011). Confined systems are e.g. found for the High Plain aquifer, along the Gulf of Mexico, and Mississippi embayment (Figure 4.9 left). The simulated flow paths show how groundwater recharge is redistributed over time and space (Figure 4.9 middle and right). Longer flow paths, crossing catchments boundaries, provide additional recharge to the importing catchment, thereby supporting water budgets in that catchment. The deference between the unconfined and confining scenario (maximum) is evident (Figure 4.9). Travel distances and travel times are generally shorter if confining layers are present. This results from the lower permeability providing higher groundwater tables, higher drainage densities and as a consequence

more local groundwater systems. Occasionally flow lines end up in the lower aquifer where they become disconnected from the surface water system over longer distances resulting in longer travel times. The flow lines in the case of unconfined aquifers are much longer with longer travel times as groundwater tables are generally deeper and groundwater systems are larger in size.

The spatial redistribution is also shown by the ratio between groundwater baseflow and groundwater recharge (Qbf : Rch) within a sub-basin (Figure 4.10). In this study the sub-basin is defined by stream-order, starting from the second stream-order. A ratio of 0.1 means 90% of the recharged water is exported, a ratio of 2 or larger means at least half of the groundwater drainage comes from neighboring catchments. The histograms in Figure 4.10 show the effect of confining units on the distribution of net groundwater importer and exporter sub-basins. The map (Figure 4.10) shows that for the deeper groundwater table regions, where confining layers are present groundwater importer ratios get smaller. Smaller ratios for the confining scenario are seen for e.g. for the Rio Grande river. In regions with more shallow groundwater tables, where ratios are close to 1, shifts to either net importing or net exporting sub-basins when confining layers are introduced. A shift in ratios is seen e.g. along the Gulf of Mexico.

4.3.5 Effects on human water use

Figure 4.11 shows a global map of total volumetric groundwater depletion per grid cell over the period 1960-2010, for the maximum confining scenario. The well-known hotspots ((e.g. de Graaf et al., 2013; Richey et al., 2015; Scanlon et al., 2012) of groundwater depletion appear, e.g. High Plain aquifer, Indus basin, and Saudi-Arabia.

We calculated the depletion trend for the maximum confining scenario and unconfined

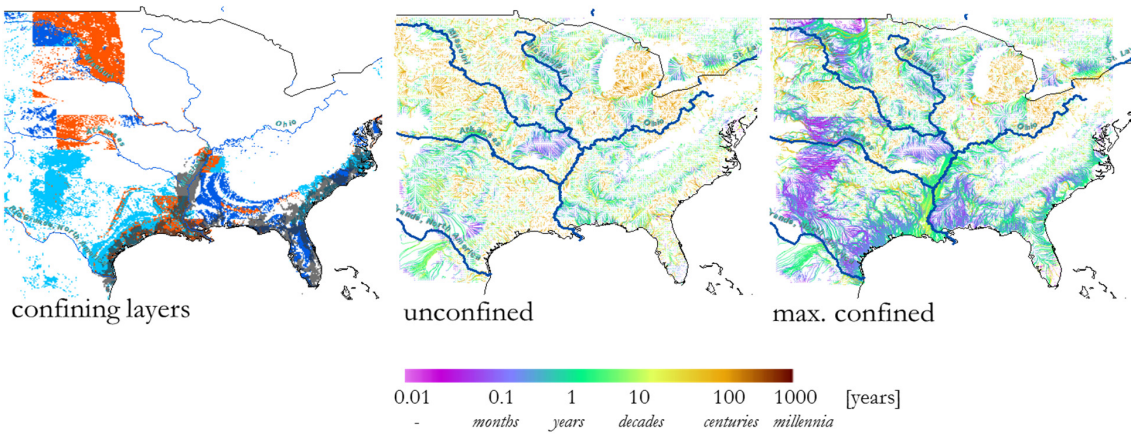

Fig. 4.9: Defined confining layers and simulated flow paths for a part of the US for the unconfined and maximum confined scenario. Flow paths are overlain by major rivers.

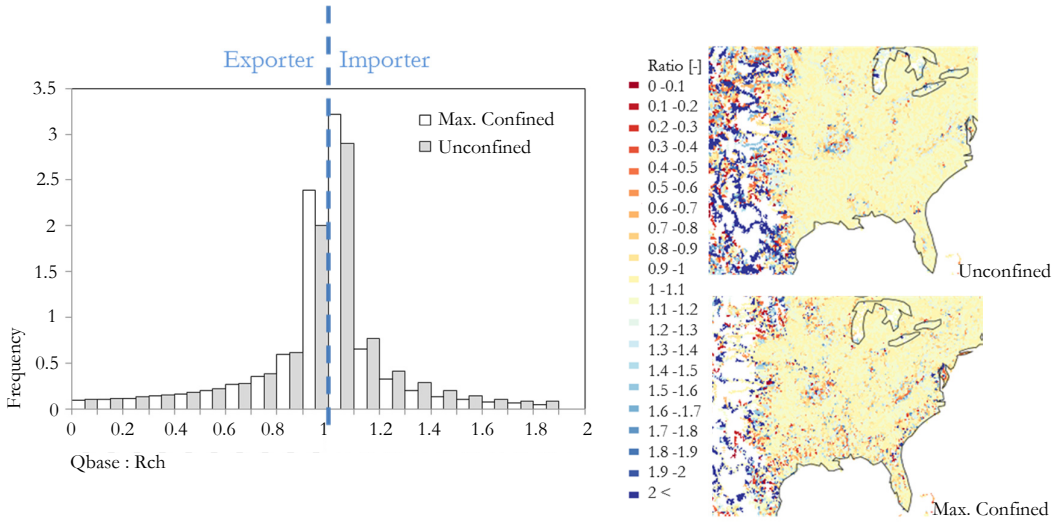

Fig. 4.10: The degree of confining shifts the ratio of groundwater importing and exporting between basins. Left: frequency of sub-basins found at a given Q_{gw} / R_{ch} ratio: comparing the results of maximal confining and unconfined scenarios. Right: Zooms for Q_{gw} / R_{ch} ratio, shows the spatial distribution. White areas present 'missing values 'where recharge is 0 md^{-1}.

scenario, calculated using head declines and storage coefficients. We compared these estimated to the difference between recharge and groundwater abstraction per grid-cell (Figure 4.12). The trend for the maximum confining scenario shows a larger inter annual variability. The noisy signal can be explained by the lack of a deep unsaturated zone in our modeling approach. It means that year-to-year variation in precipitation surplus (P-E) directly results in similar variation in groundwater recharge, allowing for a temporary recovery of areas where recharge and abstraction rates are close. The total trend shows steady groundwater depletion over the period 1960-2010. Total groundwater depletion over this period is estimated at 8307 km^3, comparable to previous published estimates of volume and flux-based approaches, see Table 4.2.

The unconfined scenario shows in general the same trend. However the estimated groundwater depletion is larger. The estimated depletion difference is 2312 km^3. This difference can be explained by the increase in river capture under the confined scenario. The presence of a confining layer results in a larger area of influence of head decline. Despite the lower permeability of the confining layer, this larger area of influence causes a larger decrease in baseflow or a larger increase in riverbed filtration. Indeed, the groundwater drainage rate of the confined aquifer model is 50 km^3 y^{-1} lower than that of the unconfined aquifer model, which adds to 3000 km^3 over 1960-2010.

The estimated depletion calculated as the deficit between groundwater recharge and abstraction for cells where more water is abstracted than recharged (flux-based method as used in e.g. (Pokhrel et al., 2012)) shows much bigger depletion volumes of 18960

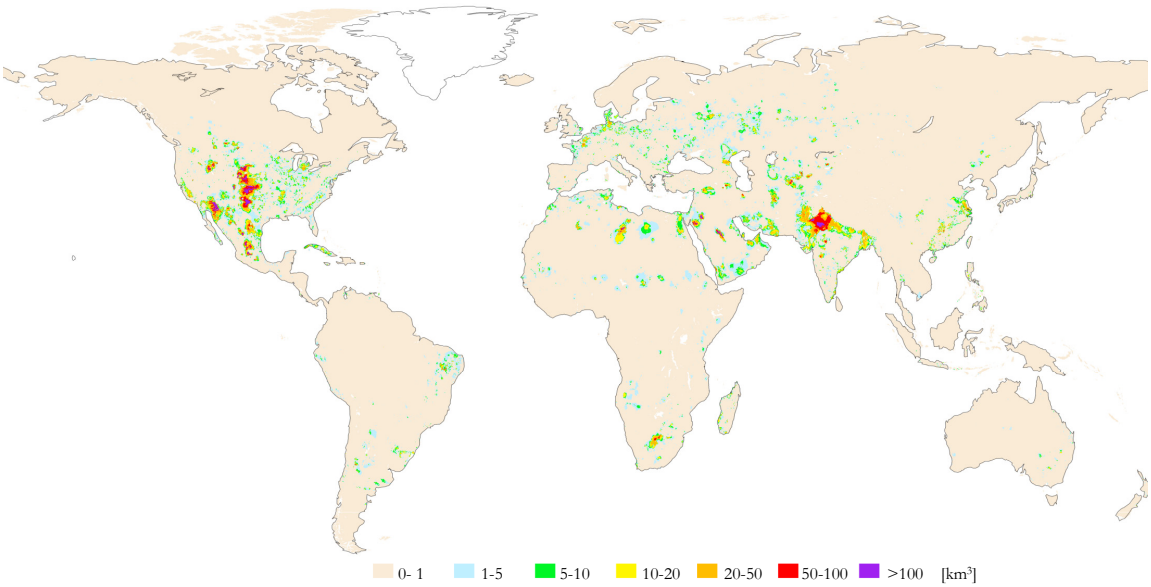

Fig. 4.11: Groundwater depletion volume (over 1960-2010) resulting from human water use for the maximum confining scenario.

km^3. Again the difference is estimated depletion can be explained by the increase in river capture, which is not accounted for by calculating the recharge-abstraction difference but is included in the groundwater model. The large difference confirms the preferred use of a lateral groundwater model, accounting for groundwater- surface water interactions, when sensitivity of aquifers to storage changes is studied. Our estimated value is still significantly higher than e.g. the estimate of the volume-based approach of (Konikow, 2011) (2000 km^3 1960-2000). The reason for this lies in the fact that Konikow et al. (2011) extrapolated U.S. depletion values to the world.

Table 4.3: Previous published depletion cummulatives (over 1960-2000) compared to this study

Global total	km^3
Pokhrel et al. (2012)	18000
Wada et al. (2010)	8000
Wada et al. (2012)	5000
Konikow (2011)	2000
this study	6700

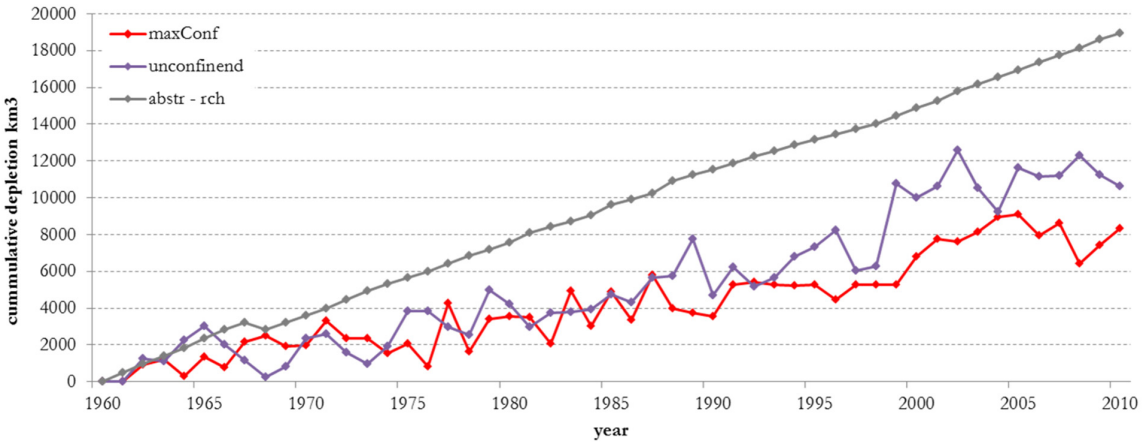

Fig. 4.12: Trend of depletion globally, estimated for the maximum confining and unconfined scenario, and calculated as the deficit cumulative between recharge and abstraction for grid-cells where abstraction is larger than recharge.

4.4 Conclusion

This paper presents a global-scale groundwater model simulating lateral flows and head fluctuations over the period 1960-2010. It is the first global-scale groundwater model that classifies the worldâs aquifers in confined and unconfined systems in order to understand aquifer sensitivity to groundwater abstractions and to properly project future groundwater level declines. Also, groundwater-surface water interactions were accounted for. The aquifer parameterization was based on global datasets of surface geology and hydraulic properties and topography-based estimates of the vertical structure of the aquifer systems. Only globally available data sets were used to keep the methods readily applicable to data-poor environments. The worldâs aquifers were classified into confined and unconfined systems to understand aquifer sensitivity to groundwater abstractions and to properly project future groundwater level declines. Confined aquifer systems are more sensitive to changes in groundwater storage than unconfined systems.

Inclusion of confined aquifer systems (estimated 6% to 20% of the total aquifer area) changes timing and amplitude of head fluctuations, as well as flow paths and groundwater-surface water interactions rates. Model performance on average heads and timing of fluctuations was slightly better when confined systems were considered. Groundwater flow paths within confining layers are shorter compared to paths in the aquifer, while flows within the confined aquifer can get disconnected from the local drainage system due to the low conductivity of the confining layer. This change in groundwater hydrology is reflected in head fluctuations and flow magnitudes.

Lateral groundwater flows between basins are significant in the model, especially for confined aquifer areas were long, slow paths are simulated crossing catchment bound-

aries, thereby supporting water budgets of neighboring catchments or aquifer systems. The spatial distribution of groundwater recharge changes for confined aquifer systems.

The estimated global depletion over the period 1960-2010 is 6777 km^3. This value is in the range of earlier published values (e.g. 8000 km^3 (Wada et al., 2010), 5000 km^3 (Wada et al., 2012)). Hotspot regions of depletion are found for intensively irrigated areas, like the High Plains aquifer (540 km^3) or Central valley (60 km^3) (both in the same range with reported values $\sim$350 km^3 and $\sim$80 km^3 (Scanlon et al., 2012). The comparison of depletion volumes for confined, unconfined, and estimated as the deficit between recharge and abstraction, showed that increase in river capture lowers the estimated depletion volume. This confirms that a lateral groundwater model, with realistic parameter settings for its aquifers, is preferred when sensitivity of aquifers to groundwater abstractions is studied.

Of course there are several limitations to our approach. Firstly, the grid-resolution (5 arc-minutes, approx. 10 km at the equator) is still too coarse to capture local aquifers in higher and steeper terrain. Groundwater heads are underestimated for these areas. Note however, that perched water tables are in general accounted for in the PCR-GLOBWB model.

Secondly, our groundwater model is not full coupled to our hydrological model, meaning the groundwater-surface water interaction is still simplified and only one way (from surface water to the groundwater). In future work the two models will be fully coupled and two-way groundwater-surface water interaction simulated, including capillary rise into to the soil, which has not been implemented yet but whose relevance was shown in several studies (e.g. Bierkens & van den Hurk, 2007; Pokhrel et al., 2012).

This study is the next step towards a fully coupled model, and already showed that used model is a useful and relevant tool to simulate effect of water abstraction on groundwater heads and baseflows. Knowledge on this is vital and needed to ensure sustainable water use, particularly for the semi-arid regions of the world, where groundwater abstractions will intensify due to an increase in drought frequency and duration combined with population growth, expanding irrigation areas, and rising standards of living.

Acknowledgements
This study was funded by the Netherlands Organization for Scientific Research (NWO) in the project Planetary Boundaries Fresh Water Cycle.

.

Chapter 5

Limits to global groundwater consumption

Groundwater is the largest accessible freshwater resource and is critical important for irrigation, and thus for global food security. Yet, many large aquifer systems are depleted and abstraction rates are unsuistainable on the long run. The main objective of this study was to estimate past and future (1960-2050) trends in groundwater levels as a result of changes in abstractions and climate and predict at what time in future limits of groundwater consumption are reached. These limits are explored by predicting where and when groundwater levels drop that low that groundwater becomes unattainable for abstractions. Also, the effect on river low flows is studied. Water availabilities, absractions, and lateral groundwater flows are simulated using a coupled version of the global hydrological model PCR-GLOBWB and a groundwater model based on MODFLOW. We estimated that in 2050 groundwater becomes unattainable for ∼20% of the global population, mainly in the developing countries of the world. Pumping cost will increase with 3980 million US$ compared to costs in 1960. Regionally, an increase or decrease in exploitation cost will be an essential factor in further economic developement and should be carefully considered in order to warrant a reliable groundwater supply under changing climate conditions

in preperation for submission: de Graaf, I.E.M., L.P.H. van Beek, E.H. Sutanudjaja, Y. Wada, M.F.P. Bierkens, Limits to global groundwater consumption.

With rising global population numbers and economic growth the earth's resources become more and more taxed. One essential resource for human existence is freshwater. Our freshwater resources are under simultaneous threat of increasing water demands and human-induced climate change, leading to more frequent and severe droughts (Taylor, 2013). Groundwater is the largest accessible source of freshwater globally and provides a reliable and substantial reserve. Groundwater is already widely exploited, with ∼70% of pumped groundwater being used to sustain irrigation and safeguard food production (Döll & Siebert et al, 2002; Siebert et al., 2010). With rising food requirements this dependency will only increase in the near future, highlighting the central place of groundwater within the food-water-energy nexus. In areas with high water demand, groundwater abstractions often exceed groundwater recharge rates, causing a permanent loss of stored groundwater and rendering these abstractions unsustainable in the long run (e.g. Rodell et al., 2009; Aeschbach-Hertig & Gleeson, 2012). Moreover, part of the

abstracted groundwater ends-up in the ocean, and will be lost as a freshwater reserve (Wada et al., 2010). The direct effect of groundwater depletion (i.e. the permanent loss of stored groundwater) is the lowering of groundwater tables, which progressively reduces the stock of attainable groundwater. In addition, falling groundwater levels induce land subsidence (Giordano, 2009), increasing the flood risk in the world's deltas particularly. Finally, falling groundwater tables lead to reduced groundwater discharge that help to sustain river flows, lake levels, wetlands, and essential ecosystem services during times of droughts (e.g. Postel, 2000; de Graaf et al., 2013).

The expected growing dependence on groundwater and the negative effects of unsustainable groundwater use pose the urgent question: What the limits are of global groundwater consumption and where and when these limits are reached? We defined these limits in terms of available groundwater that can be abstracted using conventional methods, i.e. using wells and pumps. With falling groundwater tables, the costs for the maintenance of wells and to furbish more powerful pumps will rise and groundwater abstractions will become unprofitable and eventually technically impossible (World Bank).

We explore the limits to groundwater extraction for the first time using a global physically-based surface water-groundwater model to evaluate two trends; 1) the historical development of groundwater abstraction and effects on groundwater reserves under the observed climate of the recent past (1960-2010); 2) the future developement assuming a 'constant water demand scenario' in which we assume the groundwater demand of 2010 to remain constant in the future while accounting for climate change until 2050 (using the output of the GCM HadGEM2-ES under climate scenario RCP 8.5 [available from: cmip-pcrmdi.llnl.gov/cmip5]). This constant water demand scenario highlights the possible effects of climate change in relation to high groundwater demand in a globalized industrial world while reducing the uncertainty that is associated with scenarios of future socio-economic development.

We evaluate the two scenarios by studying declines in groundwater reserves and decreases in river flows resulting from falling groundwater levels caused by abstractions. We impose water demands to evaluate abstractions and water availability using the global-scale hydrological model PCR-GLOBWB (van Beek et al., 2011), coupled to a groundwater model based in MODFLOW, simulating lateral groundwater flows (McDonald & Harbaugh, 2000; de Graaf et al., 2015, prep). The model includes a water resource module that dynamically allocates water demand to groundwater or surface water resources based on water availability in the resource (de Graaf et al., 2013). The model runs on a daily time-step at 5 arc-minutes ($\sim$10 km at the equator) resolution globally. The model parameterization is done based on the best available global data-sets, including hydrological information essential for the aquifer parameterization (Gleeson et al., 2014; de Graaf et al., 2015, prep). Model outcomes are validated to observed river flows and groundwater heads (van Beek et al., 2011; de Graaf et al., 2015, prep). Water demands are included and encompasses four sectors (irrigated agriculture, industries, households, and livestock) (see Supplementary Information (SI) for the model setup (SI 1,2,3,4)). Changes in groundwater and surface water availability are evaluated

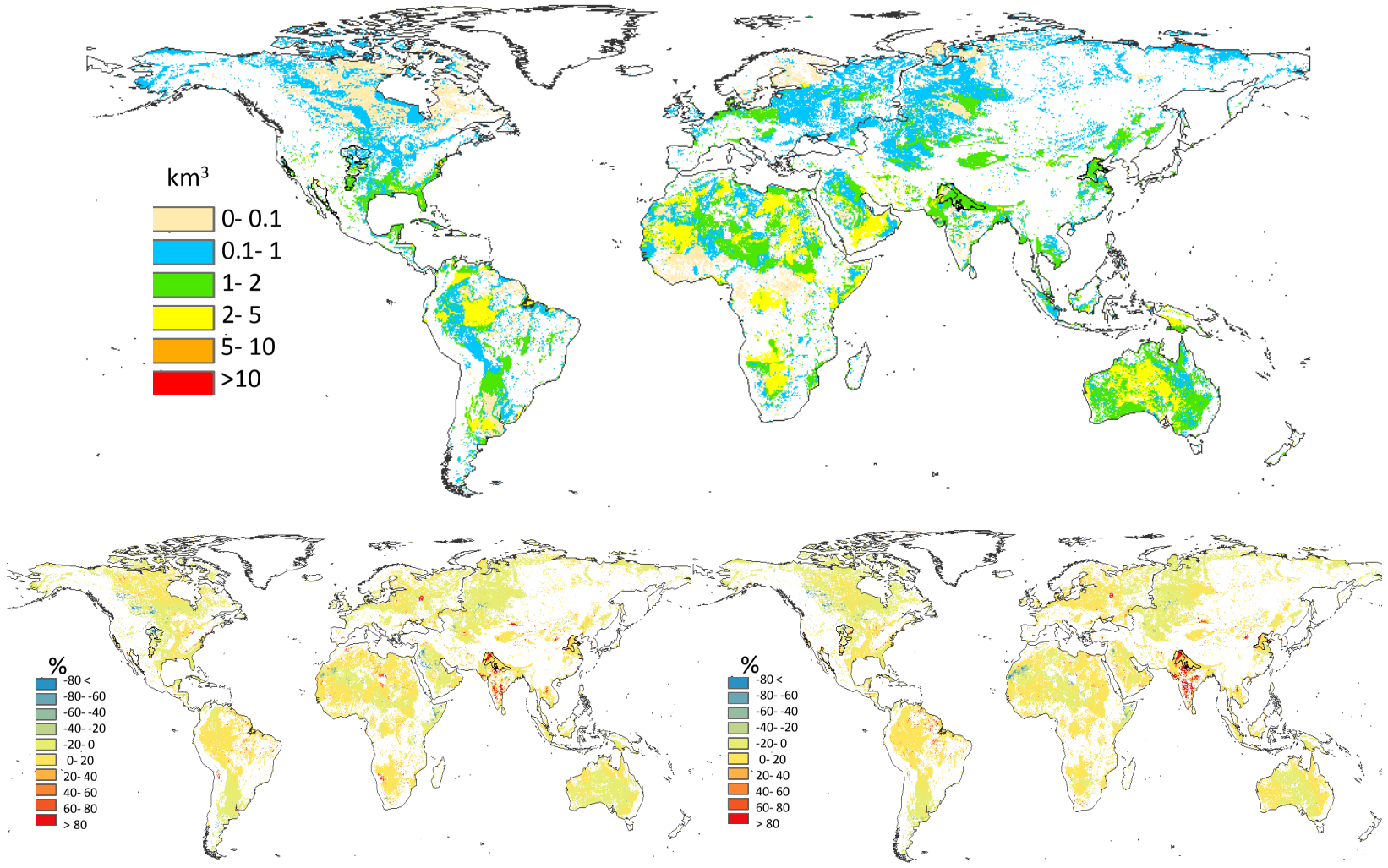

Fig. 5.1: Exploitable groundwater volume (km^3) per grid cell (5 arc-minutes) above the economical limit of 100 m below the surface over the globe in 2010; b) Relative change (%) in exploitable groundwater volume in 2010 (negative for increase); c) the same as b, but for 2050.

using 1960 as a reference. Falling groundwater levels are assessed relative to two limits: (1) a depth of 100 m below the surface at which groundwater becomes unattainable for farmers using local pumps as is the case in many irrigated areas in developing countries (World Bank); (2) a head difference larger than 300 m between phreatic groundwater heads and heads in the well, which is the typical exploitable limit of industrial scale pumps employed in developed countries (World Bank). The first depth is interpreted as an economic limit, as investments to exploit deeper groundwater cannot be borne by the farmers themselves. The second depth is interpreted as technical limit, as it would require major investments to develop new and better well-drilling and pumping techniques to access deeper groundwater. We assume the economic or technical limit is reached when the limiting depth is exceeded for at least two consecutive years. We show the spatial distribution globally when these limits are reached and calculate the increase in pumping costs related to groundwater level drops (see SI 4 cost calculations).

Figure 5.1 shows the development of the exploitable groundwater volume globally with respect to 1960 for the historical period (1960-2010). We focus here on the economic limit of 100 m as this limit is the more stringent and restrictive to local development (see Figure 5.6 in SI for the technical limit of 300 m). The figure concerns larger groundwater bodies (called aquifers hereafter) in unconsolidated and semi-consolidated sediments where substantial amounts of groundwater can be extracted for a unit drop in water level as the result (dependent on storage coefficient or storativity, see SI 2 for aquifer characterization). Areas where groundwater is mostly stored in the secondary porosity of jointed bedrock and wells are less productive (McDonald & Harbaugh, 2000) are masked out.

Figure 5.1 shows that by 2010, the economic threshold of 100 m has already been surpassed in some regions of the world (low exploitable volumes in Figure 5.1). The regions are in general intensively irrigated areas in the dryer climates of the world (see SI 3 for the reconstruction of historical water demand). Substantial groundwater volumes are still present in areas of lower demand or higher recharge, but for many areas of the world a decrease in the available groundwater storage can be observed in 2010 and 2050, relative to the reference of 1960 (Figures 5.1b and 5.1c). The largest volume declines in 2010 are seen for India, upto 80%, and these areas will further expand in the near future. Other hotspots are the High Plains and Central Valley, showing declines in 2010 upto 40% further increasing to 80% in the near future, and the North China Plains, with declines in 2010 of 60% increasing to 80%. Small recoveries of stored volume are seen for the Northern High plains, where the recovery is up to 80% in 2010, but declining again up to 2050 (up to 60%) as a result of reduced recharge under climate change.

Economically exploitable groundwater reserves (within 100 m in aquifers) decreased globally from $\sim$208,000 km^3 in 1960 to $\sim$202,000 km^3 in 2010. In several regions continued pumping causes groundwater levels to fall well below this economic limit (e.g., Central Valley (Scanlon et al., 2012) as early as 1960).

Cumulative depletion over the period 1960-2010 amounts to 7,864 km^3. Over 1960-2050 cumulative depletion is estimated to amount to 10,445 km^3 (Figure 5.2). The fixed

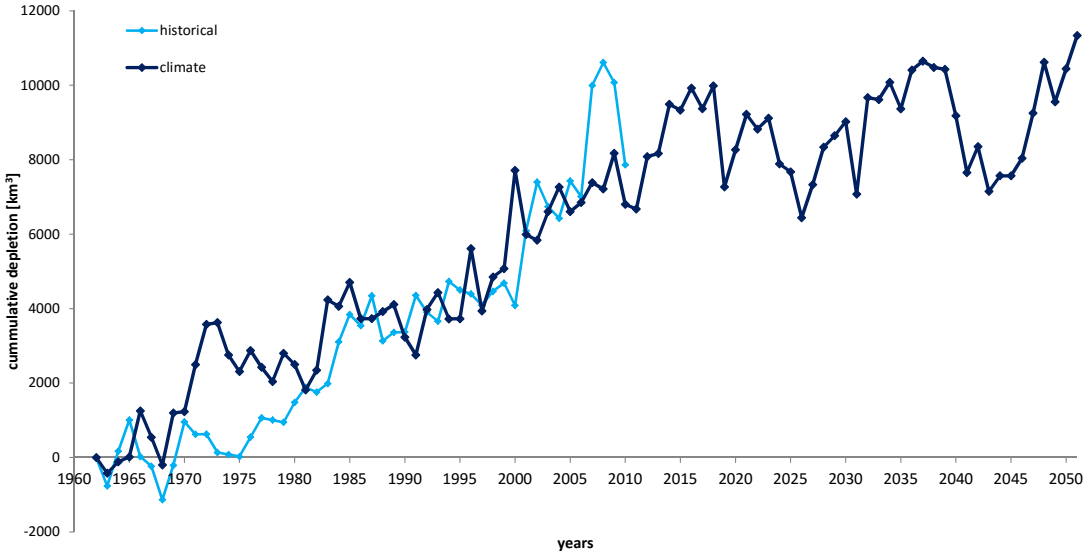

Fig. 5.2: Cumulative depletion relative to the reference 1960 using historical climate forcing and climate projection.

demand of 2010 (i.e. fixed demand for industry, households, and life stock, irrigation demand changes following climate change) results in a decrease in the rate of global depletion. The period 1990-2010 showed a depletion rate of 225 km^3 y^{-1}. This reduces to 100 km^3 y^{-1} over 2010-2050, although the higher total water demand of 2010 is used throughout. A similar change can be observed for the exploitable groundwater reserves. This break in the trend can be explained by climate change (i.e. warming temperatures and shifting precipitation patterns) by which both regional irrigation water demands and recharge will change (see SI Figure 5.7).

New areas experiencing groundwater depletion will develop in the near future, for example parts of Spain, the Middle East, and Africa. Other areas, like the Central Valley and part of the North China Plains will experience a decrease in depletion and partly recover when more recharge will get available. Notwithstanding, this regional improvement in the average groundwater status, groundwater demands will increase to buffer for more irregular streamflow occurrence (including increased hydrological drought (Dai, 2011)) under a more intense hydrological cycle in the near future (Figures SI 4 and 5). As

a result of climate change and human water use, river low flows will decrease (see SI Figure 6). The decrease due to climate change is intensified by the human water use. Largest decreases are found for irrigated regions, like for the Indus, Nile, and in future for e.g. the Danube, Rhone.

We estimate that economically exploitable groundwater (within 100 m in the aquifers) decreases to from ∼1919,000 km^3 in 2010 to ∼179,000 km^3 in 2050 whereas the technical exploitable groundwater (within 300 m in the aquifer) decreases from ∼607,000km^3 to ∼595,000 km^3. As an independent comparison to other estimates we estimated the lifespan of these aquifers as the time at which 90% of their initial storage is depleted (following (Richey et al., 2015) and found this to be in the range of 170-300 years (See SI T1). While many aquifers remain productive, economically exploitable groundwater is already unattainable or will become so in the near future, especially in intensively irrigated areas in the dryer regions of the world (Figure 5.3a). Loss of exploitable groundwater looms heavily over important agricultural areas such as the High Plains, the Indus and Ganges Basins and parts of Argentina and Australia. Locally exploitable groundwater is also falling out of reach around the Mediterranean and Middle East, in Africa, Afghanistan and Iran, and Mexico.

In terms of costs, required to sustain groundwater demand, a substantial increase can be seen over areas with noticeable depletion over the period 1960-2010, predominantly over India and Pakistan, Northern China, and the High Plains but also over fossil groundwater systems as the Nubian Aquifer and the Kalahari (Figure 5.3a). By 2050, this increase in costs is partly offset by increased recharge for Indus and Ganges Basin but they continue to increase over the eastern part of Southern Africa and for the High Plains (Figure 5.3b). Although costs partky decrease, costs remain invariably high and require major investments, especially in the case of upcoming economies. All-in-all, global costs to ensure groundwater supply amount to respectively 1798 and 3980 million US$ for 2010 and 2050 relative to the 1960 situation. Regionally, an increase or decline in exploitation cost will be an essential factor in further economic development and should be carefully considered in order to warrant a reliable groundwater supply under changing climatic conditions.

This is, to our knowledge the first global groundwater study accounting for lateral groundwater flows, groundwater-surface water interactions and abstractions for the recent past and near future. Therefore, it provides a more realistic overview of groundwater depletion and recovery due to changes in demand or climate than in previous (flux-based) studies (e.g. Döll et al., 2012; Wada et al., 2014). For the historical period, our estimates are closer to volume-based estimates over those areas where direct observations are available or indirect estimates from gravimetric anomalies can be made ((Konikow, 2011; Scanlon et al., 2012; Rodell et al., 2009); see SI T2).

However, we stress that all variables in our calculations are subject to uncertainty. Least known is the permeability of aquifers and confining layers, saturated aquifer thickness and pumping depths. In previous studies (related to this one) the uncertainty stemming from aquifer parameterization, the climate forcing, and human water demand was ex-

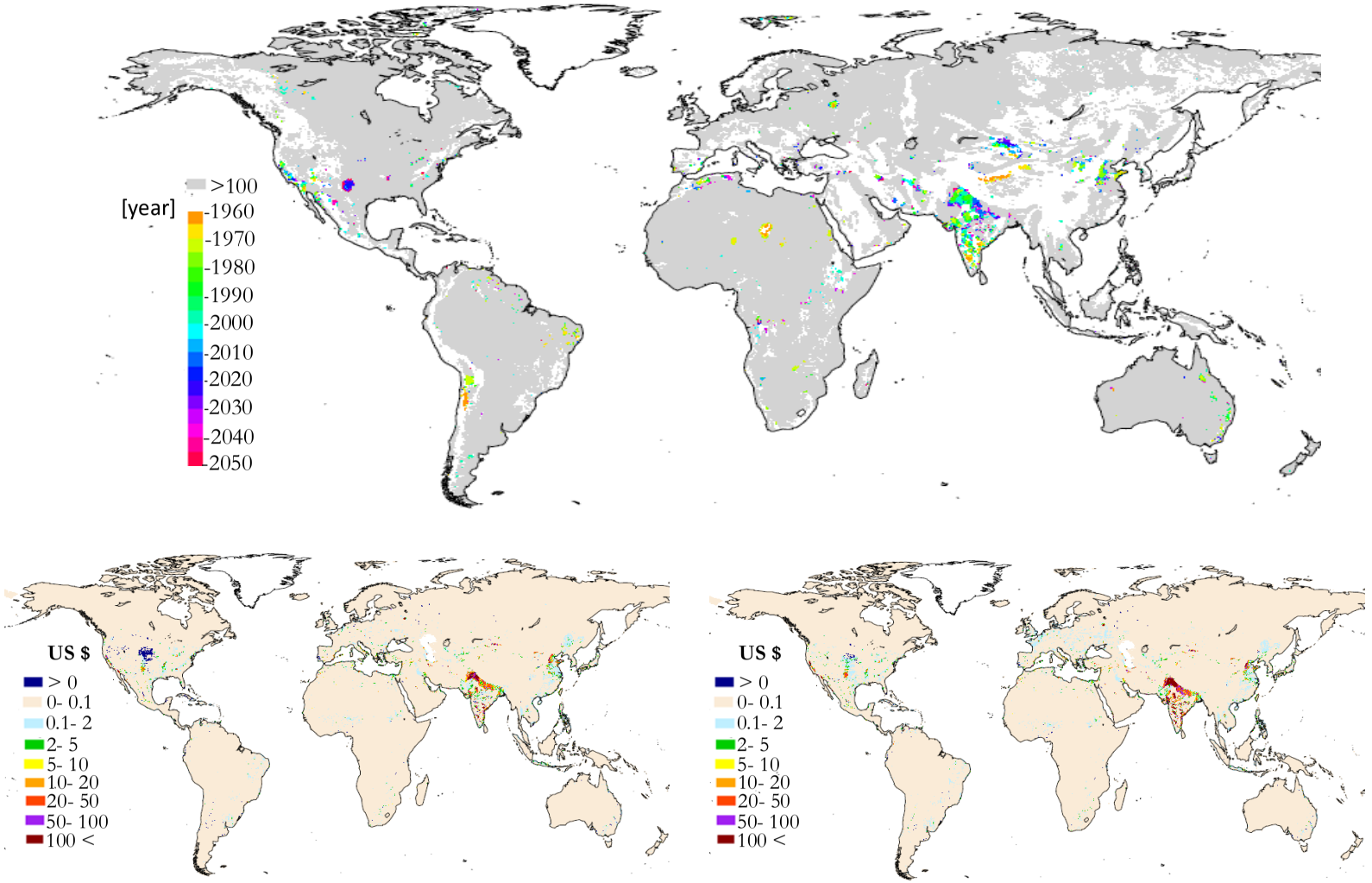

Fig. 5.3: a) First time (years) that groundwater falls below the economic exploitable limit of 100 m below the surface for two consecutive years. b) Increase in pumping costs per aquifer [US$ per 1000 m^3 extracted groundwater] for the year 2010 compared to costs in 1960; c) idem but 2050 compared to 1960

plored carefully (de Graaf et al., 2015; Wada et al., 2010, 2012). These results showed the used models can simulate river discharges and groundwater heads and fluctuations with reasonable accuracy (van Beek et al., 2011; Wada et al., 2011, 2014; de Graaf et al., 2013, 2015, prep).

It should be noted that in our assessment water demands do not increase after 2010. We opted for this 'constant water demand' approach in order to exclude the uncertainty that arises from the interplay of population growth, economic development and changing agricultural practices. We concede the presented depletion projection is therefore somewhat optimistic, as it is expected population will grow and economic development in the upcoming economies will increase water demand to levels above 2010 (UN, 2012). Still, in many regions of the world groundwater depletion continues and exploitation costs keep rising even in spite of our optimistic assumptions, indicating that locally limits of groundwater use are already being encountered or will be felt in the future; keeping the global population fixed at the level of 7 billion in 2010 we estimate $\sim$1.6 billion people are living in areas where groundwater is being depleted and has fallen below the economic limit of 100 m in the year 2010. For 2050, these numbers are estimated at respectively 1.8 and 2.5 billion people (using UN population minimumand and maximum growth projections (UN, 2012)). Evidently, this persistent and increasing level of groundwater stress will impair local development and generate tension within the global socio-economic system.

Acknowledgements
This study was funded by the Netherlands Organization for Scientific Research (NWO) in the project Planetary Boundaries Fresh Water Cycle.

Supplementary Information

I.E.M. de Graaf *et al*: Limits to global groundwater consumption

1. Model description

In this study the global-scale hydrological model PCR-GLOBWB (van Beek et al., 2011) is used to calculate the fluxes in and between two soil stores and is coupled to a lateral groundwater model (using MODFLOW (McDonald & Harbaugh, 2000; Schmitz et al., 2009). Within PCR-GLOBWB the water balance for two vertical stacked soil layers is calculated for each time-step (daily) and each grid-cell (5 arcminutes). Vertical exchange between the soil and groundwater occurs through percolation and capillary rise. Specific surface runoff, snowmelt, interflow, and base flow are accumulated along the drainage network. The original base flow calculation of PCR-GLOBWB is replaced by the groundwater-surface water exchange of MODFLOW. The drainage network consists of laterally connected surface water elements representing river channels, lakes, and reservoirs. A kinematic wave approximation at a sub-daily time-step is used to route surface water to the basin outlet.

The coupled model runs at 5 arcminute resolution globally for the terrestrial part of the world (excluding Greenland and Antarctica), for the period 1960-2050. The PCR-GLOBWB model runs at a daily time-step. The two soil stores (store 1 and 2 in Figure 5.4) have a maximum depth of 0.3 and 1.2 m respectively. The MODFLOW model runs at a monthly time-step, as this is more suitable to the slower groundwater processes, and reduces calculation times.

The groundwater model, based on MODFLOW, comprises two vertical layers. Groundwater heads, river infiltration and drainage, and capillary rise are calculated in the MODFLOW model. The recharge from the hydrological model PCR-GLOBWB is the input for the MODFLOW recharge (RCH) package, while capillary rise in the former is disabled to facilitate model coupling. The MODLFOW river (RIV) and drain (DRN) packages are used to incorporate interactions between groundwater and surface water. Three levels of groundwater-surface water interactions are distinguished: (1) large rivers, with a width greater than 25 m (2) small rivers, with a width smaller than 25 m, and (3) springs and streams higher up in the valley. When the groundwater level falls below the river or drain level, water infiltrates into the aquifer, when the groundwater levels lies above the river or drain level water is drained from the groundwater into the river. Details on the MODFLOW setup can be found in (de Graaf et al., prep).

2. Aquifer parameterization

The parameterization is based on available global datasets on permeability (GLHYMPS (Gleeson et al., 2014) and lithology (Global Lithological Map (GLiM) (Hartmann & Moosdorf, 2012), combined with an estimate of aquifer thickness (used to calculate aquifer transmissivities kD [m^2d^{-1}] (de Graaf et al., 2015) and information on the ver-

tical structure of the aquifer systems (de Graaf et al., prep). The latter includes information on the presence of confining layers, and classifies world's aquifers (that are groundwater bodies in unconsolidated and semi-consolidated sediments) in confined and unconfined systems. The inclusion of confined and unconfined systems leads to a realistic estimate of aquifer sensitivity to changes in storage by climate and human impacts. A detailed description of the aquifer parameterization method is given in the previous studies of (de Graaf et al., 2015, prep), and is summarized here.

Aquifer thicknesses were estimated based on terrain attributes, assuming that productive aquifers coincide with sediment basins below river valleys. The distinction was made between (1) mountain ranges, and (2) sediment basins representing the aquifers. The resulting map of aquifer thicknesses showed where large aquifer systems can be found, for example thick layers are simulated for the Mississippi embayment, High Plains, Central Valley, Indus and Ganges basins, and over the Sahara.

The world's aquifers were classified in confined and unconfined systems by delineating confining layers (de Graaf et al., prep). It was assumed that confining layers can be found there were unconsolidated fine grained and mixed grained sediments are described

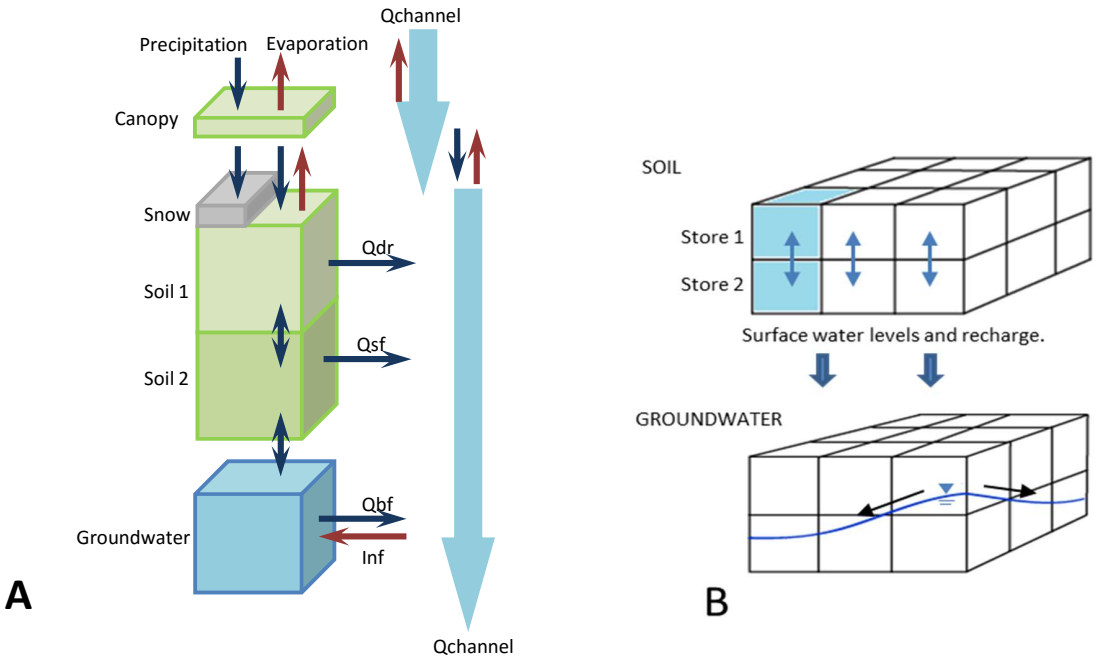

Fig. 5.4: A) schematic presentation of PCR-GLOBWB; for each grid cell the water balance and fluxes are calculated. Discharge (Qchannel) is the sum of overland flow (Qdr), subsurface flow (Qsf), and groundwater baseflow (Qbf), and is routed along the drainage network. B) The groundwater store (of A) is replaced by the groundwater model, simulating groundwater heads. PCR-GLOBWB is coupled via surface water levels and recharge to the groundwater model.

in the GLiM. Additionally, coastal zones with fine grained confining layers overlaying coarser materials were included, as these regions are underrepresented in the GLiM. This sums up to a maximum of approximately 20% of the total aquifer area covered with a confining layer (de Graaf et al., prep). The confined systems were parameterized as fine grained sediments (confining layer) overlaying coarse grained sediments (confined aquifer). For the thickness of the layer, 10% of the total thickness was assumed.

3. Water demands

PCR-GLOBWB includes a water resource model that considers water requirements for four sectors: (1) industries, (2) households, (3) irrigation, and (4) livestock.

Data on sectorial water demand for the model period were adopted from the study of (Wada et al., 2014). In their study sectorial water demands were estimated using country statistics on population numbers and spatial extend of irrigated areas, downscaled to 5 arc-minutes resolution. Generally water demand for industries and domestic uses increases with economic development (Oki & Kanae, 2006). Economic development over the model period (1960-2010) was approximated using data in Gross Domestic Product (GDP), electricity produced, and household consumption were used. For the model period 2010-2050 average water demands of 2010 were used.

In addition to inter-annual variation, seasonal variability was included for domestic demand according to air temperature fluctuations whereas industrial demand was kept constant over the year. Water recycling ratios for industries and domestic use were adopted from Wada2011 and calculated per country, based on GDP and development level, i.e. high incomes (80%), middle incomes (65%) and low income (40%) economies.

Irrigation is by far the largest water user, comprising 70% of the global gross water demand (Döll et al., 2012). Irrigation water demand was calculated for paddy and non-paddy crops (adopted from Wada et al., 2014). Optimal crop growth was assumed, reflected by maximum crop transpiration, and accounting for bare soil evaporation and soil moisture. Crop specific crop calendars and growing season lengths were used (obtained from Portmann et al., 2010) to account for seasonal variability and regional cropping practice under different climate conditions. Also, corresponding crop coefficients per crop growth stage and maximum crop routing depth were(adopted from (Siebert & Döll, 2010). The losses during water transport and irrigation application were included in the estimation of total irrigation demand by including a dynamic estimate of irrigation efficiency. This estimate is based on daily evaporative and percolation losses per unit crop area based on surface and soil water balances. For paddy fields a 50 mm of surface water depth was maintained until the late crop development stage ($\sim$20 days) before harvest (Wisser et al., 2008). Some assumptions on this water depth maintenance rule exist, which are described into more detail in Wada2014. Regions with significant paddy irrigation are e.g. India, Pakistan, China. For non-paddy crops water requirements were calculated using the actual water availability according to FAO guidelines (details also given in (Wada et al., 2014)).

Livestock water demand is for most countries very small compared to the other sectoral water demands. Globally livestock shares less than 1% of the total global water demand. However, for some African countries it cannot be neglected and livestock water demand can be larger than irrigation water demand (Els & Rowntree, 2003).

The total water demand (totDemand) per grid cell is calculated as the sum of all sectoral demands, and are used at the daily time-step:

$$totDemand = totDemand_{Industry} + totDemand_{Domestic} + totDemand_{Livestock} + totDemand_{Irrigation} \quad (5.1)$$

4. Water abstractions and return flows

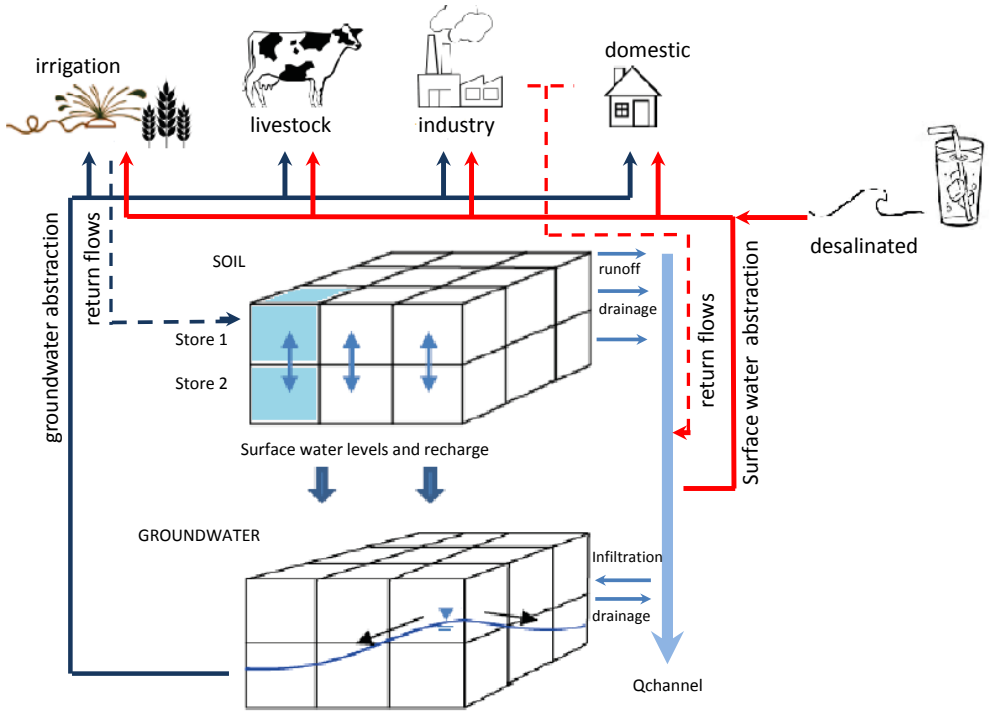

Fig. 5.5: The used allocation scheme. Water is abstracted from surface water (Qchannel) or groundwater and flows back to either the surface water or infiltrates in the soil, dependent on the user.

Total water demand can be met from (1) surface water, (2) groundwater, or (3) desalinated water. Part of the abstracted water, the part that is not consumed, flows back

as return-flow to either surface water or groundwater resources dependent on the user (de Graaf et al., 2013).

Although globally desalinated water use is small, 0.2% of the global water abstractions, it can be an important resource of water locally, e.g. in the Middle East. Country scale data of desalinated water use were taken from FAO AQUASTAT (www/fao.org/nr/aquastat), and downscaled to the coastal ribbon (∼40 km) based on gridded population intensities (Wada et al., 2011). Desalinated water use is assumed constant over the year and to be consumed entirely. Desalinated water uses can satisfy irrigation water demands within a larger grid area of 1o. This allocation over the bigger grid represents infrastructures that can transport water over larger distances.

Within the aquifer (that are the sediments basins, as described in S2) the remaining demand is attributed over groundwater and surface water resources using predefined allocation fractions of Siebert2010/2013. Outside the aquifer all demands are attributed to the surface water only. The following calculations are done:

$$Demand = TotalDemand - DWU \tag{5.2}$$

$$SWD = \text{ if } aquifer_{thickness} > 0.0 \text{ then } Demand * fSW \tag{5.3}$$

$$GWD = \text{ if } aquifer_{thickness} > 0.0 \text{ then } Demand * 1 - fSW \tag{5.4}$$

where, DWU [m] is desalinated water use, SWD [m] and GWD [m] are surface water and groundwater demands, $aquifer_{thickness}$ [m] is the estimated aquifer thickness, fSW [-] is the predefined allocation fraction.

Actual surface water abstractions are calculated evaluating surface water demand to channel discharge (routed along the drainage network, calculated in PCR-GLOBWB). Water can be abstracted from the surface water until the river runs dry. Before that, when the river discharge falls below the environmental flow condition (defined as the 90th percentile of the monthly running averaged low flow for the natural run) surface water abstractions dwindle. Surface water availabilities are positively affected by groundwater base flows (groundwater drainage, calculated in MODFLOW) and return flows, abstractions and river infiltration (calculated in MODLFOW) have a negative effect. Actual change in surface water storage, Q_{loc} [m^3d^{-1}], is calculated as:

$$Q_{loc} = Q_{runoff} - SWA - GW_{interaction} + SW_{retID} + GW_{retID} \tag{5.5}$$

where, Q_{runoff} [m^3d^{-1}] is the inflow of specific runoff (calculated in PCR-GLOBWB), SWA [m^3d^{-1}] is the actual surface water abstraction, $GW_{interaction}$ (calculated in MODFLOW) is river infiltration (flow into the aquifer, positive value) or groundwater drainage (base flow drained by the river, negative value). Whether a river infiltrated or drains depends on the groundwater head and river level; when the groundwater head lies above the river level the groundwater is drained, when the groundwater level lies under the river level, surface water infiltrates into the groundwater (de Graaf et al., 2015, prep).

The terms SW_{retID} and GW_{retID} [m^3d^{-1}] are the return flows to the surface water from industrial and domestic surface water or groundwater abstractions (illustrated in Figure 5.5. River discharge $Q_{channel}$ [m^3s^{-1}] is calculated by routing Q_{loc} along the drainage network.

When surface water demand (SWD) is larger than the available surface water, the remaining demand (SWD_{unmet}) adds up to the groundwater demand. Actual groundwater abstractions are estimated by evaluation actual groundwater storages. Groundwater storage is calculated using estimated groundwater head (calculated in MODLFOW), aquifer thickness and storage capacities. Groundwater storage is positively affected by groundwater recharge, increased by irrigation return flows, and river infiltration. Groundwater storage is negatively influenced by groundwater drainage and groundwater abstractions. Inter-basins lateral flows can contribute to the water budget of a neighboring watershed, thereby increasing water availability.

If the groundwater demand ($GWD+ SWD_{unmet}$) is larger than the available water in the groundwater store, the deficit becomes an unmet demand (GWD_{unmet}).

Both surface water and groundwater abstractions can satisfy the irrigation water demand within a larger grid area of 1°. This allocation over the bigger grid represents infrastructures that can transport water over larger distances (the same as for the desalinated water uses).

5. Calculation exploitation cost

With declining water levels, due to overexploitation of groundwater pumping costs increase. Groundwater heads and groundwater declines are calculated in this study by use of the lateral groundwater model. Actual groundwater abstractions are the output of the used allocation scheme.

Pumping cost are calculated as follows (Eq. 5.6 of Knapp et al. 2003):

First are cost calculated associated with maintaining and repairing capital (well and pump), equipment resulting from use of the well and pumps for withdrawals, plus the energy costs associated with drawdown below the water table surface as the pumps run

$$cost_{capital} = k_{cost} * wateruse \tag{5.6}$$

Where, k_{costs} is average cost per ha cm of groundwater extractions related to equipment use (e.g., US$ 0.50 (ha cm^{-1}) and wateruse is groundwater withdrawals (ha cm yr^{-1})

Second are cost calculated energy costs of lifting water from the existing water table surface to the land surface (US$):

$$cost_{energy} = e_{pumpcost} * (land_{elevation} - hydraulic_{head}) * wateruse \tag{5.7}$$

Where, $e^{pumpcost}$ denotes pumping costs per unit of lift per unit of water (e.g. US$ 0.039 (ha cm^{-1} m^{-1}).

Total costs ($) are calculated as:

$$cost_{total} = cost_{capital} + cost_{energy} \tag{5.8}$$

6. Figures and Tables

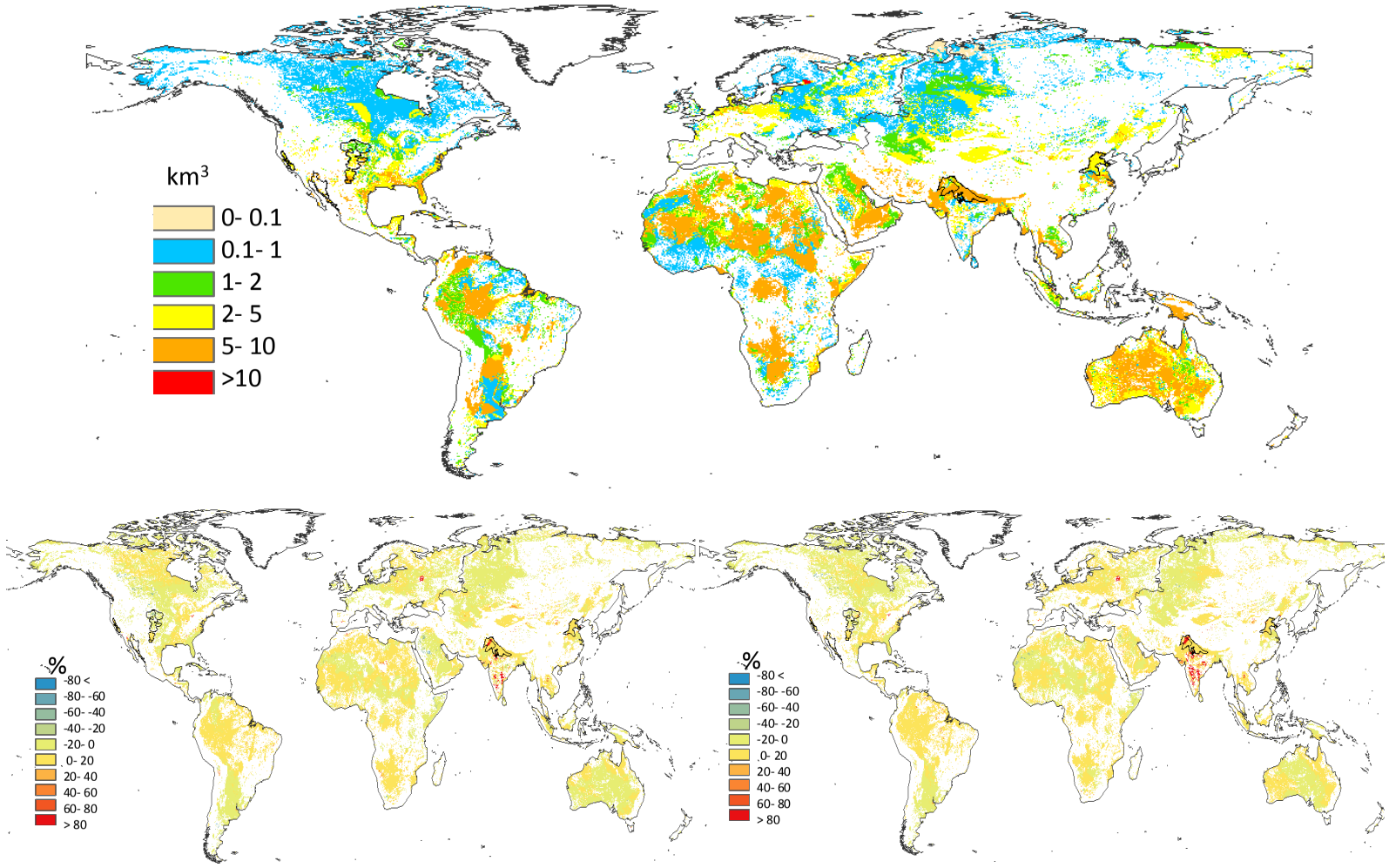

Fig. 5.6: Exploitable groundwater volume (km^3) per grid cell (5 arc-minutes) above the technical limit of 300 m below the surface over the globe in 2010; b) Relative change (%) in exploitable groundwater volume (negative for increase).

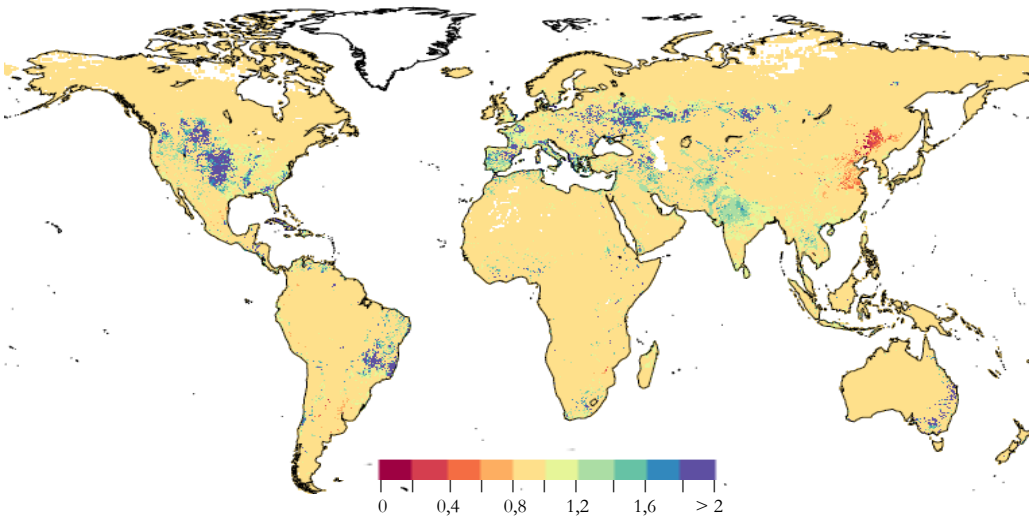

Fig. 5.7: Fraction increase in groundwater demand between 2010 and 2050 (smaller than 1 is decrease).

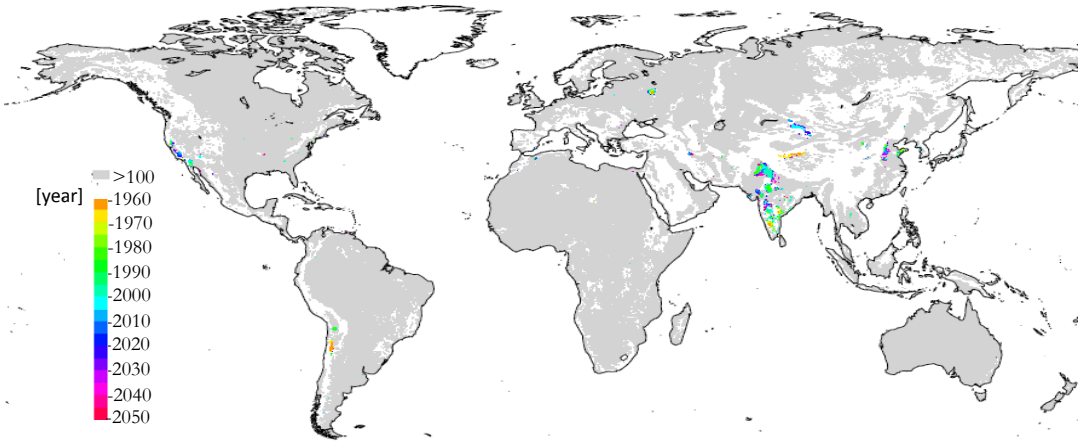

Fig. 5.8: First time (years) that groundwater falls below the economic exploitable limit of 300 m below the surface for two consecutive years.

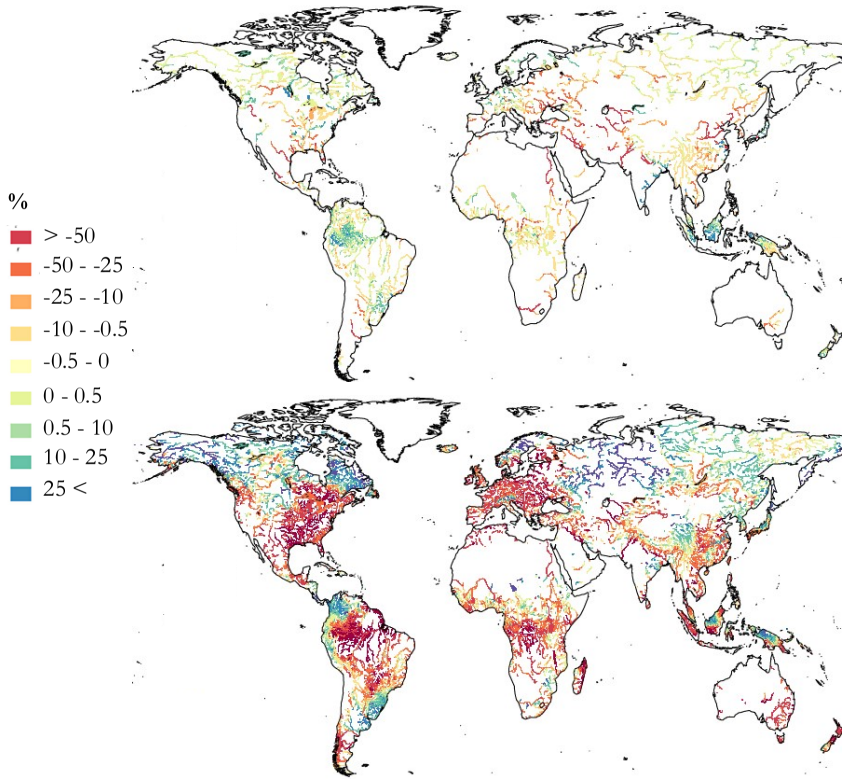

Fig. 5.9: Decrease in river low flow (Q90) in percentage, comparing Q90 for the human and pristine run over 1960-2010; b) comparing Q90 of the human run over 1960-1990 to 2021-2050. When negative Q90s decrease, when positive Q90s increase.

Table S1: Comparison this study's aquifer storage estimates and time to deplete 90% of the aquifer storage to previous published estimates

	This study			Richy et al 2015 [m^3] [e]		Time to remaining depletion [yr] [f]		
Aquifer [a]	**Initial storage [m^3]** [b]	**Storage remaining in 2050 [m^3]** [c]	**90%** [d]	**Eq (7) b= 500m**	**Eq(7) b= 1000m**	**This study**	**Richey et al (2015)**	**Konikow (2013)**
Nubian Aquifer	16674	16545	15007	11000	22000	10427	14295	57118
North West Sahara	20299	20436	18269	4900	9900		14507	
Central Valley	899	620	809	390	780	218	1333	235
High Plain	2236	1866	2012	2500	5100	447		354
Arabian Aquifer	22347	22277	20112	8600	17000	25816	32170	36628
Ganges- Brahmaputra	9456	6964	8510	3100	6200	264	100-500	
North China Plain	3312	2626	2981	2100	4300	348	436	279

a : area defined by WHYMAP
b: estimated as the average groundwater storage over 1960-1965
c: estimated as the average groundwater storage over 2045-2050
d: 90% of this study's initial storage
e: Richy et al.'s estimates that are most comparable to this study's parameterization
f: time to deplete until 90% of the initial storage starting from 2003, similar to the other studies.

This table presents that this study estimates depletion volumes in 2050 of more than 90% of the initial volume for the intensively depleted aquifers, i.e. Central Valley, High Plains, Ganges-Brahmaputra, and North China plains. This study's initial storages are comparable to previous published estimates. Taking 2003 as a start year, and using the average depletion rates over 1960-2003, it is estimated in this study the highly depleted aquifers will reach their 90% limit between 218 and 348 years. This is comparable to previous estimates, and gives a more optimistic result than the estimated storages for 2050.

Tabel S2 Published global cumulative depletion estimates over 1960-2000

	km^3
Pokhrel et al [2012][f]	18,000
Wada et al [2012][f]	5,000
Konikow et al [2011][v]	2,000
This study [v]	
historical climate	4,100
GCM	7,700

[f] flux- based approach
[v] volume-based approach

Chapter 6

Synthesis

6.1 Introduction

The main objective of this PhD study was to assess the limits of global groundwater consumption. To this end I estimated past and future trends on groundwater levels and river flows as a result of changes in abstractions and climate, and tried to predict where and when the limits of groundwater consumption are reached. These limits are explored by predicting where and when groundwater levels drop that low that groundwater becomes unattainable for abstractions, or where and when groundwater discharges no longer help to sustain river low flows.

My main research objective was **to assess the limits to global groundwater consumption from the perspective of local attainable groundwater and regional groundwater-surface water interactions**. Several sub-questions were formulated:

RQ1. What has been the effect of groundwater abstraction on low flows in rivers of the world and which trends in low flow frequency can be attributed to groundwater abstraction?

RQ2. What has been the effect of groundwater abstraction on groundwater levels worldwide and which trends in groundwater level change can be attributed to groundwater abstraction?

RQ3. What are the projected trends in groundwater levels and low flow frequencies as a result of climate change?

RQ4. At what time in the future will limits to groundwater consumption be reached? That is when and where groundwater levels drop that low that groundwater becomes unattainable for abstractions, or that baseflows no longer sustain river discharges.

In this last chapter I summarize the main contributions and results of this PhD research, and I will give recommendations and an outlook for future research.

6.2 Main contributions and results

At the start of this PhD research the available global-scale models lacked in the ability to simulate shifts in time of water use with changes in water availabilities, be it from climate change or due to abstractions. Furthermore, in general the used allocation schemes did not account for abundance of groundwater and surface water at the same time (e.g. Wisser et al., 2008; Hanasaki et al., 2010)), or base this allocation on reported data on water abstractions (e.g. Döll et al., 2012; Wada et al., 2011)).

As a first step I introduced a dynamic framework that allocates groundwater and surface water abstractions over the two resources on the basis of availability in the resource (Chapter 2). To calculate daily groundwater and surface water abstractions, estimated daily total demands per grid cell (used from Wada et al., 2011) and simulated daily water availabilities in the groundwater and surface water resources were used. Feedbacks between groundwater and surface water, like river infiltration and return flows of unconsumed abstracted water, were explicitly accounted for (Figure 2.1). With this framework the dynamic effects of groundwater and surface water abstractions and return flows on groundwater storage and river flows, particularly low flows, were studied (answering RQ1).

Daily surface water and groundwater availability and river discharge were calculated using the global-hydrological model PCR-GLOBWB (van Beek et al., 2011). In Chapter 2 the model was run at 0.5° resolution (50 km at the equator) for 1960-2010. The analysis focussed on river low flows, calculated as weekly streamflow that is exceeded 90% of the time (following Smakhtin et al., 2004)). The effects of groundwater and surface water consumption (i.e. abstraction minus return flow) on river low flows magnitude, frequency, and duration were analysed and an estimate of non-renewable or non-local groundwater abstraction was given. The latter was calculated as the deficit between groundwater demand and available renewable groundwater, calculated as groundwater storage in PCR-GLOBWB (Figure 2.1)). The results showed that the developed allocation scheme is a suitable tool to assess human induced changes in global surface water and groundwater systems and to track these changes over time. Note that local preference for surface water or groundwater was not accounted for (discussed in Chapter 2). These local preferences get more important moving to higher resolutions and should be included (see Chapter 5).

Results showed that the impact of water abstractions are largest for intensively irrigated regions of the word in arid and semi-arid climates. The large impact is reflected in significant declines in river low flows when a natural situation is compared with the human impacted situation. For example the river low flow decline for the Indus is 25-50%, for the Ganges more than 50%, and for the Yellow River 12.5-25% (Figure 2.5). Also, large unsustainable groundwater uses (i.e. non-renewable groundwater abstractions) were simulated for the intensively irrigated regions in the dry climates. Hotspot areas are India, Pakistan, North-west China, Mid-West US, and Mexico (Figure 2.7).

The results also showed that including return flows and groundwater-surface water interactions is needed to realistically simulate water availabilities and impacts of water use. For example, in the highly impacted irrigated regions return flows to the groundwater, infiltrating through the soil when used for irrigation up to 60% of the abstracted water, increase groundwater availability. Therewith, groundwater baseflows to the river are longer sustained, supporting low flow magnitudes, and changing timing and duration of these low flows (e.g. seen for the Indus River, Figure 2.9). Next to the effect on river low flows, the additional groundwater recharge results in smaller estimated non-renewable or non-local groundwater abstractions.

For industry-dominated areas, where most abstracted water flows back into the river channel (up to 80%) much smaller declines in low flows were shown (for example: Danube River 5-12.5%, Figure 2.5) or low flows even increase as additional water stemming from the groundwater is released into the river (for example: Rhine 95%, Figure 2.8). For these industrialized regions also the shifts in timing and duration of low flows is much smaller compared to what is simulated for the irrigated regions. The same holds for estimated non-renewable or non-local groundwater abstraction.

The next step in this PhD research was to focus on the groundwater, and study groundwater head fluctuations and declines caused by abstractions or climate change. At the start of this research no global-scale groundwater model was available that could simulate lateral groundwater flows and head fluctuations. In this study I constructed a global-scale groundwater model representing the large aquifers of the world using a relative simple parameterization method, such that the method can be expanded to data poor environments. The model is based on MODFLOW (McDonald & Harbaugh, 2000) and simulates lateral flows and groundwater-surface water interactions (i.e. river infiltration and drainage) over time. The last version of the model developed in this study runs at 5 arc-minutes (10 km^2 at the equator) for the recent past (1960-2010, Chapter 4) and with future climate projections (2010-2050, Chapter 5). With this model groundwater heads and fluctuations and declines are realistically simulated over time (answering RQ 2 and 3).

The main challenge in the development of this groundwater model was to overcome the data lack in hydrogeological data, such as aquifer spatial extent, aquifer thickness, permeabilities, and vertical structure of the aquifers. To overcome this data lack I used available global datasets (following Sutanudjaja et al., 2011) on lithology (GLiM Hartmann & Moosdorf, 2012) and permeability (Gleeson et al., 2014, GLHYMPS). I combined these datasets with topography-based estimates of aquifer thickness (Chapter 3) and thickness and spatial distribution of confining layers, consisting of fine-grained sediments (Chapter 4). By inclusion of confining layers the worlds' aquifer systems were categorized in confined and unconfined systems. Including confining layers in the parameterization provides vital information about accessibility and quality of the groundwater and is needed when groundwater abstractions and depletion are to be analysed (Chapter 4).

The groundwater model was forced with outputs from PCR-GLOBWB, specifically

surface water levels and groundwater recharge. In the first step, the groundwater model and PCR-GLOBWB were run consecutively and the coupling was one way, meaning from the surface water to the groundwater but not vice versa. The next step was to run the model simultaneously and groundwater-surface water interactions were fully incorporated (Chapter 5).

Results showed the regional scale groundwater table depths are well captured with the model, with high correlations compared to reported well data (R^2=0.95). However, there is a general tendency to underestimate hydraulic heads. This calls for subsequent calibration of the model and the inclusion of horizontal to vertical anisotropy. Shallow water tables are simulated throughout the coastal ribbon and expand where coastal plains meet the sea (like for the Mississippi basin). Also shallow groundwater tables are found for regions with high recharge rates at lower altitudes. Deep groundwater tables are found for low recharge rate regions and for mountainous areas. It should be noted here that, caused by the grid resolution, the regional scale groundwater table is simulated, and perched water tables in local mountain valleys are not captured by the model.

Simulated flow paths show that lateral flows often cross catchment or aquifer boundaries at significant rates, thereby supporting water budgets of neighbouring catchments or aquifer systems. This confirms lateral groundwater flows should be included in global scale water resource assessments, especially when moving to finer resolution like 5 arcminutes (suggested by Wood et al., 2012, Bierkens et al., 2015;). Inclusion of confined layers (estimated 6% to 20% of the total aquifer area, Chapter 4) significantly changes flow path patterns and flow rates. For confined aquifer systems long paths were simulated, crossing catchment boundaries and sometimes get disconnected from the local drainage. While, paths within the confined layers are short (Figure 4.9).

Next to flow path patterns also groundwater head fluctuation amplitude and timing changes when including confined layers. Simulated head fluctuation fitted observations better when confined layers are included (Figure 4.8).

In this study hotspots of groundwater depletion of confined aquifers are revealed for the first time. Total groundwater depletion globally over 1960-2010 is estimated at 7,864 km^3 (result of the fully coupled model, Chapter 5) with hotspot found for the intensively irrigated areas, like India, Pakistan, Mid US.

Depletion estimates of aquifers fit reported data better when lateral lows, confined systems, and groundwater- surface water interactions are included (e.g High Plains 540 km^3 reported 350 km^3 (Scanlon et al., 2012)). Lateral flows can transport recharged groundwater over large distances, increasing an aquifer recharge area, and the inclusion of confining layers increases river infiltration. The result shows that simulating confining layers with global hydrological models is critical for accurately simulating groundwater surface-water interactions, the water tables, and groundwater depletion.

The last step in this PhD research was to predict at what time in future the limits of groundwater consumption will be reached. To this end the developed groundwater

model was fully coupled to the hydrological model (including both infiltration from rivers and drainage by rivers as well as groundwater recharge and capillary rise) and both past estimates and future projections of climate forcing and water demand were included. To reduce uncertainty in the future demand estimates, a 'constant water demand scenario'scenario was assumed. This scenario holds industrial and domestic demand constant and similar to the average of the last 10 years while irrigation demand increases according to as a result of climate variability and change only. Past and future trends in groundwater depletion and river low flow discharges were analysed (Chapter 5). River low flows were estimated in terms of changes in the monthly Q90.

In this study I explored the limits from a physical perspective and evaluated trends over the recent past (1960-2010) and future (2010-2050) (Chapter 5, answering RQ3). Falling groundwater levels, due to abstractions and climate change, were assessed relative to two limits (answering RQ4): 1) a depth of 100 m below the surface at which the groundwater gets unattainable for local farmers, as it is the case for many irrigated regions in the developing world and 2) a head difference larger than 300 m between phreatic groundwater heads and heads in the well, which is the typical exploitable limit of industrial scale pumps employed in developed countries. The first limit is interpreted as an economic limit as investments to exploit deeper groundwater cannot be borne by the farmers themselves. The second limit was interpreted as a technical limit as it would require major investments to get access to deeper water.

It is estimated that over 2010-2050 total global depletion will increase from 7,864 km^3 to 10,445 km^3 in in 2050 (Chapter 5, Figure 5.2). A decrease is depletion rate is simulated; 225 km^3yr^{-1} over 1990-2010 to 100 km^3yr^{-1} over 2010-2050. This change is explained by climate change (i.e. warming temperatures and shifting precipitation patterns) changing both regional water demands and recharge. Next to the existing hotspots of depletion, new areas of significant groundwater depletion will develop in the near future for e.g. Southern Spain and parts of Africa.

Results showed that by 2010 the economic threshold of 100 m has already been surpassed in several regions of the world, but the intensively irrigated regions stand out (Figure 5.3). For parts of these irrigation regions also the technical limit of 300 m is already reached by 2010, and will spatially extend in the near future. Note however, that these results may be too pessimistic for e.g. India because simulated head drawdowns are on the high side due to the neglect of anisotropy and too low horizontal conductivities.

In terms of costs to sustain groundwater demand, most costs are made for regions with substantial increase in groundwater depletion, predominantly for e.g. India, Pakistan, North China, and Kalahari aquifer (Figure 5.3). Costs for these areas are high and require major investments, especially for upcoming economies. Globally, the increase in costs to ensure groundwater supply (over 1960-2050) is 399 million US$/year. Regionally an increase or decline in exploitation cost will be an essential factor in further economic development and should be carefully considered in order to warrant a reliable groundwater supply under changing climatic conditions.

In conclusion this study uses a novel approach to parameterize the world's aquifer systems, and results showed that groundwater heads and fluctuations are simulated reasonably accurately compared to reported data. This makes the developed groundwater model a useful tool to assess global groundwater resources, and shows that existing hydrological model will significantly improve when coupled to such a groundwater model. Also, the developed allocation scheme provides a useful tool to estimate groundwater and surface water demands at the grid-scale and estimates abstractions based on simulated water availability in the resources.

This study reveals hotspots of groundwater depletion in confined aquifers for the first time, and shows where and when limits of groundwater consumption will be reached globally. Limits were defined as groundwater levels that drop that low that groundwater becomes unattainable for abstraction, or groundwater discharges supporting river flows are no longer sustained. Results show that present-day hotspots of depletion are found particularly for intensive irrigated regions in dry climates, e.g. India, Pakistan, and China. Under future changes in climate and increase in human water demand, depletion for these areas will intensify and new areas will develop, e.g. South Europe. As a consequence of groundwater depletion groundwater levels will drop, increasing pumping costs and decreasing baseflows to rivers, lakes, and wetlands. The impact of abstraction on river low flows (magnitude, timing, duration)is largest for the irrigated regions, e.g. for the Indus and Ganges rivers. For many regions experiencing groundwater depletion economical limits (i.e. 100 m threshold) of abstraction are already reached or will be reached in the near future.

The results of this study provide new insights into the sustainability of water use and resilience of our water resources. It highlights regions and provides a time-frame for the limits of groundwater consumption at the global scale. This information is of value for local water managers, national governments, and international institutes concerned with global development (like UNESCO, World Bank) to ensure sustainable and efficient groundwater use as much as possible. Although the spatial resolution is probably still too coarse for practical use for local water managers, it can be used to get first insights on the status of our world‘s largest aquifer systems. Besides, it provides information for regions where local data is absent.

6.3 Recommendations and research outlook

This study provides valuable knowledge to improve existing global-scale hydrological models. Subsequently, the knowledge gained from these models is essential for water managers at all management levels to ensure sustainable and efficient (ground)water use.

However, models are never perfect and analyses can always be expanded. Here I provide recommendations related to this study and give my research outlook for further development of global-scale hydrological models.

6.3.1 More work on low flows and depletion

In this Thesis I started with exploring the limits to groundwater abstractions in relation to effects on river flows and groundwater levels critical to lakes, rivers, and wetlands. I discussed the effect of groundwater abstractions focusing on low flow magnitude, frequencies, and duration. However, I did not explicitly focus on how much groundwater can be abstracted at maximum to avoid streamflow to become too low to meet downstream water demands as well, or to sustain river flows and valuable ecosystems. This analysis can be added to the current analysis, and provides an extra environmental limit to groundwater consumption. Extra information on environmental flow requirements would be valuable in such analysis. It should be noted however, that discharge is often overestimated in basins with large semi-arid regions (i.e. the regions that are most interesting) in PCR-GLOBWB (as well as in other models), such as the Nile, Niger, and Murray-Darling (van Beek et al., 2011), most likely by the lack of a proper representation of wetlands and floodplain evaporation.

Second, the runs of Chapter 5 are limited to one Global Climate Model (GCM) and should be done again with different GCMs to obtain uncertainty bands of depletion, and to provide the worst case and best case projections of groundwater depletion. Also, aquifer vulnerability to different parameter settings is a topic to explore further.

6.3.2 Missing data links

Aquifer parameterization
In this thesis I introduced a feasible and suitable method to parameterize aquifers around the world, based on available global datasets on lithology and permeability and the estimates of aquifer thickness and spatial distribution of confining layers, generally based on terrain attributes. The results showed that using a lateral groundwater flow model (MODFLOW), and applying the parametrization method, I was able to simulate the water table, groundwater head fluctuations, and groundwater surface water interactions with reasonable accuracy when compared to reported data.

The biggest improvement of the model results are expected when accurate global-scale data becomes available and could be included. This data should hold: aquifers extent, the number of stacked aquifers, and conductivities and storativities for these layers. With this information prediction on longevity of groundwater resources will improve, as well as projections of future dependency on unsustainable groundwater.

Besides, without knowledge on vertical structure of the aquifers (hydrogeological and geomechanical knowledge) consequences of land subsidence and the effectiveness of mitigation measures cannot be predicted. A first effort to obtain the dataset needed is made by constructing the WHYMAP (World-wide Hydrogeological Mapping and Assessment Program of UNESCO www.whymap.org), but the progress here seems to be halted. A kick-start coming from the global hydrological community is needed here.

Groundwater head observations
Currently the model outcomes are validated against overserved groundwater heads (Fan et al., 2013). But, for most regions of the world no observation data is available, or is incomplete (i.e. missing elevation measurement). Next to this, observations are biased towards river valleys, coastal ribbons, and the areas where large productive aquifers occur. Besides, groundwater observations are in general taken at a certain moment in time and lengthy time series to evaluate groundwater head fluctuations, made available for a larger audience, are scarce.

To better validate model outcomes, groundwater head observations should be available globally, and preferably cover fluctuation over the year, like seasonal impacts.

Water allocation and infrastructure
In the last version of PCR-GLOBWB I used a simple method to include irrigation channels by allocation water demands over a bigger grid (50 km^2) when demands were higher than the water availability within the grid-cell itself (10 km^2). This method could be improved, when data becomes available. The current water allocation scheme can be improved when a dataset on long-distance and inter-basin water diversion (such as aqueducts) will get available, holding information on location, capacity etc. Examples of large water diversions are the California Aquaduct and the South-North Water transfer project in China. On a smaller scale, information on regional water distribution infrastructure should be included, and a network of irrigation channels. Such water diversions can substantially contribute to supply irrigation water requirements, and should be included especially when moving to finer resolutions (like 10 km^2 or 1 km^2).

Management and Technology under socio-economic change
This study (and others before, (e.g. Döll et al., 2012; Wada et al., 2011) suggest an increasing dependency of humans on unsustainable groundwater use, dropping significant doubt on the sustainability of regional water supply and food production. To feed the world population now and in future water should be used two times more efficient within the coming decennia (Hoekstra, 2005).

Technical improvements (e.g. implement drip irrigation) have the potential to reduce water demands in many countries where water is scarce. However, for many developing countries technical improvements may not be easy to realize when this requires substantial economic investments.

Governmental support works in two ways. Governments can for example subsidence the use of diesel (like in India) for pumps to increase crop growth. However this does not support efficient use of water. Governments can also support changes in agricultural practice to reduce water use, e.g. supporting a shift from three to two growing seasons (as done in Vietnam). To realize this efficiency the export value of a crop should be evaluated to the impact on local water resources. Consequently, food prices will rise

most likely. However, it should be noted here that local political choices or autonomy may be thwarted by global trade networks. Several countries heavily rely on foreign water resources and many countries have significant impacts on water consumption and pollution elsewhere (Hoekstra, 2005).

Predictions of future decision making on water related issues should thus be included in estimates of future water demands.

6.3.3 The next generation

One of the shared goals of the hydrological world is to develop models that 'are everywhere and locally relevant' (Bierkens et al. 2015). Global-scale models, such as the one in this study running at 5 arc-minutes, are a big step forward to reach this goal. The model estimates of groundwater and surface water abstractions are comparable to reported data, and effects of abstractions can be simulated, including hotspots of groundwater depletion for confined and unconfined groundwater systems. These model outcomes can give water managers a first insight what is happening with the groundwater and surface water systems, and to see if sustainable water management is needed or not, now and in the future. This is especially useful for areas were regional scale models are absent, like for most of the developing world. But, the grid resolution of the current global-scale hydrological models is still too coarse to be relevant for local water managers, interested in more than the global overview.

A general ambition would be to have the next generation models globally available at hyper-resolutions (e.g. 1 km or 250 m) so that it would be relevant for local water managers too. However, this goal is very ambitious and will take years to accomplice. Model efforts of regional scale models, running for example at 1 km resolution for the contiguous United States or for Europe, can be a lead.

A first step to improve the current model efforts would be to use the model outcomes to see which regions are of special interest and are worth it the increase model resolution.However, just making the grid finer would not help to make the results locally more relevant. For this, some major challenges have to be overcome.

First, the used input data should be available at the finer resolution too. The major limitation here is the climate models, not providing high resolution data. Also, more complete data on abstractions, including sector specific preferences to use surface water or groundwater, as well as data on infrastructure (e.g. irrigation channels, sewer systems) is needed to realistically allocate water demands at the finer resolution. This data should become available first, for example from remote sensing, observations, or global science community initiatives before the existing model can be sufficiently improved. Before a complete data-set on groundwater head observations is available, data from GRACE can be used.

Next to this, simple sub-grid concepts need to be replaced by explicit physical representations (e.g. Wood et al., 2012, Bierkens et al., 2015), for example to estimate saturated

overland flow. This requires additional data to parameterize and extra computational power to solve the new physical representations. Here, the increase in resolution should not be traded with accuracy (Beven & Cloke, 2012), new datasets to compare and calibrate models would solve this issue. Also, multi-model ensemble predictions can be used to reduce parameterization errors. In an ideal world there would be sub-grid concepts and parametrizations that change consistently with scale (e.g. Bloschl & Sivapalan, 2006).

At last, a main challenge lays in the large computational demands in terms of CPU time and storage requirements (Maxwell et al. 2015). An increase in spatial resolution by a factor 10 will increase computational time by a factor 100. Moreover, as mentioned, simple sub-grid parameterization will be replaced by explicit process dynamic when running at hyper-resolution, demanding more computational time. Tech giants such as Google, Microsoft, and Amazon are lending their computation muscle to crunch data on the environment and help communities plan for an altering landscape. This facility would be very useful also to run the high-resolution hydrological models at. Running the models parallel or using grids of variable size may reduce computational time, but such methods have to be developed for global-scale models.

Bibliography

Aeschbach-Hertig, W. & Gleeson, T. (2012). Regional strategies for the accelerating global problem of groundwater depletion. *Nature Geoscience*, *5*(12), 853–861.

Allen, R., Pereira, L., Raes, D., & Smith, M. (1998). Crop evapotranspiration- guildelines for computingcrop water requirements. *FAO Irrigation and Drainage Paper 56, FAO, Rome*.

Bierkens, M. F. P. & van den Hurk, B. J. J. M. (2007). Groundwater convergence as a possible mechanism for multi-year persistence in rainfall. *Geophys. Res. Lett.*, *34*(L02402).

Bloschl, G. & Sivapalan, M. (2006). Scale issues in hydrological modelling: A review. *Hydrological processes*.

Clark, B. & Hart, R. (2009). The mississippi embayment regional aquifer study (meras): Documentation of a groundwater-flow model contructed to assess water availability in the mississippi embayment. *Tech. Rep. 5172, US Geological Survey Scientific Investigations Report*(US Geological Survey,Reston, Virginia,).

Dai, A. (2011). Dought under global warming: A review. *Wiley Interdisciplinary Reviews: Climate Change*.

de Graaf, I. E. M., van Beek, L. P. H., Gleeson, T., Moosdorf, N., Schmitz, O., & Bierkens, M. F. P. (in prep). A global-scale two-layered transient groundwater model: development and application to groundwater deletion.

de Graaf, I. E. M., van Beek, L. P. H., Sutanudjaja, S. H., & Bierkens, M. F. P. (2015). A high-resolution global- scale groundwater model. *HESS*, *2*(19), 823–837.

de Graaf, I. E. M., van Beek, L. P. H., Wada, Y., & Bierkens, M. F. P. (2013). Dynamic attribution of global water demand to surface water and groundwater resources: effects of abstractions and return flows on river discharges. *Adv. Water Resour.*, *64*, 21–33.

Dee, D., Uppala, S., Simmons, A., Berrisford, P., Poli, P., & S., K. (2011). The era-interim reanalysis: configuration and performance of the data assimilation system. *Quarterly Journal of the Royal Meteorological Society*, *137*(656), 553–597.

Döll, P., Müller Schmied, H., Schuh, C., Portmann, F. T., & Eicker, A. (2014). Global-scale assessment of groundwater depletion and related groundwater abstractions: Combining hydrological modeling with information from well observations and grace satellites. *Water Resources Research*, *50*(7), 5698–5720.

Döll, P., Hoffmann-Dobrev, H., Portmann, F., Siebert, S., Eicker, A., & Rodell, M. (2012). Impact of water withdrawals from groundwater and surface water on continental water storage variations. *Journal of Geodynamics*, *59-60*, 143–156.

Döll, P. & Lehner, B. (2002). Validation of a new global 30-min drainage direction map. *Journal of Hydrology*, *258*(1-4), 214–231.

Döll, P. & Siebert, S. (2002). Global modeling of irrigation water requirements. *Water Resources Research*, *38*(4), 81–811.

Dürr, H., Meybeck, M., & Dürr, S. (2005). Lithologic composition of the earth's continental surfaces derived from a new digital map emphasizing riverine material transfer. *Global Biogeochemical Cycles*, *19*(4).

Els, A. & Rowntree, K. (2003). Water resources in the sananah regions of botswana. Technical report, EU INCO/UNEP/SCOPE Southern African Savananas Project.

Fan, Y., Li, H., & Miguez-Macho, G. (2013). Global patterns of groundwater table depth. *Science*, *339*, 940–943.

Fan, Y., Miguez-Macho, G., Weaver, C. P., Walko, R., & Robock, A. (2007). Incorporating water table dynamics in climate modeling: 1. water table observations and equilibrium water table simulations. *J. Geophys. Res.-Atmos.*, *112*.

FAO (2010). Fao aquastat on-line database. food and agricultural organization rome, italy. available: http://faostat.fao.org.

Faunt, C. C. E. (2009). Groundwater availability of the central valley aquifer. *US Geological Survey Professional Paper 1766, US Geological Survey, California,*, p. 255.

Foster, S. S. D. & Chilton, P. J. (2003). Groundwater: the processes and global significance of aquifer degradation. *British Geological Survey*.

Giordano, M. (2009). Global groundwater? issues and solutions. *Annual Review of Environment and Resources*, *34*, 153–178.

Gleeson, T., N., M., Hartmann, J., & van Beek, L. P. H. (2014). A glimpse beneath earth's surface: Global hydrogeological maps (glhymps) of permeability and porosity. *Geophys. Res. Lett.*, *41*.

Gleeson, T., Smith, L., Moosdorf, N., Hartmann, J., Dürr, H. H., Manning, A. H., van Beek, L. P. H., & Jellinek, A. M. (2011). Mapping permeability over the surface of the earth. *Geophys. Res. Lett.*, *38*.

Gleeson, T., van der Steen, J., Sophocleous, M. A., Taniguchi, M., Alley, W. M., & Allen, D. M. (2010). Groundwater sustainability strategies. *Nature Geoscience*, *3*(6), 378–379.

Gleeson, T., Wada, Y., Bierkens, M. F. P., & Van Beek, L. P. H. (2012). Water balance of global aquifers revealed by groundwater footprint. *Nature*, *488*(7410), 197–200.

Haddeland, I., Matheussen, B. V., & Lettenmaier, D. P. (2002). Influence of spatial resolution on simulated streamflow in a macroscale hydrologic model. *Water Resources Research*, *38*(7), 291–2910.

Hagemann, Botz, Dmenil, & Machenhauer (1999). Derivation of global gcm boundary conditions from 1 km land use satellite data. *Rep. 289. Tech. Rep., Max Planck Institude for Meteorology, Hamburg, Germany*.

Hanasaki, N., Inuzuka, T., Kanae, S., & Oki, T. (2010). An estimatetion of global virtual water flow and sources of water withdrawal for major crops and livestock products using a global hydrological model. *J. Hydrol.*, *384(3-4)*, 232–44.

Hartmann, J. & Moosdorf, N. (2012). The new global lithological map database glim: a representation of rock properties at the earth surface. *Geochem. Geophy. Geosy.*, *13*.

Hoekstra, A. Y. (2005). Globalization of water. *Water Resource Development and Management*, *x*.

Ingebritsen, S. & Manning, C. (1999). Geological implications of a permeability-depth curve for the continental crust. *Geology*, *27*, 1107–1110.

Konikow, L. F. (2011). Contribution of global groundwater depletion since 1900 to sea-level rise. *geophysical research letters*, *38*.

Kraaijenhof van der Leur, D. (1958). A study of non-steady groundwater flow with special reference to a reservoir coefficient. *de ingenieur*, *70*, 87–94.

Krakauer, N. Y., Li, H., & Fan, Y. (2014). Groundwater flow across spatial scales: importance for climate modeling. *Environ. Res. Lett*, *9*.

Lacey, G. (1930). Stable cchannel in alluvium. *P. I. Civ. Eng.*, *229*, 259–292.

Lam, A., Karssenberg, D., van den Hurk, B. J. J. M., & Bierkens, M. F. P. (2011). Spatial and temporal connections in groundwater contribution to evaporation. *Hydrol. Earth Syst. Sci.*, *15*, 2621–2630.

Lehner, B. & Döll, P. (2004). Development and validation of a global database of lakes, reservoirs and wetlands. *Journal of Hydrology*, *296*(1-4), 1–22.

Manning, R. (1891). On the flow of water in open cchannel and pipes. *Transactions of Institution of Civil Engineers of Ireland, Dublin,*, 161–207.

McDonald, M. G. & Harbaugh, A. W. (2000). Modflow-2000, the us geological survey modular groundwater model – user guide to modularmodular concepts and the ground-water flow process. *Tech. rep., US Geological Survey, Reston, Virginia*.

Miguez-Macho, G., Li, H., & Fan, Y. (2008). Simulated water table and soil moisture climatology over north america. *B. Am. Meteorol. Soc.*, *89*(663-672).

Mitchell, T. D. & Jones, P. D. (2005). An improved method of constructing a database of monthly climate observations and associated high-resolution grids. *International Journal of Climatology*, *25*(6), 693–712.

New, M., Lister, D., Hulme, M., & Makin, I. (2002). A high-resolution data set of surface climate over global land areas. *Climate Research*, *21*(1), 1–25.

Oki, T. & Kanae, S. (2006). Global hydrological cycles and world water resources. *Science*, *313*(5790), 1068–1072. cited By 0.

Pokhrel, Y., Hanasaki, N., Koirala, S., Cho, J., Yeh, P. J. F., & Kim, H. (2012). Incorporating anthropogenic water regulation modules into a land surface model. *Journal of Hydrometeorology*, *13*(1), 255–269.

Pollock, D. (1994). User's guide for modpath/modpath-plot, version 3: A particle tracking post-processing package for modflow, the us geological survey finite-difference groundwater flow model. *Tech. rep., US Geological Survey Open-File Report 94-464, US Geological Survey, Reston, Virginia*.

Portmann, F. T., Siever, S., & Döll, P. (2010). Mirca2000-global monthly irrigated and rainfed cop areas around the year 2000: A new high-resolution for agricultural and hydrogeological modelling. *Global Biogeochemical Cycles*, *24*, GB1011.

Postel, S. L. (2000). Entering an era of water scarcity: The challenges ahead. *Ecological Applications*.

Richey, A. S., Thomas, B. F., Lo, M.-H., Famiglietti, J. S., Swenson, S., & Rodell, M. (2015). Uncertainty in global groundwaer storage estimates in a total groundwater stress framework. *Water Resource Research*.

Rodell, M., Velicogna, I., & Famiglietti, J. S. (2009). Satellite-based estimates of groundwater depletion in india. *Nature*, *460*(7258), 999–1002.

Rohwer, J., Gerten, D., & Lucht, W. (2007). *Development of functional irrigation types for improved global crop modelling*. No. 104 in PIK Report.

Rost, S., Gerten, D., Bondeau, A., Lucht, W., Rohwer, J., & Schaphoff, S. (2008). Agricultural green and blue water consumption and its influence on the global water system. *Water Resources Research*, *44*(9).

Savenije, H. H. (2003). The width of a bankfull channel; lacey's formula explained. *J. Hydrol.*, *276*, 176–183.

Scanlon, B. R., Faunt, C. C., Longuevergne, L., Reedy, R. C., Allley, W. M., McGuire, V. L., & McMahon, B. (2012). Groundwaer depletion and sustainability of irrigation in the us high plains and central valley. *PNAS*, *109*(24).

Schaller, M. F. & Fan, Y. (2009). River basins as groundwater exporters and importers: implications for water cycle and climate modeling. *J. Geophys. Res.-Atmos.*, *114*.

Schmitz, O., Karssenberg, D., van Deursen, W., & Wesseling, C. (2009). Linking external components to spatio-temporal modeling framework: coupling modlfw and pcraster. *Environ. Modell. Softw.*, *24*, 1088–1099.

Shiklomanov, I. (1993). *World freshwater resources. In P. H. Gleick (ed.), Water in Crisis: A Guide to the Worlds Freshwater Resources.* New York, Oxford University Press.

Shiklomanov, I. & Rodda, J. (2003). *World Water Resources at the Beginning of the Twenty-First Century*. cambridge university press.

Siebert, S. & Döll, P. (2010). Quantifying blue and green virtual water contents in global crop production as well as potential production losses without irrigation. *J. Hydrol.*, *384(3-4)*, 198–217.

Smakhtin, V. U., Revenga, C., & Döll, P. (2004). A pilot global assessment of environmental water requirements and scarcity. *Water Int.*, *29*, 307–17.

Stanley, D. J. & Warne, A. G. (1994). Worldwide initiation of holocene marine deltas by deceleration of sea-level rise. *Science*, *265*, 228–231.

Sutanudjaja, E. H., van Beek, L. P. H., de Jong, S. M., van Geer, F. C., & Bierkens, M. F. P. (2011). Large-scale groundwater modeling using global datasets: a test case for the rhine-meuse basin. *Hydrol. Earth Syst. Sci.*, *15*(2913-2935).

Sutanudjaja, E. H., van Beek, L. P. H., de Jong, S. M., van Geer, F. C., & Bierkens, M. F. P. (2014). Calibrating a large-extent high-resolution coupled groundwater-land surface model using soil moisture and discharge data. *Water Resourc. Res.*, *50*(687-705).

Syvitski, J. P. M., Vörösmarty, C. J., Kettner, A. J., & Green, P. (2005). Impact of humans on flux of terrestrial sediment to the global coastal ocean. *Science*, *308*, 376–380.

Todini, T. (1996). The arno rainfall-runoff model. *J. Hydrol.*, *175*, 339–382.

Toscano, M. A. & Macintyre, I. G. (2003). Corrected western atlantic sea-level curve for the last 11,000 years based on calibrated 14c dates from acropora palmata framework and intertidal mangrove peat. *22*(3), 257–270.

Toth, J. (1963). A theoretical analysis of groundwaterflow in small drainage basins. *J. Geophys. Res.*

UN (2012). The 4th edition of the un world water development report (wwdr4). Technical report, Unesco.

van Beek, L., Wada, Y., & Bierkens, M. (2011). Global monthly water stress: 1. water balance and water availability. *Water Resources Research*, *47*(7).

Vergnes, J.-P., Decharme, B., Alkama, R., Martin, E., Habets, F., & Douville, H. (2012). A simple groundwater scheme for hydrological and climate applications: description and offline evaluation over france. *J. Hydrometeorol.*, *13*, 1149–1171.

Vörösmarty, C. J., Green, P., Salisbury, J., & Lammers, R. B. (2000). Global water resources: Vulnerability from climate change and population growth. *Science*, *289*(5477), 284–288. cited By 0.

Vörösmarty, C. J., McIntyre, P. B., Gessner, M. O., Dudgeon, D., Prusevich, A., Green, P., Glidden, S., Bunn, S. E., Sullivan, C. A., Reidly Liermann, C., & Davis, P. M. (2010). Global threats to human water security and river biodiversity. *Nature*, *467*.

Wada, Y., Van Beek, L., Van Kempen, C., Reckman, J., Vasak, S., & Bierkens, M. (2010). Global depletion of groundwater resources. *Geophysical Research Letters*, *37*(20).

Wada, Y., Van Beek, L. P. H., & Bierkens, M. F. P. (2011). Modelling global water stress of the recent past: On the relative importance of trends in water demand and climate variability. *Hydrology and Earth System Sciences*, *15*(12), 3785–3808.

Wada, Y., van Beek, L. P. H., & Bierkens, M. F. P. (2012). Nonsustainable groundwater sustaining irrigation: A global assessment. *Water Resources Research*, *48*(1).

Wada, Y., Van Beek, L. P. H., Viviroli, D., Dürr, H. H., Weingartner, R., & Bierkens, M. F. P. (2011). Global monthly water stress: 2. water demand and severity of water stress. *Water Resources Research*, *47*(7). cited By 68.

Wada, Y., Wisser, D., & Bierkens, M. (2013). Global modeling of withdrawal, allocation and consumptive use of surface water and groundwater resources. *Earth Syst Dynam Discuss*, *4*, 355–392.

Wada, Y., Wisser, D., & Bierkens, M. F. P. (2014). Global modeling of withdrawal, allocation and consumptive use of surface water and groundwater resources. *Earth Syst. Dynam.*, *5*, 15–40.

Wisser, D., Frolking, S., Douglas, E. M., Fekete, B. M., Vörösmarty, C. J., & Schumann, A. H. (2008). Global irrigation water demand: Variability and uncertainties arising from agricultural and climate data sets. *Geophysical Research Letters*, *35*(24).

Wood, E. F., Roundy, J. K., Troy, T. J., van Beek, R., Bierkens, M., Blyth, E., de Roo, A., Döll, P., Ek, M., Famiglietti, J., Gochis, D., van de Giesen, N., Houser, P., Jaffe, P., Kollet, S., Lehner, B., Lettenmaier, D. P., Peters-Lidard, C. D., Sivapalan, M., Sheffield, J., Wade, A. J., & Whitehead, P. (2012). Reply to comment by keith, j. beven and hannah, l. cloke on "hyperresolution global land surface modeling: Meeting a grand challenge for monitoring earth's terrestrial water". *Water Resour. Res.*, *48*.

.

Appendix

Supplement to Chapter 3

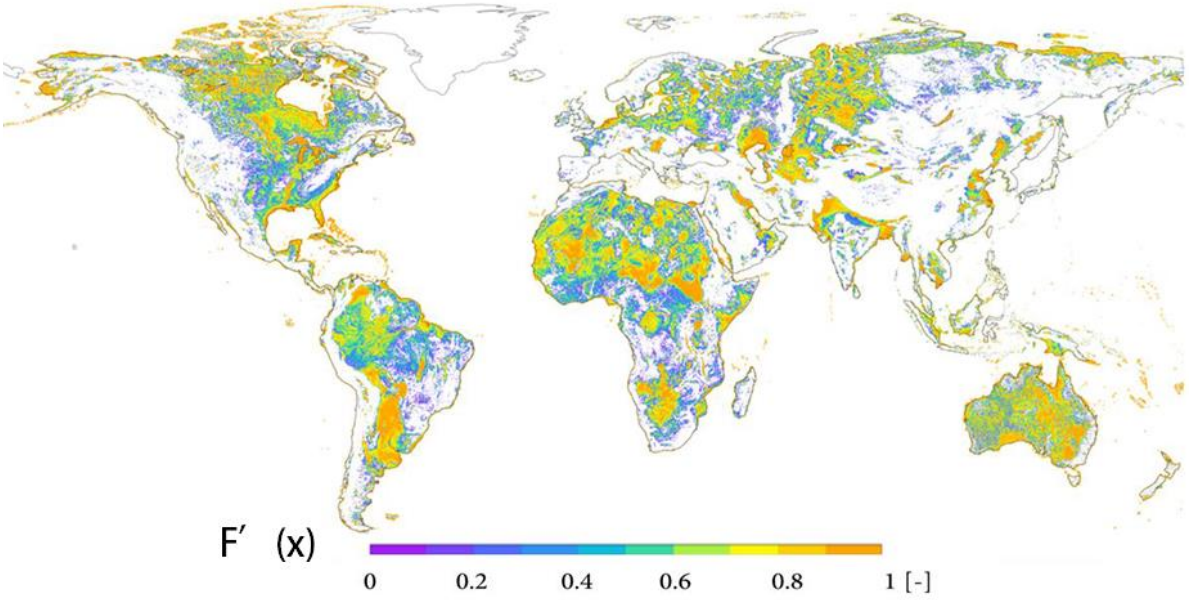

Fig. 6.1: Spatial distribution of $F^{'}(x)$, representing the likelihood of finding a thick aquifer

e-folding depth
The near surface permeability is described by the sediment-bedrock profile at a location, which depends strongly on terrain slope; the steeper the land, the thinner the regolith and the sharper the decrease in permeability with depth (e.g. Miguez-Macho et al., 2008). This is expressed through the e-folding depth. The range of the e-folding depth (f) is given in the graph below, and its spatial distribution in the map below.

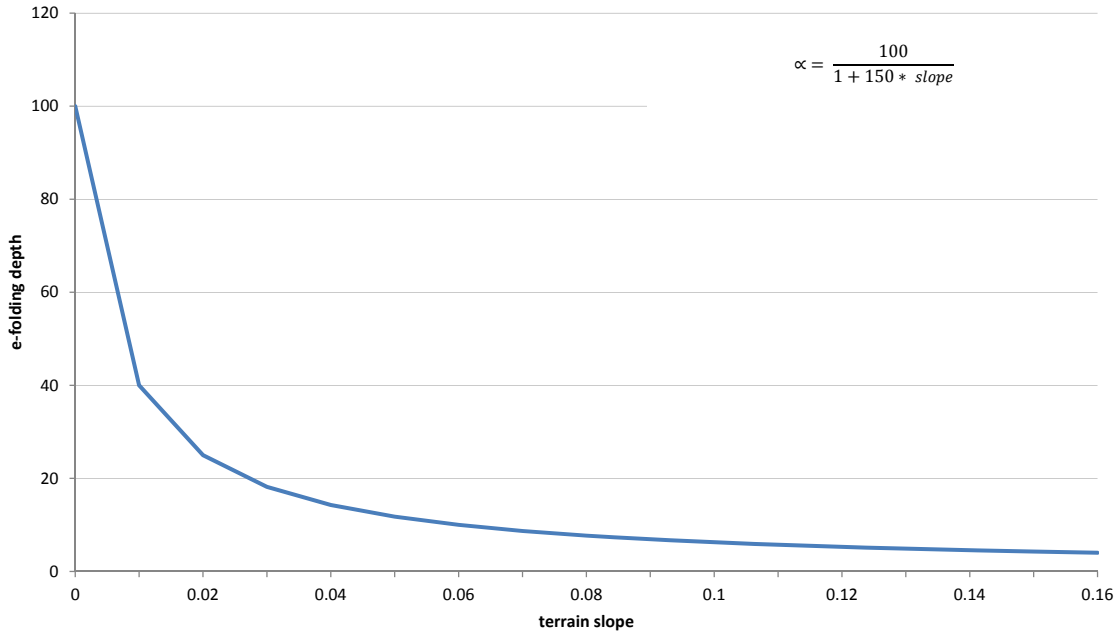

Fig. 6.2: e-folding depth as a function of terrain slope, using constants of Miguez-Macho et al. (2008).

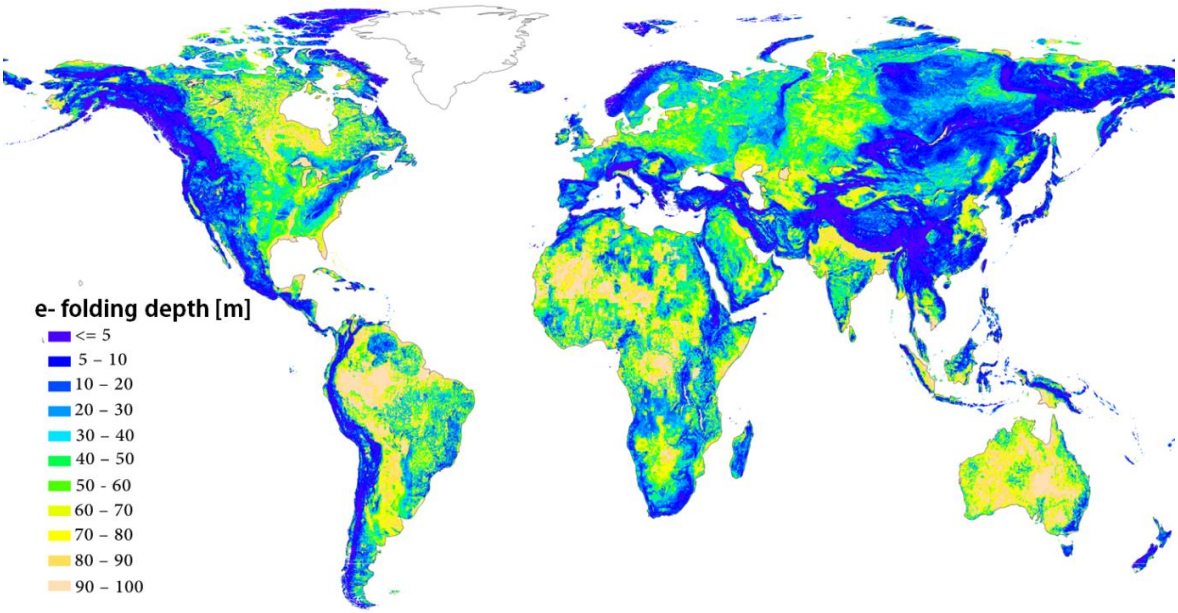

Fig. 6.3: e-folding depth

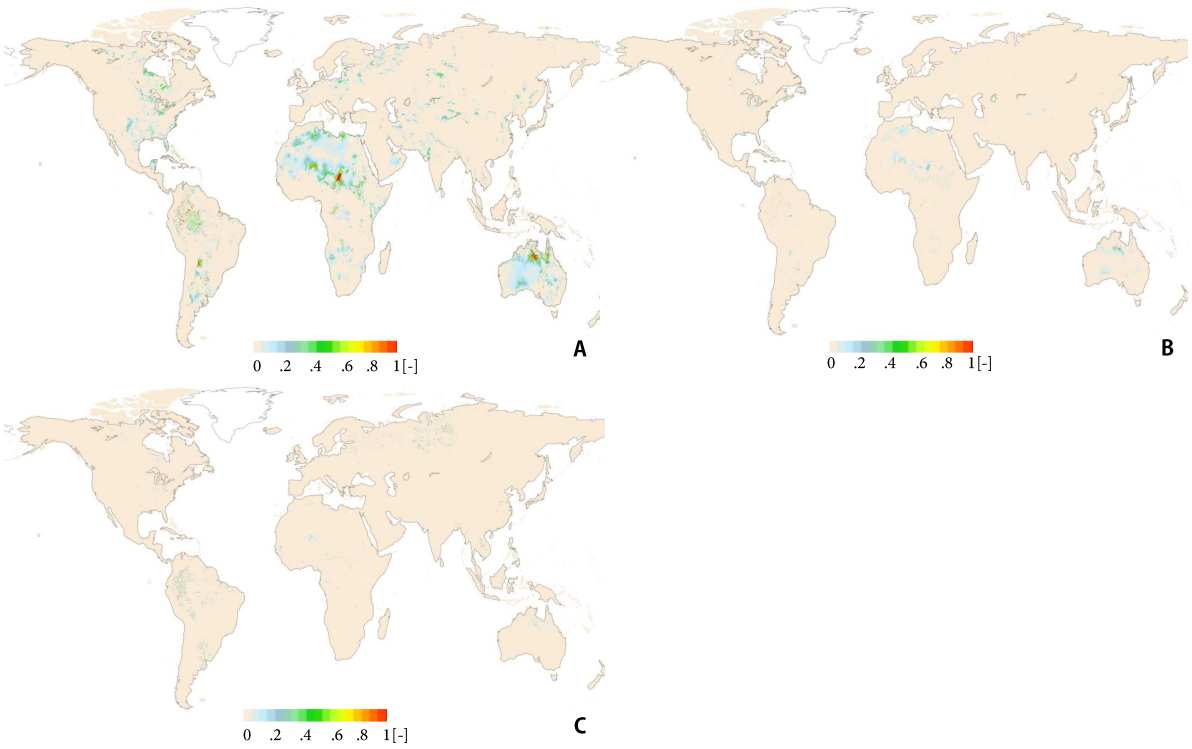

Fig. 6.4: Coefficient of variation of groundwater depth of 100 runs with different parameter settings for (A) saturated conductivity, (B) aquifer thickness, and (C) groundwater recharge.

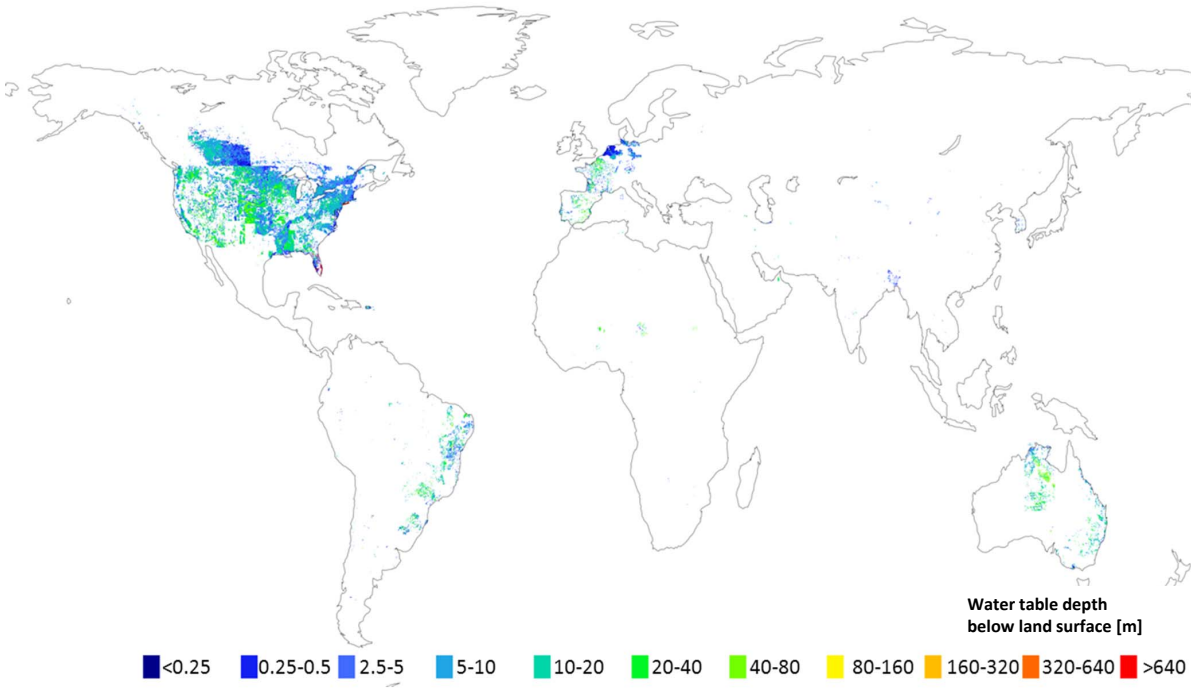

Fig. 6.5: Global piezometer observations; groundwater depths in meters below the land-surface (from Fan et al., 2013).

Samenvatting

De grenzen van mondiaal grondwaterverbruik

Zoetwater is essentieel voor ons bestaan. Door de groei in wereldbevolking en economie is de wereldwijde vraag naar zoetwater bijna verdrievoudigd in de afgelopen decennia. De grootste waterverbruiker is geïrrigeerde landbouw, goed voor 70% van de totale watervraag. Niet overal op de wereld is voldoende water beschikbaar in rivieren, meren, of stuwmeren. Om toch aan de watervraag te kunnen voldoen wordt er daarom vaak water uit ondergrondse reservoirs opgepompt (ofwel grondwater). Wereldwijd is dit opgeslagen grondwater de grootste beschikbare zoetwater voorraad. Maar, in veel gebieden wordt er meer grondwater onttrokken dan er wordt aangevuld door bijvoorbeeld het infiltreren van regenwater. Het grondwater reservoir wordt langzaam maar zeker uitgeput, met grote problemen tot gevolg.

Een eerste gevolg is dat door het uitputten van het grondwater reservoir zullen grondwaterstanden gaan zakken (dit is de diepte waar we grondwater vinden). Als gevolg van de zakkende grondwaterstanden nemen pompkosten toe, het water komt tenslotte van dieper. Er zal meer brandstof moeten worden verbruikt om dezelfde hoeveelheid water op te pompen. Bovendien, moet er geïnvesteerd worden in nieuwe pompen en technologische ontwikkelingen om in de toekomst het water van nog dieper te kunnen halen. De toename in pompkosten, en daarmee de toename in voedselprijzen, zal de aller armste op de wereld het hardst treffen.

Een tweede gevolg is dat door het oppompen van water bodems gaan zakken, net als de veengebieden in Nederland. In kustgebieden verhoogt dit het risico voor overstroming van zowel de zee als rivieren. Een voorbeeld is de Jakarta delta, waar overstromingen een vaak terugkerend fenomeen zijn als gevolg van een zakkende bodem.

Een derde gevolg van dalende grondwaterstanden is dat de grondwaterstroming richting rivieren afneemt (de gradiënt neemt af). Het grondwater aandeel in de rivierafvoer wordt minder. Dit heeft vooral een groot effect gedurende droge periode met weinig neerslag en lage rivierafvoeren. Rivieren vallen droog en belangrijke ecosystemen worden niet langer behouden.

De verwachting is dat in de toekomst de vraag naar water verder zal toenemen. Daarnaast zal water schaarser worden als gevolg van klimaatveranderingen. Door deze verwachte toenames en de genoemde gevolgen van grondwater uitputting, reist de vraag wanneer en waar hebben we de grenzen van onze watervoorraad bereikt? De vraag die ik me gesteld heb is hoeveel grondwater kan worden onttrokken in de verschillende delen van de wereld voordat grondwaterstanden te diep wegzakken of rivieren droogvallen?

Maar waarom bekijk ik dit probleem op mondiale schaal, terwijl grondwater vaak toch beschreven wordt als lokale bron van water? Ten eerste, grondwater reservoirs kunnen duizenden vierkante kilometers omvatten, overschrijden landsgrenzen en hebben grote invloed op de sociaaleconomische ontwikkelingen in de regio. Zelfs als grondwater wel lokaal is kan het verbruik een mondiale impact hebben: de import en export van goederen is ook een import en export van grondwater verbruikt voor de productie van deze goederen. Biljoenen liters water worden op deze manier herverdeeld over de wereld. Ten tweede, als we meer weten over de verschillende grondwatersystemen over de wereld draagt dit bij aan meer kennis van welk grondwatersysteem dan ook en kunnen we beter aangeven hoe we duurzamer water kunnen gaan verbruiken. Als laatste is de mondiale schaal belangrijk om te zien wat problemen, dreigingen en kansen zijn wereldwijd. Dit draagt bij aan het stellen van prioriteiten voor management acties.

Om mijn onderzoeksvraag te beantwoorden heb ik gebruik gemaakt van een hydrologisch model (PCR-GLOBWB) en een grondwater model (gebaseerd op MODFLOW), beide op mondiale schaal op hoge resolutie ($\sim$10 km^2 op de evenaar met tijdstappen van een dag). De modellen simuleren grondwaterstromingen en grondwater standen, rivierafvoeren en de hoeveelheid opgeslagen water in bodem en grondwater. De modellen zijn gekoppeld, zodat alle interacties tussen grondwater, rivier, en bodem mee genomen kunnen worden. Het is het eerste mondiale model dat laterale grondwater stroming simuleert, de stroming tussen de verschillende model cellen. Met dit model en data over het klimaat en watervraag heb ik gesimuleerd wat er is gebeurd en zal gebeuren met grondwaterstanden en rivierafvoeren, in de afgelopen decennia (1960-2010) en in de nabije toekomst (2010-2050).

De grootste uitdaging van dit onderzoek was het maken van het grondwater model, omdat er weinig of geen data beschikbaar is over de eigenschappen van de grondwaterreservoirs: hoeveel water kan er worden opgeslagen en hoe gemakkelijk wordt het los gelaten. Om dit data probleem op te lossen heb ik gebruik gemaakt van alleen beschikbare mondiale datasets, en heb ik geschat hoe dik de grondwaterreservoirs zijn op mondiale schaal. Ik heb nu dus over de hele wereld een idee van de eigenschappen vande reservoirs, ook voor de gebieden waar er geen data beschikbaar is. Omdat ik op deze manier het grondwater systeem karakteriseer kan ik, als eerste, een realistisch beeld geven van de effecten van grondwater onttrekkingen op grondwaterstanden wereldwijd.

Aan de hand van de kaarten en tijdsreeksen die uit de verschillende modelruns komen, kan ik zien wat het effect van grondwater onttrekking is geweest, of zal zijn, op rivierafvoeren en grondwater standen op mondiale schaal. Ik kan bepalen in welke gebieden water nu al schaars is en waar er al problemen zijn, en welke gebieden hier bij zullen komen in de nabije toekomst als gevolg van toenemende watervraag en een droger klimaat. Ik kan berekenen hoeveel grondwater er is onttrokken en een schatting maken van de hoeveelheid beschikbaar water en hoelang we hier nog mee kunnen doen.

De resultaten uit deze studie laten zien dat vooral geïrrigeerde gebieden in droge klimaat zones gevoelig zijn voor toename in watervraag. We zien grondwateruitputting hotspots voor India, Pakistan, Noord China, Midden en West USA (Fig. 1.1). Nieuwe gebieden

waar grondwateruitputting zal gaan plaatsvinden zijn de gebieden waar de watervraag zal gaan toenemen door een droger klimaat, zoals Spanje of Italië (Fig. 5.7). Op mondiale schaal zal de uitputting verdubbelen (Fig. 5.2).

De afname in rivierafvoeren laat het zelfde patroon zien; het grootst voor de drogere geïrrigeerde gebieden, en veel kleiner in gebieden waar minder grondwater wordt onttrokken. In de toekomst zullen rivierafvoeren verder afnemen door afname in neerslag en toename in watervraag en grondwater onttrekking (Fig. 5.9).

Voor sommige gebieden met grondwateruitputting zijn de grondwaterstanden al zo diep weggezakt dat een gewone, lokale boer er niet meer bij kan (de vuistregel hier is 100 m diep) (Fig. 5.3). In de toekomst zullen deze gebieden groeien en zullen er nieuwe bijkomen. Pompkosten zullen toenemen (Fig. 5.3) . Dit laat zien dat, om in de toekomst nog steeds water te kunnen onttrekken, er grote investeringen gedaan moeten worden om putten niet te laten opdrogen. Aan de andere kant, laten de kaarten met uitputting en de mondiale trend zien dat ons waterverbruik nu niet duurzaam is. Om in de toekomst nog over water te kunnen beschikken moet er naar duurzame oplossingen gezocht worden.

Deze informatie is van grote waarde voor water managers op regionale schaal, nationaal, en ook internationale organisaties (bv UNESCO, World Bank). Modellen zoals deze geven informatie op mondiale schaal, dus ook voor de gebieden waar regionale modellen niet beschikbaar zijn.

.

About the Author

Inge (Ingeborg Elisabeth Maria) de Graaf was born 5-5-1987 in Nijmegen. She grew up in Wijchen.

Inge finished her pre-university education at het Dominucus College in Nijmegen in 2005. She always was interested in 'system earth' and decided to study Soil, Water, and Atmosphere in Wageningen. After the first year, Inge chose to continue the hydrology route of the BSc. and MSc. program. For her MSc thesis, Inge visited the University of Idaho to do fieldwork. In this research she explored the spatial and temporal distribution of subsurface water flows recharging the underlying aquifer in the Paradise Creek watershed in Idaho. It was during this stay that Inge realized that doing scientific research was something she loves to do. Back in the Netherlands, Inge did her internship at Alterra in Wageningen, modelling the urban water balance for different cities in Europe. In 2011 Inge graduated as a Master of Science in Hydrology and Water Quality at Wageningen University.

In September 2011 Inge started her PhD research on large-scale hydrology at Utrecht University. This research gave her the opportunity to broaden her hydrologic point of view from the catchment scale, to the global scale. The findings of her PhD research are published in peer-reviewed journals, and bundled in this Thesis.

In October 2015 Inge moved to Colorado and started as a postdoctoral fellow at the Colorado School of Mines. Here she works on the development of a high-resolution hydrological model for the US, focussing on the groundwater part. This project is part of a larger project, aiming on enabling better, faster, and cheaper computational science and engineering capabilities for extreme-scale computing.

.

List of Publications

First autor publications

de Graaf, I.E.M., E.H. Sutanudjaja, L.P.H. van Beek, and M.F.P. Bierkens (2015), A high resolution global scale groundwater model, *HESS*, 19, 823-837, doi:10.5194/hess-19-823-2015, *editors highlight*

de Graaf, I.E.M., L.P.H. van Beek, Y. Wada, and M.F.P. Bierkens (2013), Dynamic attribution of global water demand to surface water and groundwater resources: Effects of abstractions and return flows on river discharges, *Adv. in Water Res.*, 64, 21-33, doi:10.1016/j.advwatres.2013.12.002

Publication in preperation

de Graaf, I.E.M., L.P.H. van Beek, E.H. Sutanudjaja, Y. Wada, M.F.P. Bierkens, Limits to global groundwater consumption.

de Graaf, I.E.M., L.P.H. van Beek , T. Gleeson, N. Moosdorf, O. Schmitz, E.H. Sutanudjaja, M.F.P. Bierkens, A global-scale two-layered transient groundwater model: development and application to groundwater depletion, *submitted to HESS*.

Y.Wada, I.E.M. de Graaf , L.P.H. van Beek, High-resolution modeling of human and climate impacts on global water resources, *submitted to JAMES*

S. Koirala, M. Jung, I.E.M. de Graaf, M. Reichstein, N. Carvalhais. Determinants of the groundwater-vegetation interaction at the global scale.

Conference contributions (selection)

de Graaf, I.E.M., L.P.H. van Beek, E.H. Sutanudjaja, Y. Wada, M.F.P. Bierkens (2015), Limits to global groundwater consumption, AGU Fall Meeting, San Francisco, California, *oral presentation.*

de Graaf, I.E.M., L.P.H. van Beek , T. Gleeson, N. Moosdorf, O. Schmitz, M.F.P. Bierkens (2015), A global-scale two-layered transient groundwater model, EGU General Assembly, Vienna, Austria, *oral presentation.*

de Graaf, I.E.M. (2015), Water Underground, EGU General Assembly, Vienna, Austria, *oral presentation, early carreer activity.*

de Graaf, I.E.M., L.P.H. van Beek , T. Gleeson, N. Moosdorf, O. Schmitz, M.F.P. Bierkens (2014), Reconstruction of Groundwater Depletion Using a Global Scale Groundwater Model, AGU fall meeting, San Francisco, USA, *oral presentation.*

de Graaf, I.E.M., L.P.H. van Beek, M.F.P. Bierkens (2014), Categorizing Large-Scale Aquifers of the World, GEWEX, den Haag, *poster presentation.*

de Graaf, I.E.M., E.H. Sutanudjaja, L.P.H. van Beek, and M.F.P. Bierkens (2013), A High Resolution Global Scale Groundwater Model, AGU fall meeting, San Francisco, USA, *oral presentation.*

de Graaf, I.E.M., L.P.H. van Beek, Y. Wada, and M.F.P. Bierkens (2013) Dynamic Attribution of Global Water Demand to Surface Water and Groundwater Resources: Effects of Abstractions and Return flows on River Discharges, EGU General Assembly, Vienna, Austria, *oral presentation.*

de Graaf, I.E.M., L.P.H. van Beek, Y. Wada, and M.F.P. Bierkens (2012), Effects of Water Abstractions on River Low Flows, EGU General Assembly, Vienna, Austria, *poster presentation.*

Dankwoord

Despite only my name is printed on the cover this thesis, the underlying research certainly was not a solitary exercise. In the past 4 years I have been able to work with passionate and inspiring people who have made this PhD research a valuable and instructive period for me. I will switch to Dutch for the final words of this thesis to say a proper and honest thanks to those who supported me in completing this PhD research.

Als eerste wil ik natuurlijk mijn begeleiders duo bedanken. Marc en Rens, bedankt dat jullie mij hebben geïntroduceerd in de wereld van de mondiale modellen, ik had me geen leuker PhD onderzoek kunnen wensen. In het begin was het voor mij wel even wennen bij jullie, maar gelukkig is alles goed gekomen en ben ik blij met alles wat ik van jullie heb geleerd.

Ik wil graag mijn collega's van FG bedanken voor alle ontspannen gesprekken bij het koffieapparaat en de verfrissende lunch wandelingen in de botanische tuin. In het bijzonder wil ik Edwin en Yoshi bedanken. Guys, thanks for all your help and inspiring discussions that we had and the good friends that we became! Ik wil ook Wouter bedanken. Wouter, ik vond het heerlijk om af en toe lekker samen te klagen over van alles en nog wat, maar ook altijd met een lach. Je was een gezellig kantoorgenootje en ik kom snel een kop koffie drinken.

Next, a special thank goes to Tom, who invited me to come to McGill University. Although it was for a short period only, for me it was a very refreshing and valuable experience.

Naast de braintraining, wat promotie onderzoek doen wel is, moet er natuurlijk ook aan het gezonde lichaam gewerkt worden. Ik wil graag mijn roeiploeg en coaches bedanken voor alle gezellige uurtjes die we samen hebben doorgebracht op het water, op de ergometer en in de gymzaal. Het is heerlijk om na een dag hard nadenken lekker te zweten op een ergometer met zunami op de 'achtergrond ', of om het weekend goed te beginnen met een training in de acht. Daarnaast wil ik ook de dames van de Bike Babes bedanken. Het was heerlijk om met jullie rond te fietsen en ondertussen lekker bij te kletsen, met een taartje onderweg.

Ik wil ook graag al mijn goede vrienden en familie bedanken die vaak geïnteresseerd luisterden als ik over mijn onderzoek vertelde maar ook voor de nodige ontspanning zorgden als dat nodig was.

Als laatste wil ik Chris bedanken. Chris, ik ben super blij met jou. Bedankt voor je onvoorwaardelijke steun en liefde. Je steunde me ook toen ik besloot naar Colorado te verhuizen, daar ben ik je heel dankbaar voor.

Februari, 2016
Golden, Colorado